Risk Analysis of Power Electronics-based Power Systems Using Physics-of-degradation in Power Electronic Converters

Kjær, Martin

DOI (link to publication from Publisher):
10.54337/aau561804316

Publication date:
2023

Document Version
Publisher's PDF, also known as Version of record

RISK ANALYSIS OF POWER ELECTRONICS-BASED POWER SYSTEMS USING PHYSICS-OF-DEGRADATION IN POWER ELECTRONIC CONVERTERS

BY
MARTIN VANG KJÆR

DISSERTATION SUBMITTED 2023

AALBORG UNIVERSITY
DENMARK

Risk Analysis of Power Electronics-based Power Systems Using Physics-of-degradation in Power Electronic Converters

Ph.D. Dissertation

Martin Vang Kjær

Dissertation submitted June, 2023

Dissertation submitted: June 2023

PhD supervisor: Professor Frede Blaabjerg
Aalborg University

PhD committee: Associate Professor Peter Omand Rasmussen (Chair)
Aalborg University, Denmark

Professor Giovanna Oriti
Naval Postgraduate School, USA

Professor Thomas Ebel
University of Southern Denmark, Denmark

PhD Series: Faculty of Engineering and Science, Aalborg University

Department: AAU Energy

ISSN (online): 2446-1636
ISBN (online): 978-87-7573-687-4

Published by:
Aalborg University Press
Kroghstræde 3
DK – 9220 Aalborg Ø
Phone: +45 99407140
aauf@forlag.aau.dk
forlag.aau.dk

Printed in Denmark by Stibo Complete, 2023

Biography

Martin Vang Kjær

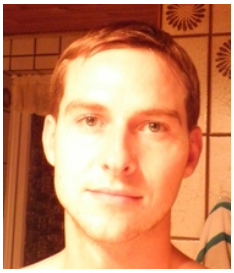

Martin Vang Kjær received the B.Sc. and M.Sc. degrees in Energy Technology, with specializing in Electrical Energy Engineering and Power Electronics and Drives from Aalborg University, Aalborg, Denmark, in 2017 and 2020, respectively. Martin is currently pursuing a Ph.D. degree in applied power electronics also at the Department of Energy. His current research interests include intelligent power processing, reliable operation of distributed generation systems and prognostics and health management of power converters. Martin is the section representative in the IEEE student activities committee of IEEE Denmark. He is a member of the Ph.D. board at the Faculty of Engineering at Aalborg University. And finally, he is the technical and industry officer at the IEEE student branch AAU at Aalborg University.

Abstract

The conservation and development of modern society are highly dependent on reliable power systems, which can ensure a high degree of continuously available electrical energy supply. The primary function of power systems is to provide its customers with electrical energy as economically possible while preserving adequate system reliability. Due to the present global energy supply transition from fossil-based to zero carbon emitting, the sector is witnessing a significant increase in the installed capacity of renewable-based energy sources. The large-scale integration of renewable energy sources and power electronics-based generation introduces some distribution and grid utility challenges. One of the main challenges is the increased risk of failure-related downtime, which is an outcome of power electronics converters being known to constitute the fragile subsystems and are, therefore, likely to constitute the system bottleneck in terms of reliability. To address this challenge, it is crucial that these costly undesired events can be predicted and thereby prevented through means of time-to-failure assessment methods of power electronic-based generators. These assessment methods can help to preserve a high system availability through predictive maintenance, which can lead to a reduction in the levelized-cost-of-energy.

The reorganization of power systems gives rise to issues related to assessing the system reliability, as the classical methods might no longer guarantee optimal operation. These methods were developed for conventional power systems comprised of large generators supplying the power and, in combination with the bulk transmission system, that formed a single utility system with significantly less power electronic converters. In order to achieve a successful transition to power electronics-based power systems, it is crucial to gain the possibility of assessing the localized reliability of distribution systems when including the likelihood of power electronic converter failures. Additionally, bridging the gap that enables the merging of the converter assessment methods with those of power system reliability should be employed using models that describe a more realistic failure tendency of power converters and less dependent on assumed failure rates with lack of considerations on the physics-of-failure and actual operation conditions.

To address those issues, this Ph.D. study proposes models, concepts, and modeling frameworks for reliability assessment of power electronics-based power systems. First, a mission profile-based methodology on how to assess the reliability of modern power systems is proposed, based on a case study using a low-voltage distribution network consisting solely of renewable-based generation units. The study includes time-to-failure modelling of power converters and the modelling of long-term state probabilities used to gain the availability of power electronic-based generation units. The availability is then exploited to present risk modelling concepts, which can assess the risk of generator downtime and the consequences of particular failure events and how to exploit this knowledge for maintenance planning.
A great deal of effort is made to gather an understanding of the issues related to the existing converter reliability methods, which may lead to inaccurate lifetime predictions. This study exploits the concepts of physics-of-degradation to deal with the relevant issues. One of the main challenges is identified as being the relatively large distribution spread of the failure distributions caused by multiple uncertainties, such as the usage of the extrapolation of accelerated tests to real-field usage conditions. This study presents a concept which is capable of reassessing the converter time-to-failure distributions through the means of the monitoring of a unified efficiency-based health precursor. This methodology proves to be effective in terms of its capability of decreasing the distribution spread as the unique degradation trend gets increasingly transparent. The time-to-failure can therefore be stated with relatively high precision at the crucial time of imminent failure. Due to its loading dependency, the condition monitoring concepts have abstained from using efficiency as a health indicator. This study presents a method to detect the end-of-life of converters, which deals with the issue of efficiency being dependent on loading conditions. This detection mechanism makes use of a maximum margin classifier that is able to construct non-linear decision boundaries in the feature plane. The combination of the physics-of-degradation concepts presented in this thesis constitutes a holistic approach that can be useful in regard to maintenance coordination, which can help to advance the availability of power electronic-based power systems.

Resumé

Den løbende opretholdelse og udvikling af det moderne samfund er yderst afhængig af, at der er et pålideligt elektrisk forsyningssystem til rådighed, som kan garantere en høj grad af kontinuert tilgængelig elektrisk energi. Den primære funktion af det elektriske elnet, er at kunne forsyne nettets kunder med elektrisk energi på en måde hvor de økonomiske omkostninger minimes til en grad, hvor der samtidigt bevares en tilstrækkelig mængde af system pålidelighed. Som følge af den nuværende globale energiforsynings overgang fra fossil-baseret energikilder til energikilder som ikke bidrager til den samlede CO_2 udledning, er energisektoren vidne til en betydelig forøgelse af den samlet installeret kapacitet af vedvarende energikilder. Storskala integreringen af vedvarende energikilder og effektelektronik baseret generationsenheder giver anledning til visse udfordringer i elforsyningsnettet. En af de centrale udfordringer er den øgede risiko for fejl relateret nedbrud, som er et resultat af skrøbelighed som effektelektroniske omformere udviser. Effektelektroniske omformere er generelt kendt for at være blandt de mest fejltilbøjelige delsystemer og det er derfor ofte sandsynligt at de udgør de kritiske elementer i forhold til elforsyningssystemets overordnede pålidelighed. For at imødekomme denne udfordring er det afgørende at man er i stand til at forudsige disse omkostningsfulde og uønskede begivenheder. Dette muliggøres ved brug af livstidsestimeringer af effektelektronisk baseret generationsenheder. Disse vurderingsmetoder kan bidrage til at opretholde en høj systemtilgængelighed af el-nettet gennem brug af tilstandsbaseret vedligehold, som kan lede til en reduktion af de totale enhedsomkostninger af elforsyningen.
Omstruktureringen af elnettet i forbindelse med den grønne omstilling giver desuden anledning til udfordringer relateret til måden, hvorpå pålideligheden af system skal vurderes, da brugen af de eksisterende metoder muligvis ikke længere er garant for den optimale drift. Dette skyldes at disse vurderingsværktøjer er udviklet til anvendelse på konventionelle elforsyningssystemer som udelukkende består af store centrale synkrongeneratorer som i kombination med det centrale transmissionsnet har udgjordt et enkelt samlet forsyningsnet, hvori der indgik en betydelig mindre andel af effektelektro-

niske omformere. Hvis der skal opnås en vellykket overgang til et grønt forsyningsnet som i høj grad baserer sig på effektelektroniske systemer, så er det essentielt at muligheden for at evaluere pålideligheden lokalt opnås og hvor der samtidigt tages højde for sandsynligheden for omformer nedbrud. Derudover er det også essentielt at realistiske fejl tendenser af omformere anvendes, når der skal udvikles modeller som muliggør at pålidelighedsevaluerings metoderne, der bruges i forbindelse med omformerne skal omfattes og indarbejdes i pålidelighedsevalueringen af elforsyningssystemer. Dette betyder at fejltendensen af omformerne ikke skal beskrives ved brug af konstante fejlrater, som hidtil hverken tilgodeser de fysiske fænomener som leder til nedbrud og de lastbetingelser som påvirker enhederne.
Med henblik på at imødekomme de nævnte problemstillinger, fremviser dette Ph.D. studie en række modeller, koncepter og modelleringsprincipper til brug af pålidelighedsevaluering af effektelektronisk-baseret elforsyningssystemer. Dette inkluderer blandt andet en belastnings-baseret metodik, som beskriver hvordan pålideligheden af fremtidens elforsyningssystem skal vurderes.
Metodikken tager udgangspunkt i et lavspændingsdistributionsnet, som udelukkende består af generationsenheder baseret på vedvarende energiteknologier. Studiet inkluderer modeller, som kan beskrive den resterende levetid af omformere inden nedbrud kan forventes, langsigtet tilstandssandsynligheder som kan opgive tilgængeligheden af effektelektroniske generationsenheder. Denne opnåede information om enhedens tilgængelighed udnyttes derefter til at præsentere modeller til risikovurderinger, som er i stand til at vurdere risikoen for generator nedbrud og hvilken negativ effekt sådan et eventuelt nedbrud kan forventes at medføre i forhold til uleveret elektrisk energi. Denne information udnyttes herefter til at kortlægge et fremtidigt præventivt vedligehold af generationsenhederne.
I projektet er der ydet en stor indsats for at opnå en god forståelse for hvilke problemstillinger der er relateret til de eksisterende pålidelighedsmetoder som anvendes på omformere i dag, og som i værste fald kan lede til upræcise livstids estimeringer. For at imødekomme de relevante problemstillinger gør projektet nytte af den fysik, som underligger en degraderingsproces af omformer komponenter. En af de centrale problemstillinger er identificeret som værende den relative store spredning i fordelingsfunktionerne som angiver nedbrudsfordelingen og som er forårsaget af et betydeligt antal usikkerheder i modellerne. En af de centrale usikkerheder, som bidrager til denne spredning, skyldes anvendelsen af extrapolering af resultater som er opnået under accelererede tests til anvendelse under rigtig praktiske forhold. Denne Ph.D. afhandling fremviser et koncept, som muliggør kontinuerte revurderinger af fordelingen af den estimerede tid til forventet nedbrud. Denne revurdering opnås gennem tilstandsovervågning, der gør brug af omformerenhedens samlet effektivitet som indikation for den aktuelle helbredstilstand.

Metoden viser sig at være effektiv i forhold til at reducere spredningen i observationer af tiden indtil fremtidige nedbrud. Denne spredning reduceres i takt med at en stigende del af omformerens brugbare levetid forbruges og den unikke degraderings tendens i stigende grad bliver mere åbenlys. Dette medfører at tiden til et fremtidigt nedbrud kan estimeres med relativ høj præcision og på det afgørende tidspunkt, hvor et nedbrud er nært forestående. De eksisterende tilstandsovervågnings koncepter har afholdt sig fra at anvende omformeres effektivitet som en helbredsindikator på grund af dens afhængighed af omformerens lastforhold. Dette studie fremviser en metode, hvorved det er muligt at opdage når omformerenhedens livscyklus ophører og som samtidigt tager højde for effektivitetens afhængighed af lastforholdende. Denne metode gør brug af en maximal margen klassifikations algoritme, som er i stand til at definere ikke lineære beslutnings grænser i det plan hvor de essentielle signalindikatorer indgår. Kombinationen af de koncepter som er præsenteret i denne afhandling og som baserer sig på fysikken bag omformer komponenters degraderingsprocesser, kan tilsammen udgøre en holistisk tilgang, som kan være brugbar i forhold til koordinering af el-systemets vedligehold, og kan bidrage til at øge tilgængeligheden af effektelektronisk-baseret elforsyningssystemer.

Preface

The content presented during this dissertation is a summary of the outcome of the Ph.D. study "*Risk Analysis of Power Electronics-based Power Systems Using Physics-of-degradation in Power Electronic Converters*," which was carried out at the Department of Energy, Aalborg University, Denmark. The Ph.D. study was part of the REliable Power Electronics-based Power System (REPEPS) research project. I wish to express my sincere gratitude to the Villum Foundation, which funded this study.

I want to express genuine gratitude to my supervisor, Professor Frede Blaabjerg, for his exceptional supervision and, most of all, the patience he had with me throughout my study. He is undoubtedly blessed with extraordinary skills in leadership and management of Ph.D. students, and it was a great learning experience working with him. I would also like to express my sincere gratitude to my co-supervisor, Professor Huai Wang, whose unrivaled knowledge within reliability engineering of power converters was indispensable for my progress countless times. His technical assistance got me through several cases of feeling lost and prevented me from taking my study in a direction which would not have benefited the final result. I also want to express appreciation to Professor Yongheng Yang, who took a significant part in that i got the opportunity to have this experience, and also for his valuable supervision and kind nature.

Lastly, I would like to thank everyone who was part of this inspiring research environment, all the talented guest students of Section C originating from all over the world, meeting all of you enriched my life in so many ways. In particular, I would like to say special thanks to Shih-Feng Chou, Amirali Davoodi, Saeed Peyghami, and all the remaining Ph.D. students of REPEPS.

Martin Kjær
Aalborg University, June 18, 2023

Contents

Part I

Project Summary

Chapter 1

Introduction

The benefits of electrical power systems are an integrated part of modern society to such an extent that it is impossible to imagine society without a continuously available electrical energy supply. This emphasizes the importance of power systems' reliability, which is the subject of this thesis. The main function of power systems is to supply its customers, large as well as small, with electrical energy as economically possible, while maintaining adequate system reliability [1]. Due to the current transition of the global energy sector from fossil-based to zero-carbon emitting, the capacity of renewable energy sources (RES), such as solar and wind based generation units, have seen a substantial increase in the past decades [2]. With the continuously increasing deployment of distributed energy resources (DER), the conventional centralized power grid is being replaced by a large variety of distributed networks. The large-scale integration of DER posses some challenges to the distribution networks and to the utility. One of the main challenges is due to the intermittent nature of RES, causing the injected power to be highly fluctuating and thereby affecting the network stability [3, 4]. While another significant challenge, is the increased risk of failure related downtime. This is a consequence of power electronic converters being, according to the literature [5], identified as the most fragile subsystems and is therefore likely to constitute the bottleneck of the entire system in terms of reliability. The fragility of the power electronic converters will not only induce the risk of a reduction in supplied energy but also alter the cost of generated energy negatively as a result of the failure related downtime. Recent research efforts are therefore concerned with the subject of estimating the lifetime of power converters and with the developed lifetime predictions, the system availability can be increased by means of predictive maintenance, which will result in a reduction in the Levelized-Cost-of-Energy (LCOE) [6].

The challenges affecting the short- and long-term performance of power systems can be quantified by the power system reliability. By definition, *reliability is the ability of a system to perform its purpose adequately in a specified finite time interval while subjected to some defined operating conditions*. The long-term performance can be quantified by how well the power system is able to supply the demand at all times, which puts some requirements on the existing generation capacity, transmission facilities and a sufficient level of reserve. This ability is known as the system adequacy [1] [7]. In contrast, the short-term performance can be quantified by how well the power system is able to withstand sudden contingencies in the form of abrupt disturbances and abnormal operation such as power outages. This ability compromises the system security. The system adequacy can be ensured by proper long-term planning of sufficient generation facilities to accompany the load demand, whereas the security aspect can be accomplished by conducting a stable system operation. The planning is conducted on several different timescales in which the long-term planning considers the facility planning, which is associated with developing the infrastructure that can accompany the future growth in energy consumption. The facility planning includes the installation of generation units and expansion of the current transmission and distribution systems and is often considering a time frame of 5-30 years ahead [8]. In contrast, the short-term planning involves the operation of the existing facilities in terms of scheduling the seasonal and day-ahead commitment of the units. In addition, the short-term planning also compromises the maintenance-scheduling with the objective of optimizing the operation in regards to generation cost and reliability. The structure of the operation and planning and its corresponding timeline is shown in Fig 1.1

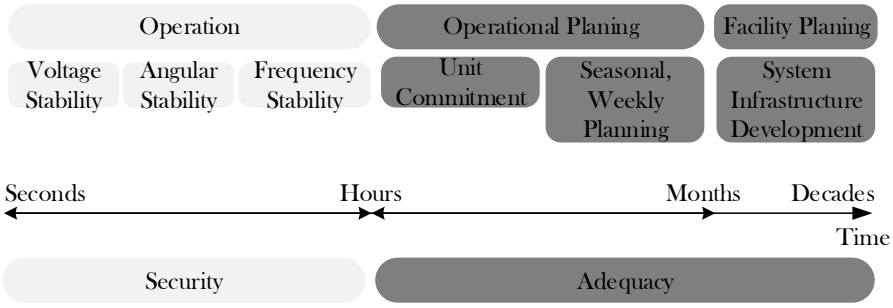

Fig. 1.1: Structure of power system planning and operation including its corresponding timeline where Gx denotes conventional synchronous generators, DG denotes distributed generation units and DS denotes distributed storage units.

Low security of supply can result in energy not being supplied to the

customers, which may lead to high monetary costs. From a national perspective, Denmark has a relatively high-level of supply security, which benefits the electrical consumers and the society as a whole. On average, Danish consumers experienced approximately 22 outage minutes in 2018, corresponding to the electricity being available 99.996% of the time. Among the total amount of yearly outage, 0.2 minutes was caused by disturbances, while the remaining 21.7 minutes caused by failures occurring in the distribution grid. Even though Danish consumers are experiencing one of Europe's highest ranked level-of-security-of-supply, the outage minutes are expected to increase in the future. The current high level-of-security-of-supply is mainly due to the electricity grid being relatively new and wear-out related faults have remained relatively low until now. Also, the future grid is going to include many new types of components, which will lead to an increased risk of failure. During recent years, the grid adequacy has come under pressure, due to the increasing failure probability, that the aging grid induces [9]. When looking across the domestic borders, a statistical survey [10], states that the energy not supplied (ENS) in the Nordic, as well as Baltic countries, amounts to an annual average of nearly 7 GWh. Several studies are concerned with the social and economic impact of failure related outages by considering the severe consequences of recent European blackouts. For example, the disruption of a power line in Switzerland in 2003 resulted in a cascade of effects on the neighbouring countries and caused a financial loss of approximately €1.2 billion as a result of interrupting millions of people for several hours [11]. While it is difficult to assign the momentary value to the impact of interruptions of private homes, it is somewhat straightforward to make rough estimates for businesses and according to the U.S. Department of Energy (DoE), outages are costing the U.S. economy $150 billion annually [12]. Due to the cost of interruptions, there is an essential need to further enhance the reliability of power systems. Additionally, the transition from fully adjustable power generation to the intermittent generation, that is linked to RES, is adding further challenges to the generation adequacy. In order to meet the challenges and uncertainties related to future trends, grid operators need to make reinvestments and implementations that can prevent inadequate operation and at the same time ensure a greater amount of system flexibility.

1.1 Reliability of Future Power Systems

During the past decade, considerable efforts have been made to make society more sustainable, which is due to the pollutive nature of the utilization of fossil-based energy sources, that affects the climate negatively. Consequently, global efforts have been directed towards replacing the traditional centralized power generation with decentralized renewable based power sources such as

wind and solar [4]. The decentralized RES is grid-interfaced by power electronics, which provides the advantages of flexible power control and high efficient, static power conversion [13]. In contrast to these advantages, the reorganization of power systems also arises new issues in terms of assessing the system reliability, as the old methodologies might no longer guarantee optimal operation. The reliability of conventional power systems is assessed by adequacy and security indices, that states the systems ability to supply its demand [1]. These concepts are developed for cases where the entirety of the system elements of power system services were supplied by a single integrated utility. This comprised large generators, that supplied the power and combined with the bulk transmission system formed an extensive generation system with loads connected to the distribution network. Due to the simple structure of single utility systems, the reliability assessment is fairly straight forward. However, as the power system gets more dominated by RES, a large share of the generation mix will consist of distributed generation, which requires a fundamental rethinking of how the reliability of the system is assessed. The impact, that the restructuring of power systems will have on the reliability assessment has already been addressed by the Cigre C1.27 working group [14]. Based on the inclusion of RES, DGs and storage systems, the working group redefined the reliability of power systems, so that service is considered bidirectional, meaning that it is considered to be both to and from the end-user. This implies, that the top-down approach of reliability evaluation used for conventional power systems no longer applies, which can be understood by observing Fig 1.2, which depicts the fundamental difference in the physical structures of conventional and modern power systems. From Fig. 1.2, it can be recognized that there is a need for a reliability definition that can deal with the two-way nature of power flow in the modern utility environment, which is in harsh contrast to the conventional systems dominated by large-scale thermal power plants, that delivered power to the end-consumers by means of a top-down structure. As the integration of DG is gaining momentum, large-scale renewable plants such as Wind farms and PV parks are becoming an increasingly part of the transmission and medium voltage distribution systems which forms an active network with multiple sources of power generation. The increasing amount of RES and their intermittent nature of power generation induces some requirements on the system flexibility, in order to cope with the increase of net load variability. It implies the need to employ energy storage units to restore the balance between supply and demand, that is, the combined variability in power consumption and non-dispatchable generation [15]. As the power system is moving towards a high penetration of RES, it will require employment of both utility-scale and small scale energy storage. This can aid to energize distribution systems to locally support the demand and thereby ensure reliable operation. The operation of such systems will require real-time monitoring of generation units to

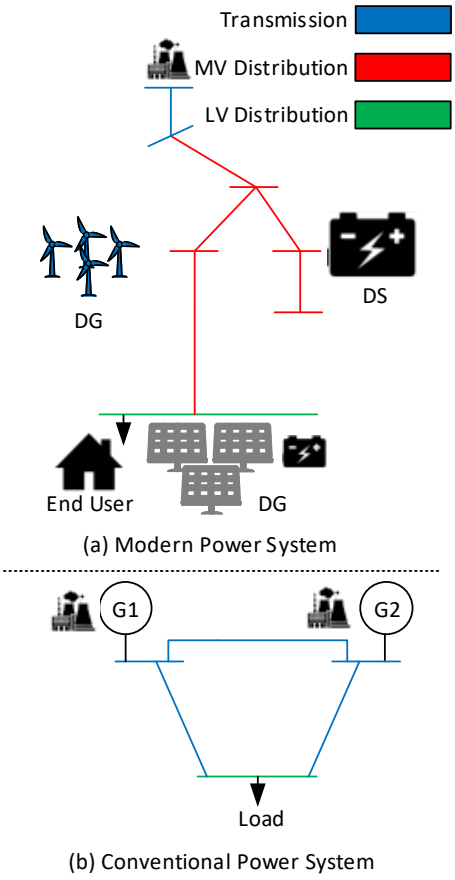

Fig. 1.2: Difference in structure in conventional and modern power systems

optimize the decision-making, that can be executed in a distribution or decentralized manner, which can show to be advantageous in terms of efficiency, stability and availability. These active distribution subsystems are generally known as microgrids and they normally include a variety of DER and end-users. In terms of the DER units, this includes both DG and distributed storage (DS) units, inhibiting different capacities and characteristics. The microgrid normally operates in grid-connected mode through a substation transformer to the utility grid, but it is also expected that it is able to provide a sufficient amount of generation capacity and have proper operational strategies to support its load demand in case of being disconnected from the utility grid and thereby remain operational as a self-governing islanded entity [16]. None of the existing literature has covered the requirements and assessment of localized reliability of distribution systems operating as microgrids when

including the likelihood of converter failures. This is a fundamental requirement as future power systems must be able to guarantee energy adequacy locally.

A DG unit consists of a primary energy source, an interface unit and switch gear located at the point of connection, as shown in Fig. 1.3. It should be

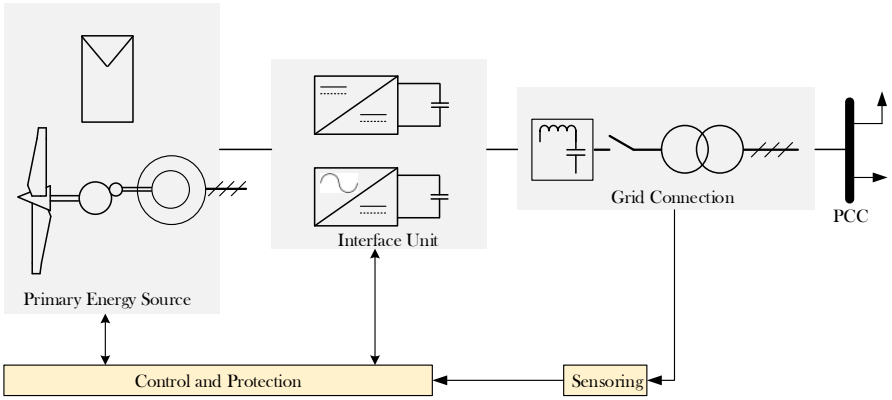

Fig. 1.3: Block diagram representation of DGs

noted, that the primary energy source in Fig. 1.3 can also be a distributed storage unit. In the case of power electronic interfaced DG units, the power electronics offers flexible control of e.g., voltage and/or frequency and the input power can be AC at either fixed or variable frequency or DC. The output power of non-dispatchable units is generally controlled to ensure the optimal operating condition of the given energy source. For example, wind based generators are commonly operated based on the extracting the maximum power of the wind regime. Thus, the loading of non-dispatchable units varies according to the environmental conditions, which has a critical impact on the failure prone power electronic components causing wear-out related failures. As a result, the reliability modelling should consider the real-field mission profile that is subjected to the power electronics operation in RES [17].

Up until now, the integration of power electronics in power system analysis has been based on the assumption, that the failure rates of the power electronic devices remain constant during the entire life-cycle [18]- [25]. The employment of constant failure rates does not coincide well with the true failure tendency of power converters and will therefore introduce incorrect reliability and risk evaluations when used in power system analysis. This will result in non-optimal planning of power systems with a high degree of RES and as power electronics is a fundamental part of renewable generators, they

are required consideration in power system analysis, in order to gain realistic and accurate results. This includes the consideration of the relative short life-cycle of power converters for planning purposes, so that cost-effective replacement policies can be developed. Finally, the time-varying and condition dependent failure-rate of power electronics should be employed when assessing the system reliability as this will inflict the system performance significantly. It is, therefore, of utmost importance, that the analysis of converter reliability is incorporated into the future power system reliability assessment methods.

1.2 Reliability of Power Electronic Converters

Due to the rapid increase of renewable energy sources, there is a fundamental requirement for novel operational strategies that can help to ensure a high-degree of power-supply reliability. A key enabling technology, which is commonly used within renewable generation, is power electronics and in recent decades, the advancements in power devices and passive components, converter topologies, control strategies and system integration methodologies have been significant. The overall performance of power converters, is dictated by how the individual components perform, the used circuit topology, the applied control procedure, and the application and usage condition. One of the fundamental performance factors of power electronics is their ability to perform as required without failures when exposed to some defined usage conditions. As previously stated, power electronic converters are often the life-limiting factor of systems and field experience show, that they constitute the critical assemblies in terms of failure frequency and maintenance cost within renewable generation [26]. In particular, it shows that converters made up 13% of the failures and 18.4% of the total downtime in a study covering 350 onshore wind generators [27]. In addition, another survey shows that PV-inverters are causing 37% of unscheduled maintenance and 59% of failure related costs during a 5 year of operation of a 3.5MW PV park [28,29].

1.2.1 Key Concepts in Reliability

In order to provide some insight in how the reliability of power converters are evaluated in terms of metrics and key terminology, the following will provide a brief introduction to the reliability engineering concepts used in the thesis. First and foremost, the frequency of failure of a population of power electronic components are presented in the form of a failure distribution as shown in Fig. 1.4. The distribution of failures is modelled by a parametric function known as a probability density function (pdf) and the failures of power electronic components follow a Weibull distribution, which

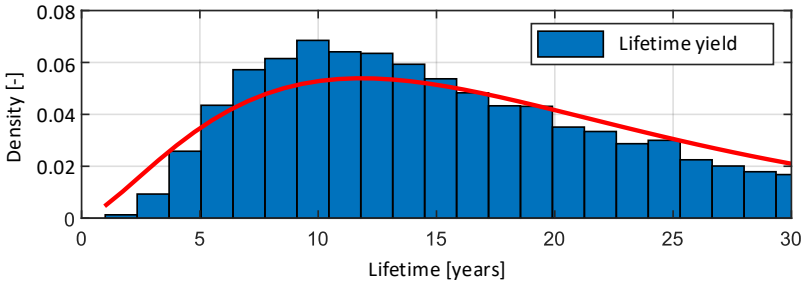

Fig. 1.4: An example of the failure distribution of power devices and its corresponding fitted Weibull function (Red).

describes scenarios, in where the failure-rate is non-constant during the wear-out phase [30]. This is in stark contrast to the converter reliability being employed in power system analysis nowadays, which considers constant failure rates, that are obtained from historical data. The lifetime of the components, is based on when they reach their defined failure criterion. The criteria could either be an abrupt failure or a certain level of degradation e.g., a 20% increase of the thermal resistance of the active power devices. In practice, the lifetime is stated in terms of the percentile life, which denotes when a certain percentage of a population of units has reached this defined failure criteria. The concept of percentile life is depicted in Fig. 1.5. The B_{10} value corre-

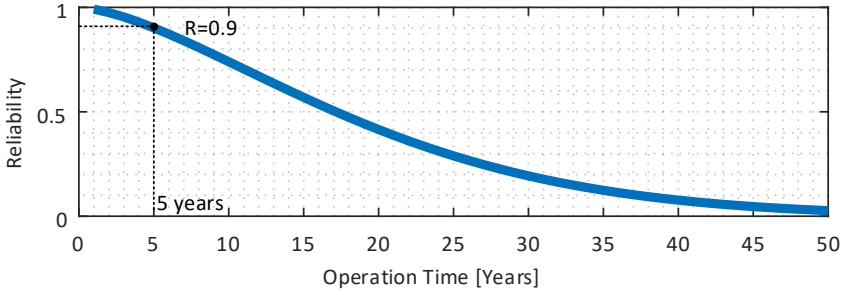

Fig. 1.5: An example of the percentile lifetime of power devices.

sponds to when 10 percent of the population has entered its failed state, that is, when the reliability equals 0.9. Fig. 1.5 describes the relationship between reliability and percentile life based on the example shown in Fig. 1.4.

The bathtub curve is a means to display how the failure rate evolves through-

out the life time of power electronic components. It is a superimposition of three distinct time intervals of the life-cycle; the failure rates for early failures (extrinsic), random failures (useful life) and wear-out failures (intrinsic) as depicted in Fig. 1.6. The extrinsic failures are caused by unintended defects and

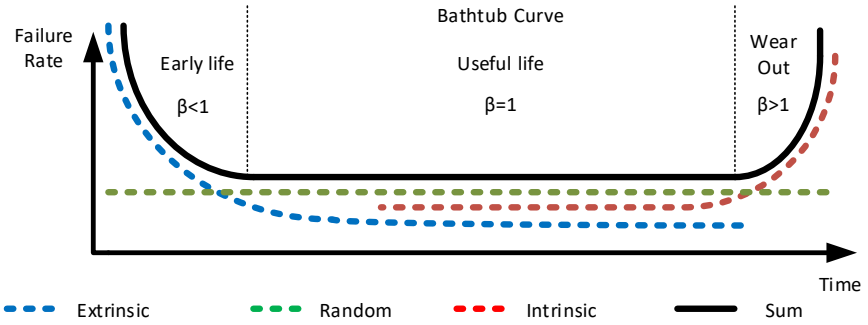

Fig. 1.6: The bathtub curve and the superimposed failure rates including the corresponding Weibull parameter β.

deviations fabricated during the manufacturing process of the components, this failure is distinctive for infant mortality and also installation defects. The intrinsic failures are caused by the natural deterioration (wear-out), as the processed materials age. If there exists a reasonable time-separation between the extrinsic and intrinsic failures, then the time occurring in-between represents the useful life of the components [31]. One of the objectives of this thesis, is to predict the wear-out phase, in order to provide advanced warning of failures, so that the life-cycle cost can be reduced through the minimization of unscheduled maintenance.

1.2.2 Physics-of-Failure Methodology

The state-of-the-art of converter lifetime predictions is based on the physics-of-failure methodology (PoF). The PoF methodology utilizes the knowledge of the life-cycle loading and the potential failure mechanisms in order to assess the time-to-failure of power converters [32]. The failure of the power electronic components can be understood as being present when the applied loading exceeds the design strength. The load refers to the relevant stressor e.g. voltage, temperature cycling etc. whereas the strength refers to the resisting physical properties e.g, adhesion, melting point etc. [30]. The load and strength of the components are dispersed within some specific ranges, which can be stated by using PDFs. As time passes, the strength of the components degrade and the occurrence of load-strength interference is increasingly likely, which is conceptually exemplified in Fig. 1.7. The method emphasizes

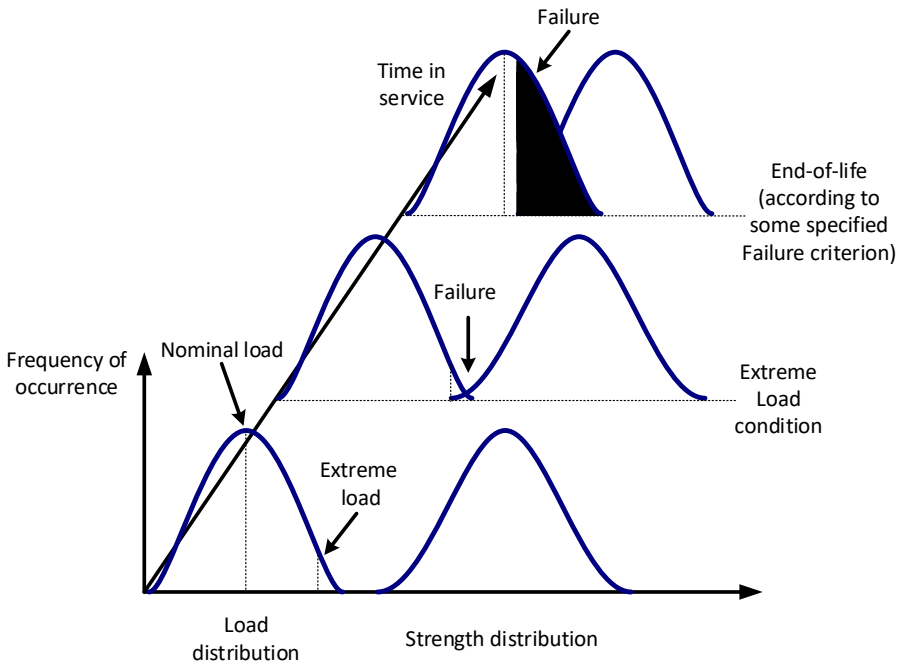

Fig. 1.7: Load-strength curves to illustrate overstress and wear-out with time in service.

the fundamental requirement of understanding the reliability physics of the power electronic components when assessing the reliability of power electronic systems. In those systems, special attention needs to be given to active power devices and capacitors, as they are considered the most liable components. Namely, the IGBT modules and the capacitors for AC filtering and DC-link applications [33]. The first step of the methodology involves the prioritization of the critical failure modes and mechanisms, which will vary based on the specific design and how the particular converter is loaded. One commonly used approach to identify what will be the critical failure mechanisms and where do these failures occur, is the Failure Modes, Mechanisms, and Effects Analysis (FMMEA). The inputs required to the FMMEA are the design data, the expected life-cycle data and historical maintenance and inspection data. Then subsequently, the actual load subjecting the device, that can lead to wear-out of the components, is collected. The stress features, that lead to the deterioration, which is linked to the specific failure mechanisms, are extracted and the damage caused by the specific loading profile can be assessed by use of PoF models, as outlined in Fig. 1.8. The PoF methodology seems like a good approach for systems with sufficient legacy, but one major concern, which might lead to inaccuracies in lifetime predictions, is the

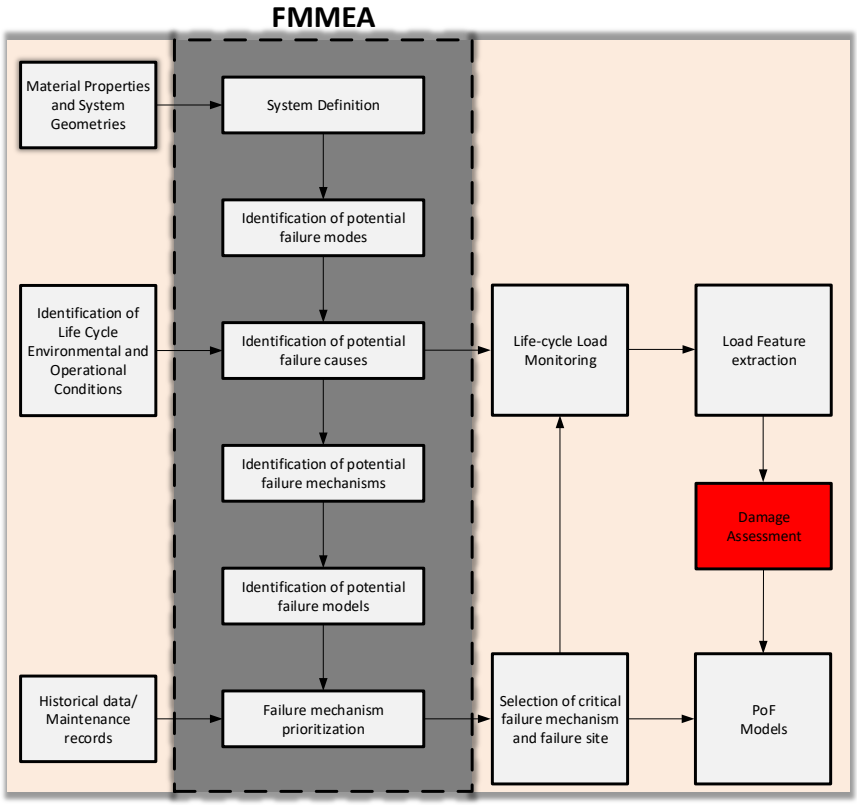

Fig. 1.8: Physics of Failure based reliability approach used in power electronic systems.

tendency to inherently base the prediction on one single failure mechanism. Often, PoF models are not available and therefore FMMEA is practically non-existing in current literature studies, which instead assumes that bond-wire lift-off is the single existing failure mechanism in the case of power devices. This is an idealistic assumption, as in reality, multiple failure mechanisms can co-exist and some can even be related in terms of sharing the driving forces that govern multiple failure mechanisms [34].

1.2.3 Reliability of Power Modules

The reliability of power modules requires knowledge across different fields such as the thermo-mechanical design capabilities, the underlying material properties science of the PoF models and power electronics in terms of its application field. Manufacturer of power modules have made considerable

efforts to develop lifetime models, as they occupy the required product data and expertise to handle it. The majority of these models are empirical lifetime models, strictly based on experience, and used to state the power cycling capabilities [35]. The models are commonly used for end-of-life estimations of power modules and thereby for the reliability estimation of power electronic systems when they are subjected to application-specific mission profiles. However, the major concern linked to this approach, is the establishment of the useful life by means of extrapolating accelerated test results to real-field usage conditions in order to obtain the parameters of the failure fatigue model. The validity of this extrapolation is often times doubtful [33]. This is due to the fact that the testing data are often based on a restricted number of constant loading conditions, which is in stark contrast with the real applied use cases [35, 36]. The loading profiles linked to renewable generation is of a highly dynamic nature, inhibiting a wide variety of stress ranges and gradients, which has a large influence on the mechanical stress that may excite the failures of power devices [37].

1.2.3.1 Life limiting factors of power modules

Lifetime models can be used as a tool for making end-of-life (EOL) estimations of power modules, that are subjected to cyclic, thermal loading. When carefully controlling the conditions of the accelerated tests in such a manner that failures will solely be triggered due to the wear-out, the most commonly reported failures are interconnection failure. The critical failure sites observed during tests, are the interconnections of the wire bonds, the chip solder joints and the substrate-baseplate solder layer. The first two failure modes are categorized as chip related failures, which are due to the heat losses caused by the internal loading of the chip, and will cause the temperature to fluctuate according to the applied mission profile. As a result of the different mechanical properties of the multilayered module, each respective layer, presented in Fig. 1.9, inhibits different coefficients of thermal expansion (CTE). The heat loss is primarily transferred vertically downwards and the temperature gradient, which differs from layer-to-layer arises from top-to-bottom and with alternating electrical stress, the resulting mechanical stress causes the bond wires to bend, eventually leading to cracking between the aluminium lead of the bond-wire and the silicon of the power chip. The cracking may eventually spread during the continuously applied thermal stress, which in the worst case can lead to bond-wire lift off [38]. The substrate-baseplate solder failure falls into the category of packaging related failures, due to the change in the local ambient temperature, also known as thermal cycling (TC). The CTE mismatch of the copper baseplate material and the ceramic substrates, in combination with the thermal stress, generate solder strains. Repetitive loading can lead to solder cracking and thereby

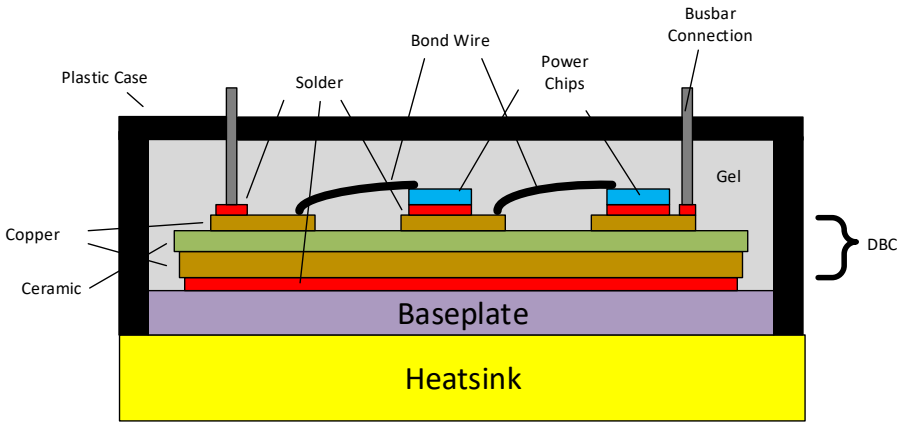

Fig. 1.9: Internal structure of IGBT module mounted on a heatsink. DCB denotes the direct copper bonding layers.

increase the thermal impedance between the chip and the baseplate [39]. In [40], it was proven that bond-wire lift-off and solder fatigue failure modes exhibit different physical presence and do therefore require to be treated differently. In case of analysing these failure modes by use of empirical models, it will require one specific model to cover each failure mode separately. This, naturally, requires to separate the failure modes in the first place, which, as stated previously, is not a common practice among existing literature. Additionally, the prediction accuracy for systems with an insufficient amount of legacy will always be limited, due to the fact that the models are solely statistical. They do therefore not assess the deformation mechanisms of power modules, that are imposed during complex loading profiles.

Lifetime models play an important role in the thermal and electrical design of power electronic systems, as they portray the power cycling (PC) and TC capabilities of power modules. Namely, the number of cycles to failure N_f, which is a measure of the modules lifetime, when certain conditions are assumed. Therefore, lifetime modelling constitutes a crucial part of the reliability of power converters. The main root-cause of the wear-out of power modules is the thermo-mechanical stress induced in the multiple layers compromising the module structure. As stated previously, the interconnections of the module dictate the lifetime of the entire assembly. In practice, it is challenging to fully separate the failure modes, as there are close interactions, that lead to positive feedback of the driving forces of failure. For example, as solder fatigue results in an increase in the thermal resistance, it leads to higher thermal stress at the bond-wires, and thereby accelerates the possible

event of lift-off. In addition, the event of bond-wire lift-off causes uneven current distribution and a reduction in the conduction path. This produces higher power losses and hence an increase in the thermal stress applied to the solder interconnections. These interactions of driving forces cause the evolution of damage to accelerate as the module degrades. This is in stark contrast to the extensive use of Miner's rule used for linear damage accumulation, which is a simplistic assumption, as it does not consider the interactions and can therefore also lead to inaccuracies, when predicting the lifetime of power converters [41, 42]

1.2.3.2 Lifetime modelling

The power modules of power electronic converters are subjected to high switching currents and also blocking voltage levels. The power losses that are generated during field operation leads to large temperature variations, that gradually degrades the modules and its primary functionality and eventually leads to wear-out. The process of assessing a quantitative measure of the modules functional life-span includes several steps, as outlined in Fig. 1.10. The initial step acquires to decompose the loading profiles, so the

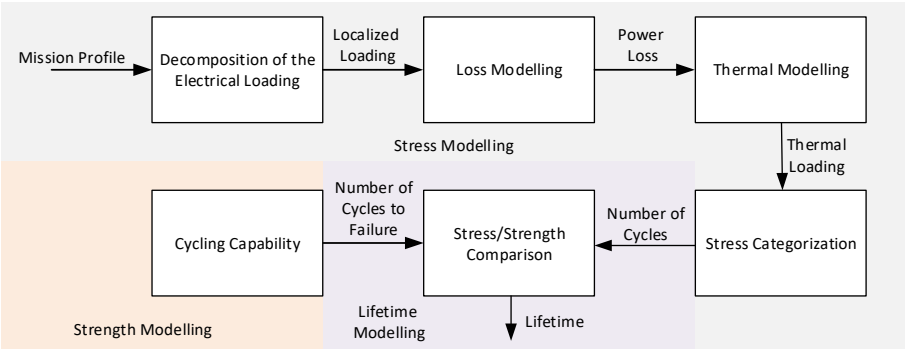

Fig. 1.10: The process of assessing the lifetime of power modules

power losses can be known for any characteristic mission profile by means of converter circuit simulations. The power losses are then translated into the corresponding thermal loading profiles that subjects the power modules through means of thermal models. The simulations and the modelling can be understood to be a constitutive part of the lifetime assessment as direct temperature measurements are not practically possible. As stated previously, the main principle of the lifetime modelling is based on extrapolating the accelerated test results to the specific field application usage condition.

The thermal modelling can be simplified by using one-dimensional thermal

networks, known as the Cauer and Foster network model respectively [43]. The networks consist of thermal circuit elements such as the thermal resistance, R_{th} and the thermal capacitance, C_{th}, which is, analogous to electrical circuits, used to model the transient behavior and can therefore be excluded for long-term steady-state simulation purposes. The Cauer model shown in Fig. 1.11(a), has a real physical interpretation as each of the nodes can be associated with one of the particular layers of the power module. In contrast, in

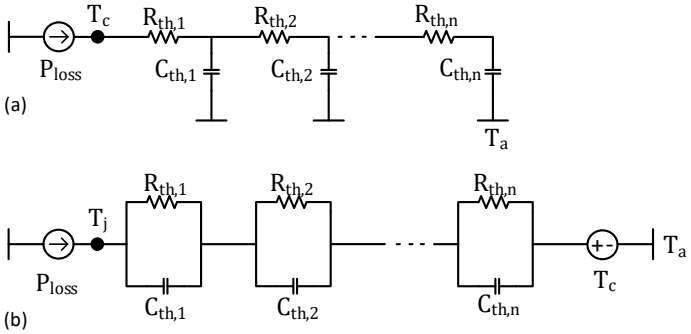

Fig. 1.11: One-dimensional thermal networks used to model the thermal behaviour of the power modules. (a) Cauer model. (b) Foster model. P_{loss} is the applied power loss that generates the heat dissipation, $R_{th,x}$ is the thermal resistance of each respective layer, $C_{th,x}$ is the thermal capacitance of each respective layer, T_c is the casing temperature and T_j is the junction temperature.

the Foster model, which is shown in Fig.1.11(b), the input node at the power source exclusively has any physical representation, as the model parameters are obtained by heating up the module and fitting the response during the cool-down phase. Both models have the same overall thermal impedance and does therefore return the same thermal response at their respective input nodes. The Foster model does prove to be advantages with respect to mathematical convenience, which enables the possibility to easily gain the thermal response across different applications and mission profiles.

Finally, the empirical models are deducted from accelerated tests and they describe the cycling capability of a given module technology, i.e., the number of cycles to failure, N_f. More specifically, the models describe this N_f-dependency on the test parameters such as the junction temperature cycling amplitude, the mean junction temperature and the heating time etc. A case of the dependency of the temperature cycling amplitude and the mean junction temperature is depicted in Fig. 1.12. The commonly used Coffin-Manson law relates the cycling capability to the junction temperature variation ΔT_j, that is applied via power cycling. The model constants are obtained by fitting the accelerated test curves that are presented in Fig. 1.12. Through

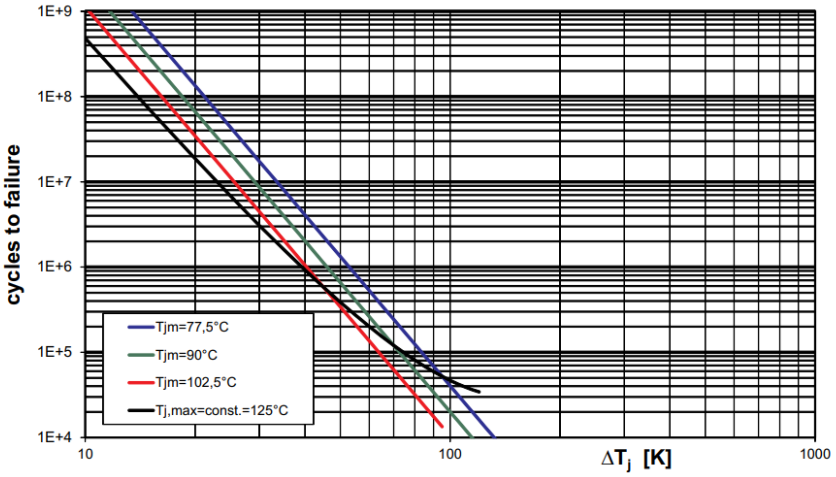

Fig. 1.12: Power device cycling capability dependency on the junction temperature cycling amplitude ΔT_j and the mean junction temperature T_{jm} [44]

experience gathered from PC experiments in the LESIT project [45], indications proved that the cycling capability was influenced by other factors than simply the temperature variation. As a result, the influence of the average junction temperature $T_{j,mean}$ was included in the model by the implementation of the Arrhenius approach. In addition, ABB [46] conducted PC tests, in order to quantify the influence of the heating time t_{on} on the thermal induced fatigue. These tests proved, that the heating time has a significant impact on the useful life and is therefore fundamental to include as a factor that effects ageing.

1.2.4 Reliability of DC-link Capacitors

Capacitors are known to distinctively being one of the components that are prone to high rates of failures when operating in the field of power electronic systems [5, 26, 47]. This is partly because global competition has forced the design margins to be highly dictated by the minimum cost, without considering the risk of failure. Additionally, the capacitors in field operation are exposed to harsh environmental conditions with fluctuating ambient temperature and humidity build-up. This combined with thermal stress caused by the power loss related heat dissipation, which is further impaired by the trending demands on high power density of power converters.

The capacitor technology considered in this thesis, is the electrolytic capacitors, which introduces some reliability related issues, such as their inher-

ent tendency to wear-out as a result of electrolyte evaporation and electrochemical reaction, that are highly dependent on the applied electro-thermal stresses [48]. The main source of the electro-thermal stresses, is the internal self-heating caused by the ripple currents affecting the resistive elements, which in its entirety is commonly referred to as the equivalent series resistance (ESR). Fig. 1.13, presents a lumped electrical circuit model of capacitors, where C, ESR and ESL denotes the capacitance, equivalent series resistance

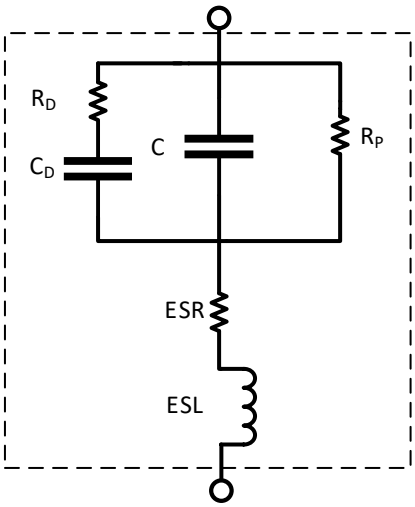

Fig. 1.13: Equivalent electrical circuit model of capacitors. R_D is the dielectric loss, C_D inherent dielectric absorption, C is the main capacitance, R_P is the insulation resistance, ESR is the equivalent series resistance and ESL is the equivalent series inductance.

and equivalent series inductance respectively. R_P is the insulation resistance, R_D is the dielectric loss caused by dielectric absorption and C_D is the inherent dielectric absorption [49]. One thing to keep in mind, is that the values of C, ESR and ESL vary according to the applied operating conditions and if these variations are not taken into account, it can lead to inaccurate analytical results. This implies that not only will the self-heating cause an increase in the hot-spot temperature, but it can also lead to an increase in the ESR, which in turn leads to an increase of losses and thereby accelerates the ageing process [47]. This signifies the importance of considering the reliability aspect, when designing the capacitors. As shown in the flowchart in Fig 1.14, which outlines the required steps in assessing the lifetime of capacitors, the initial step encapsulates the determination of the harmonic current spectrum contained in the DC-link. The harmonic content depends on the topologies used on the input and output sides, e.g., the use of an active front-end will lead to a different harmonic content compared to the case of a passive front-end as depicted in Fig. 1.15 [50]. In general, the harmonic spectrum consists of lower

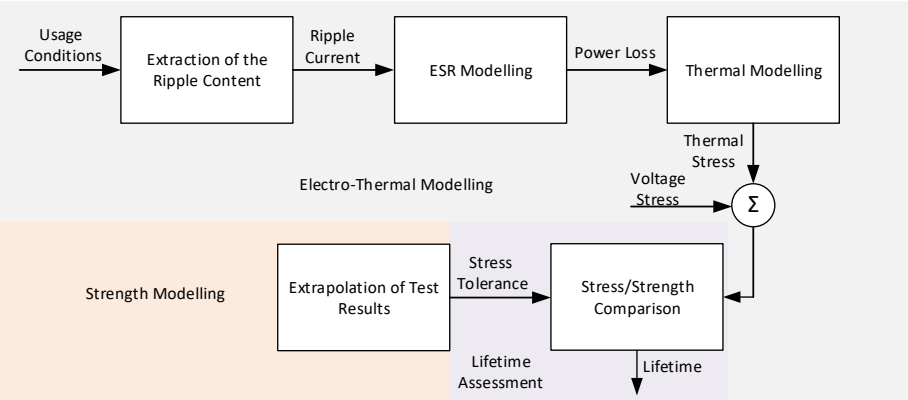

Fig. 1.14: Flowchart outlining the lifetime assessment of DC-link Capacitors.

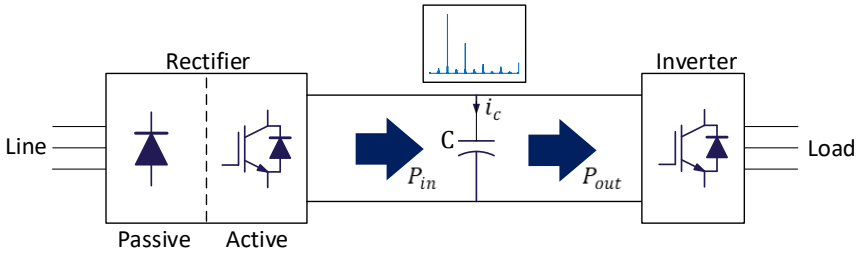

Fig. 1.15: Illustration of which factors influences the DC-link harmonic spectrum, which generally consists of a combination of lower-order components caused by power unbalance and high-order switching harmonics.

order harmonics caused by unbalanced input and output power and also high-order switching components [51]. At each given frequency, the power loss is obtained as the product of the ripple current and the ESR, implying that it is fundamental, that the frequency dependence, the ESR inhibits, are considered, in order to obtain the correct stress-levels. Additionally, as with the case of the lifetime assessment of power modules, the damage is also inherently assumed to be linear in the case of capacitors. This assumption is likely to lead to inaccurate prediction results, as this does not consider the drift of the ESR, which accelerates the accumulated damage as the capacitors degrade. In respect to the thermal modelling of the capacitors, the thermal stress can be obtained by applying the power loss to the model shown in Fig. 1.16. The failure of capacitors can both be due to intrinsic and extrinsic factors, such as manufacturing defects, wear-out of materials or overstress related failures. The electrolyte evaporation is a major known failure mechanisms of smaller sized snap-in type Al-Caps. This is due to their small heat dissipation area and their relatively large valued ESR. In contrast, the

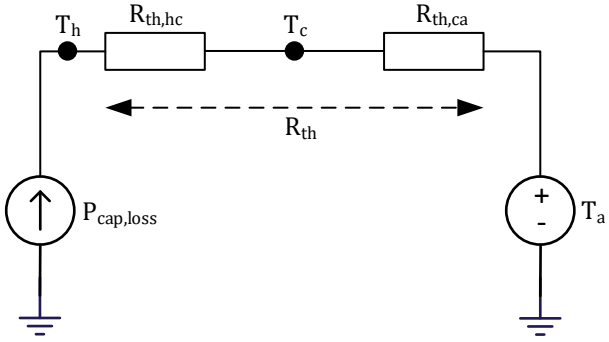

Fig. 1.16: Thermal model of capacitors.

wear-out of the large sized Al-caps is in largely sovereign cases determined by the increase of leakage current, which is related to the electro-chemical reaction of the oxide-layer [52]. The dominant failure modes of Al-caps are all linked to the same critical driving forces of failure, such as voltage stress, capacitor ripple current stress and the ambient temperature surrounding the capacitors, which are all summarized in Table 1.1. The most common lifetime models of capacitors considers the impact of voltage and temperature, while once again extrapolating test results to real-field usage conditions.

Table 1.1: Summary of the critical failure modes, failure mechanisms and driving forces related to aluminum electolytic capacitors.

Technology	Failure Modes	Failure Mechanisms	Driving Forces of Failure
Al Caps	Wear Out/Overstress	Electrolyte Vaporization Degradation of Oxide Layer Dielectric Breakdown	T_A, V_C, I_C

1.2.5 Uncertainty Linked to the Physics-of-Failure Methodology

Even though the lifetime models enable the opportunity of assessing the remaining useful life, the implementation of the uncertainties into the reliability assessment is crucial in order to assess the impact of each considered uncertainty on the remaining useful life distributions, in order to make risk-informed operational decisions. A common practice, on how to account for

issues such as differing conditions and future usage uncertainty is to model the failure fatigue model parameters as distribution functions and thereby represent the lifetime prediction as a failure probability like described in [36]. Initially, the sources of uncertainty are identified and categorized into several different types of uncertainties; measurement uncertainty, parameter uncertainty, failure criteria uncertainty and future usage uncertainty. A sensitivity analysis is executed in order to identify which input variables i.e., uncertainties can be characterized as the dominant ones that have a significant impact on the remaining useful life model output. When the correct input parameter variance is known, a random sampling Monte Carlo simulation is utilized to provide a distribution of the accumulated damage of power electronic components as shown in Fig 1.17. When all possible uncertainties

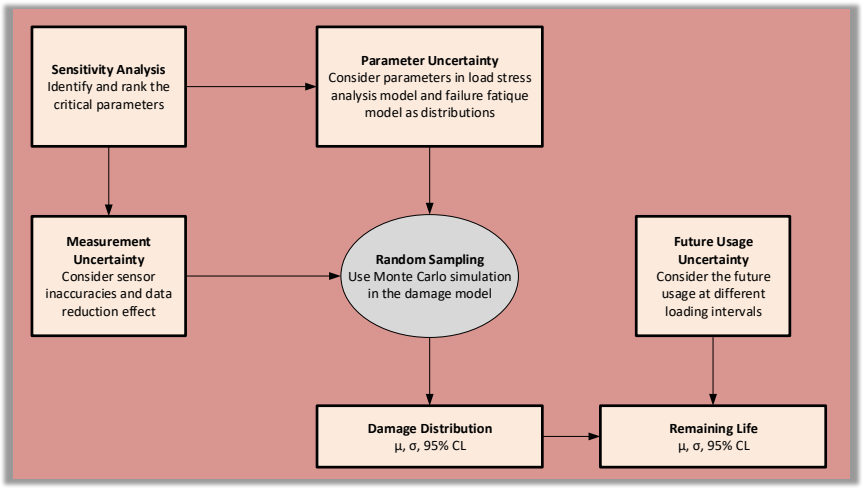

Fig. 1.17: A base implementation of the uncertainty implementation for reliability assessment of power converters, where the typical inputs are related to the future usage, model uncertainty caused by extrapolation of accelerated test results and sensor inaccuracies. μ is the mean of the damage and remaining life distributions, σ is the standard deviation of the damage and remaining life distributions and CL is the confidence level of each of those respective distributions.

are considered, the resulting lifetime distribution tends to inhibit a variance compromising several years, as exemplified in Fig. 1.18, and does therefore end up lacking sufficient precision for any unique cases under study [53]. As shown in Fig. 1.18, a common useful reliability metric, when dealing with failure distributions, is the percentile life, which denotes, at which point in time, a certain percentage of the distribution is accumulated. The suitable chosen percentage value to indicate the end-of-life, is application dependent e.g., when considering power converters with the functionality of operating

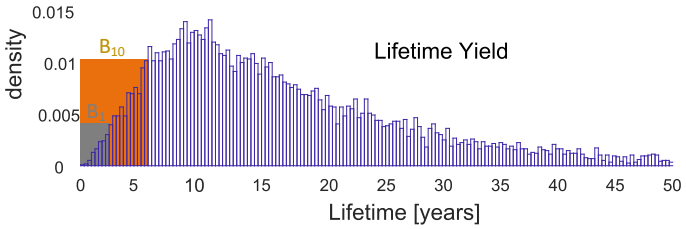

Fig. 1.18: Lifetime probability yield of a PV-inverter including the application dependent percentile lifetimes of 1 and 10 percent, which are labeled B_1 and B_{10} respectively.

as interface between the RES and the power grid, a failure percentage of one, or even less, is considered suitable. Allowing a risk of a higher percentage of generation units to enter a failed state must be regarded as improper system operation. The stringent reliability requirements rightfully forces the consideration of only a small fraction of the distribution, when in reality any unique case could fail at anytime and could therefore be located anywhere in the distribution.

1.3 Physics-of-degradation

A promising way to deal with the shortcomings of the PoF based methodology, is to exploit prognostic and health management methods and in particular exploit the physics-of-degradation that occurs as power converters wear. In physics-of-degradation based methods, the long-term changes in the electro-thermal parameteres are used as component health state indicators. The degradation of power electronic components will likely occur at the material and interconnection-level and as these changes in materials and interconnections influence the electro-thermal parameters, they can indirectly signify the gradual wear-out of the components and can therefore be harnessed to assess information about the current state of the converter [54]. The classical indicators includes the increase in the forward voltage of an IGBT or a diode and also the thermal resistance of power modules. The variation of the forward voltage is influenced by temperature, gate oxide integrity, metalization reconstruction and lastly, the quality of the electrical connections, specifically bond-wire fatigue and lift-off as discussed previously. A steady increase of the forward voltage is an indication of aluminium surface metalization affecting the overall ohmic resistance, while, on the other hand, sudden steep increases in the voltage drop can be observed in the case of the occurrence of bond-wire lift-off. This is due to the fact, that the remaining operational bond-wires now have to carry an additional load and the overall conduction path has decreased [55–59]. Finally, the evaluation of the thermal

resistance can be harnessed to indicate degradation in the physical form of solder or ceramic cracks, that degrades the power modules ability to conduct heat from the power device and onto the heat sink [55,60,61]. For capacitors, the commonly used health precursors includes the capacitance, the ESR, the dissipation factor and the insulation resistance that describes to which extent the dielectric material is able to resist the leakage current. [47,62].

Fig. 1.19 shows a generic degradation curve of a health precursor, which relates to some failure mechanism, where y is the monitored value of the given health precursor, Δy is the parameter drift with respect to its initial value y_0. The y-axis shows the absolute value of the parameter change in percentage.

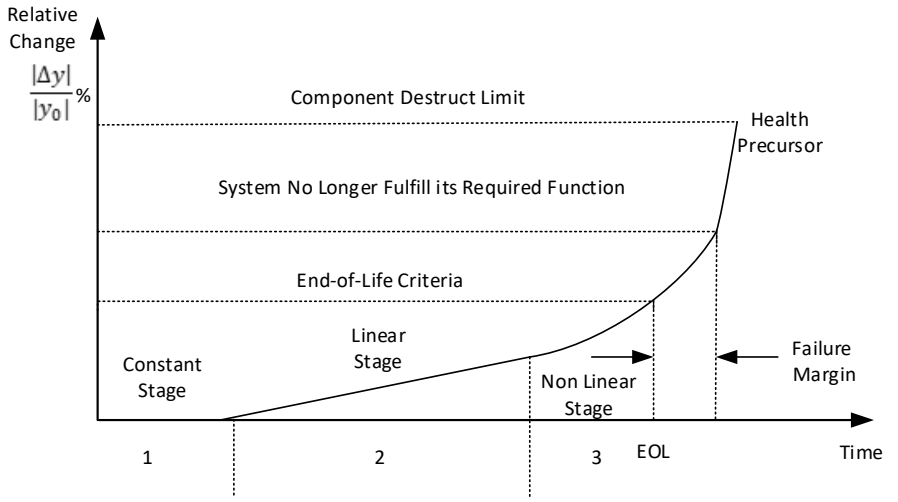

Fig. 1.19: A generic degradation curve outlining the three typical stages of power electronic component degradation process i.e., the initial constant stage, the linear stage and the non-linear stage. Δy is the parameter drift of the given health precursor y, y_0 is the initial value of a component operating in a "as good as new" state. *EOL* is the end-of-life criterion, which states the maximum value that the health precursor is allowed to have and maintenance is therefore required.

A power electronic component usually has three distinctive stages that are prominent during an entire degradation process. The process compromises the stages 1, 2 and 3, that for each has a time interval where the health precursor either keeps constant, changes linearly, increases or decreases at an accelerated pace respectively. It should be noted, that all three stages do not necessarily occur in all types of used health precursors but the process is generally a combination of one or more of the listed stages. Additionally, the curve characteristics can change according to the used health precursor and also for different stress conditions. As shown in Fig. 1.19, the end-of-life cri-

terion should be defined based on some historical knowledge of the destruct limit and the inclusion of some margin in order to prevent failure related downtime. E.g., a 20 % increase in the forward voltage of active switches and power diodes is consistent with a large share of existing publications as end-of-life criteria [63], whereas a 2-3 times increase of the ESR of electrolytic capacitors is commonly used [47]. In certain cases, the rate-of-change can also play an essential role in terms of defining the end-of-life as an alternative to an absolute value based end-of-life criterion.

Based on the existing research, it is quite evident, that exploiting the aforementioned health precursors are effective in terms of covering the occurrence of several types of failure induced degradation modes. With the high failure related costs and the increasing use of power electronics in failure critical applications, the relevance of the physics-of-degradation based methods is without doubt justified. So, if failure is no longer an acceptable option, then degradation modelling becomes essential. The major asset is to benefit from the fact that a degradation curve retains all the information gathered from historical data, while, on the other hand, a lifetime model is only based on one single point estimate, i.e., the end-of-life. Nevertheless, all existing methods are limited to cover one single type of component or an individual component [54, 62, 64, 65]. This is a severe limitation, due to the fact that the degradation is highly likely to occur on multiple components concurrently at the application-level. This is a direct consequence of different types of occurring parameter shifts, that all contribute to the overall degradation of the converter. However, it is not possible to verify these mutual effects, when assuming that one single component exclusively degrades and it would certainly be a tedious affair, if not impossible, to estimate the health of every single component operating in the converter. Additionally, due to the long and exhaustive process of locating and remedying any particular component defect, it is very unlikely that one component is replaced in case of failure and it is therefore essential to monitor the health status of the entire converter by exploiting converter-level signals as alternative solutions [41].

1.4 Power System Adequacy Assessment Concepts

This section briefly explains the concepts linked to reliability assessments of conventional power systems. Initially, the power utilities estimate the proper level of power reserve required to maintain an acceptable level of system reliability, which can be realized using either a deterministic or a probabilistic approach [1]. A common deterministic approach is to state a capacity reserve margin, which corresponds to some excess generation capacity in respect to the peak load demand. A fixed percentage of the installed capacity is used

to state the reserve margin, which should consider the uncertainty of load advancements and generation unit failures in order to avoid loss of load [66]. The main issue when applying this method, is the assumption of basing the margin on the installed capacity instead of the derated capacity. This does not provide a rightfully representation of the actual margin of the particular system operation, since it assumes, that all plants are 100 percent available at any time regardless of the specific technology. Another commonly used deterministic approach, is to base the spinning reserve so it corresponds to the capacity of the largest generation unit. This method simply compares the peak demand of the system with the available generation capacity in the case of losing the largest unit. This is also commonly known as the firm capacity. It should be noted that none of these methods accounts for the availability of the generation units [1].

In general, the adequacy evaluation of power systems requires three fundamental steps; create a generation model that reflects the operating characteristics of the generation units, create the load model and finally combine the generation model with the load model to obtain a risk model. Using the risk model, a reliability index of choice can be used to evaluate the system as shown in Fig. 1.20 [1]. In regards to the generation model, a generation unit

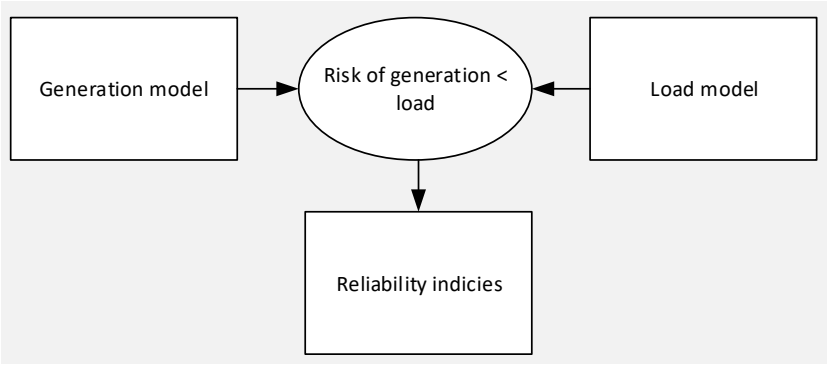

Fig. 1.20: The steps needed to assess the power system adequacy.

can either be available or out for service, which is commonly referred to as being in the up state and being in the down state respectively. When the unit is in its operational state, it may enter the down state as a result of a fault and vice versa, it may transit from the down state to the up state through the process of repair. The random process that a generation unit undergoes can be illustrated as shown in Fig. 1.21. The fraction of the long-term average

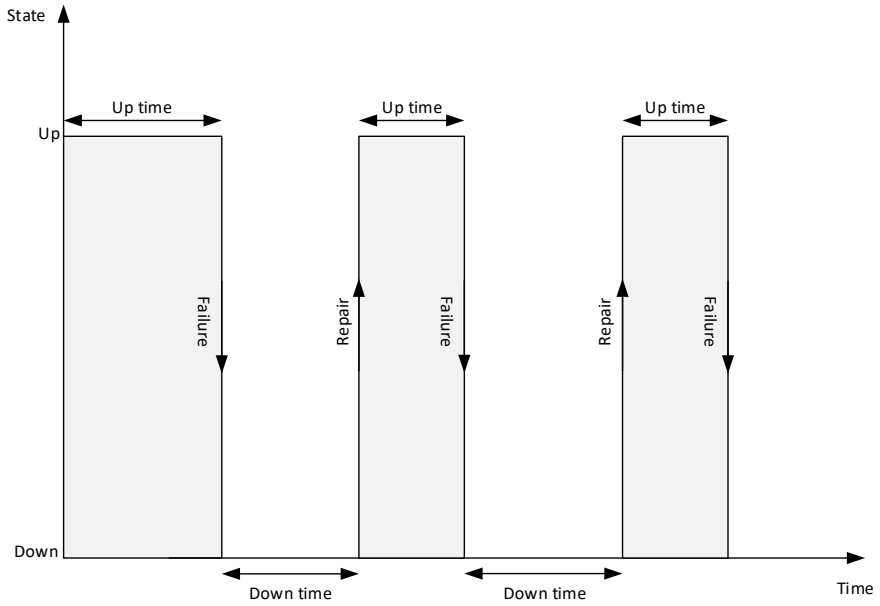

Fig. 1.21: Illustration of the random process a generation unit undergoes with time when ignoring scheduled outages.

cycle time of when the unit operates in the up state results in the probability that the unit is available, also known as the unit availability. In contrast, the long-term average of the down time fraction results in the probability, that the generation unit is unavailable, also known as the unit forced outage rate (FOR) [1].

The main mathematical tool used in power system reliability assessment is the Markov model. It is used to model each respective state, that the generation unit can reside in and at which rates it transits among those states. A two-state model is used to represent a unit that can only reside in either fully operational state or in a forced outage state as shown in Fig. 1.22. The transition rates λ and μ are the failure rate and repair rate respectively. The failure rate can be obtained as the reciprocal value of the mean-time-to-failure (MTTF), which is the average time that the unit resides in the up state. Similarly, the repair rate can be obtained as the reciprocal value of the mean-time-to-repair (MTTR), which is the average time that the unit resides in the down state. These parameters are quite essential as the probability of the unit being unavailable in a distant future is commonly known as the unavailability and is one of the key parameters used in the reliability assessment of power systems.

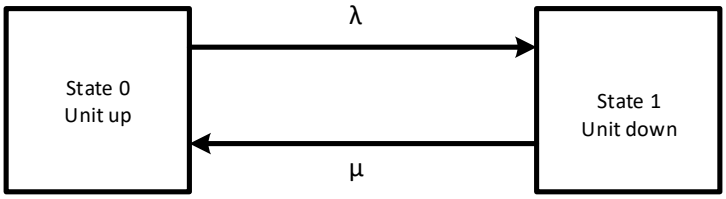

Fig. 1.22: Two-state Markov model used to model the availability (unit up) and unavailability (unit down) of a generation unit. λ is the failure rate and μ is the repair rate of the unit.

Load models are used to represent the system energy demand within some finite time intervals. The models come in a variety of level of complexity, where the simplest representation is to use a fixed load, during the entirety of the study, which often corresponds to the peak load. The most commonly used models used for adequacy studies compromise the daily peak load variation curve and the load duration curve. The daily peak load variation curve consists of individual daily peak load data and it is arranged in descending order. The load duration curve is created using the individual hourly peak load and does therefore provide a more realistic representation of an actual system load demand [1].

Finally, the system risk model is obtained by combining the generation model with the load model. The model can be used to evaluate the system risk indices, such as loss of load expectation (LOLE) and loss of energy expectation (LOEE). The LOLE is the average number of days of which the generation capacity is insufficient to satisfy the load demand and LOLE is therefore not an energy based index and does therefore not indicate the severity of the system deficiency [67]. The LOEE is the expected energy that will not be supplied due to insufficient generation capacity, which is a more appealing index, as it indicates the severity of a possible system deficiency, rather than simply a number of occasions. It is therefore more likely that this index will be used in future studies, where the replacement of energy sources will consider renewable energy sources. The index is often normalized with respect to the total energy demand, which results in the energy index of reliability (EIR), which is useful for the comparison of adequacy studies of different systems of different sizes [67].

1.5 Thesis Perspective

Based on the subjects and challenges addressed in the introduction, the motivation for conducting the research presented in the thesis will be now be stated. Due to the high cost of interruptions in the power grid, there is an essential need to enhance the reliability of power systems while coping with the challenges related to the transition from fully adjustable power generation to the intermittent generation linked to RES. The reorganization of the power grid requires rethinking of how the system reliability is assessed, as the methodologies might no longer guarantee optimal operation. The old concepts were developed for systems, compromised by large generators, that supplied the power and combined with the transmission system, formed an extensive generation system. However, as the system gets more dominated by RES, DGs and storage systems, the top-down approach of the reliability evaluation of power systems no longer applies, as the service is now considered to be bidirectional i.e., a power flow to and from the end-user. As the integration of DG is gaining momentum, large- and small-scale renewable plants will become a substantial part of the grid, forming an active network with multiple sources of generation. The operation of such systems requires decision-making, that can be executed in a distribution or decentralized manner, which can prove to be advantageous in terms of efficiency and availability. These active distribution systems are commonly known as microgrids, which includes a variety of DER and end-users. The DER units can comprise both DG and DS units, which are required to cope with the increase of the net load variability, that is a result of intermittent generation. The microgrid can both be operated as grid-connected but also as an self-governing islanded entity while still remaining able to support its load demand. This project will cover and address unsolved issues related to the subject of assessing the localized reliability of distribution systems operating as microgrids, as it is a fundamental requirement in future power systems that they must be able to locally guarantee energy adequacy [16].

The existing research related to the subject of integrating power electronics into the domain of power system reliability analysis, assumes that the failure rates of power electronic components remain constant during the entire lifecycle. However, this assumption do not coincide well with the true failure tendency of power converters and will therefore result in non-optimal risk based planning of power systems with a high penetration of RES. This project will address this issue by modelling the power electronic components with time-varying and condition-dependent failure rates in order to gain more accurate and realistic results. In general, it is of great importance that methodologies are developed, which ensures that the subject of converter reliabil-

ity analysis is firmly incorporated into the existing power system reliability methods.

It is not sufficient to accompany the power electronics analysis with that of the power system without addressing the existing concerns linked to power electronics reliability analysis. The existing power electronics research is based on the PoF methodology, which utilizes the knowledge of the life-cycle loading and the potential failure mechanisms, in order to assess the time-to-failure. The PoF methodology seems like a good approach for systems with sufficient legacy but one of the major concerns, which can lead to inaccuracies in the lifetime predictions, is the inherent tendency to base the predictions on one single failure mechanisms. Often PoF models are not available and FMMEA is therefore practically non-existing in the current power electronics reliability analysis, which instead assumes that bond-wire lift-off is the single existing failure mechanism in the case of power devices. This is an idealistic assumption as in reality multiple failure mechanisms can be coexisting and some can even be related in terms of sharing the driving forces that govern multiple failure mechanisms [34]. It is therefore essential, that methods which can cover multiple failure mechanisms are used for lifetime predictions of power converters.

Still, the single most critical concern linked to the PoF approach, is the establishment of the useful life by means of extrapolating accelerated test results to real-field usage conditions, in order to obtain the parameters of the failure fatigue model. The validity of this extrapolation is often doubtful, due to the fact that the testing data is often based on a restricted number of loading conditions, which is in stark contrast with the real-field use. Additionally, in practice, it is quite difficult to fully separate the failure modes due to the interactions, which can cause positive feedback on the driving forces of failure. For example, as solder fatigue results in an increased thermal resistance, it leads to higher thermal stress at the bond-wires and thereby accelerates a possible lift-off failure event. Similarly, the event of bond-wire lift-off causes uneven current distribution and a reduced conduction path, which results in increased power losses and hence an increase in the thermal stress applied to the solder interconnections. These interactions cause the evolution of damage to accelerate as the module degrades. This is in stark contrast to the extensive use of Miner's rule used for linear damage accumulation, which is a simplistic assumption, as it does not consider the interactions. The use of Miner's rule can therefore lead to inaccurate lifetime predictions and there is therefore a fundamental need for alternative methods, which can consider the acceleration of damage as the converter degrades. Analogous to the case of lifetime assessment of power devices, the damage is also inherently assumed to be linear in the case of capacitors, which is prone to lead to inaccurate pre-

dictions. This is due to the fact that it does not consider the drift of the ESR, that will cause an acceleration of the accumulated damage as the capacitor wear.

Also, while the PoF based lifetime models do enable the opportunity of assessing the remaining useful life, the implementation of the uncertainties into the reliability assessment, is fundamental to assess the remaining useful life distributions used to make risk-informed operational decisions. A common practice for accounting the issues of differing conditions and future usage uncertainty, is to model the failure fatigue model parameters as distribution functions and thereby represent the lifetime prediction as a failure probability. When all possible uncertainties are considered, the resulting lifetime distribution tends to inhibit a variance compromising several years and does therefore end up lacking sufficient precision for any unique cases under study.

A promising way to deal with the concerns of the PoF based methodology, listed in this section, is to exploit physics-of-degradation methods. In particular, to exploit the long-term changes of the electro-thermal parameters by using them as as health-state indicators. The classical health state indicators includes the forward voltage of power devices and the ESR of capacitors, which effectively covers several types of failure inducing degradation modes. The major asset is to benefit from the fact that a degradation curve retains all the information gathered from historical data, while on the other hand, a lifetime model is based solely on one single-point estimate. Nevertheless, all the existing methods are limited to one single type of component or an individual component, which is a severe limitation, as the degradation is highly likely to occur on multiple components concurrently at the application-level.

Based on the content discussed in this section, the main tasks and issues, that will be addressed in this study and which can be used to improve the reliability analysis and operation of modern power systems, are outlined in Fig. 1.23.

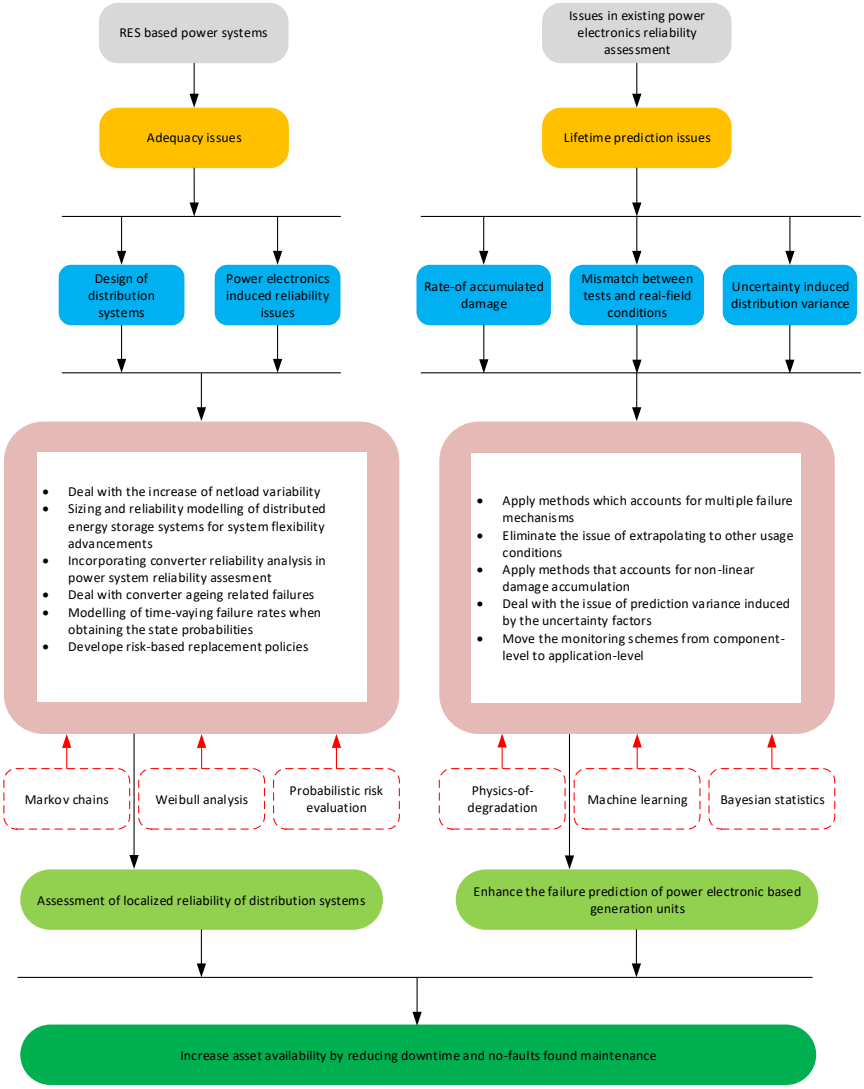

Fig. 1.23: The main tasks and challenges of future power systems which are dealt with in the Thesis.

1.5.1 Thesis Hypothesis and Objectives

The main objective of this Ph.D. study is to broaden the knowledge on how to incorporate the art of power electronics reliability into the domain of power system reliability assessment and also how to deal with the issues linked to

the lifetime estimations based on empirical models by incorporating physics-of-degradation based methods. The hypothesis can be stated in terms of a problem formulation as:

"Is it possible to merge the domain of power electronics reliability with that of power system reliability in order to assess the reliability of modern distribution systems and simultaneously exploit physics-of-degradation based methods for risk evaluations?"

In order to solve the research problem, modelling of power converters reliability is required, such as mission profile translation with the purpose of gaining the driving-forces-of-failure, that is based on real-field data. Models with some degree of physical interpretation in terms of describing how the stressors induce failures are required as well as statistical models that support the reliability of power converters. These models aids to the failure prediction of power converters operating in RES.

The overall study can be divided into the following sub-problem formulations

- How should the increase in netload variability, which is caused by the intermittent nature of renewable-based energy sources, be dealt with in terms of system reliability?
- How should the distributed energy storage systems be modelled in terms of sizing and reliability in order to aid to the system flexibility and aid to the localized reliability of distributed energy systems?
- How can converter reliability analysis be incorporated into the power system reliability assessment, in order to ensure the proper operation of systems with a high penetration of renewable energy sources?
- How can the time-varying failure rates of power converters be modelled when obtaining the state probabilities of the generation units?
- How can risk based replacement policies be developed in distributed generation systems?
- Which methods can be applied that accounts for multiple failure mechanisms, eliminates the issues of the extrapolation to other usage conditions, accounts for non-linear damage accumulation and deals with the uncertainty aspects of the physics-of-failure based methodology?

- Is it possible to define a health precursor which is able to move the existing monitoring methods from component-level to the application-level and thereby indicate the health state of entire converters?

To analyse the mentioned problem formulations, the following subsequent objectives are formulated:

Understand and deal with the reliability issues caused by the intermittent nature of renewable based energy sources and the impact the incorporation of power electronic converters has on the system-level reliability
As discussed previously, the proliferation of renewable energy sources introduces some issues in regards to the security of supply. The existing concepts used for power system reliability studies are developed for cases with fully-dispatchable generators. In order to analyze and accommodate this, the thesis will seek to do adequacy studies of stand-alone low voltage distribution networks. This study will also strive to cover the inclusion of the design of the units, including the modelling of supplementary storage units, that can compensate for the intermittent nature of the generation units and thereby add to the system flexibility and ensure adequate operation. Another challenge introduced by the proliferation of renewable energy sources, is the increased risk of failure related downtime, due to the failure prone nature of power electronic converters. The failure tendencies of power converters needs to be clarified, when they are operating in distributed energy systems.

Model and investigate the impact of using time-varying failure rates, that reflect the true wear-out tendencies, in power converter based generation units
Until now, the integration of renewable energy sources in power system reliability is based on the assumption that the failure rates of the generation units remain constant during the entire life-cycle. The employment of constant failure rates does not coincide well with the true nature of power electronic based generation units. There is a need to model the time-varying failure rates using concepts, which extend the Markov process, so it no longer only applies for stationary processes. This is a fundamental requirement for these tendencies to be translated into long-term state probabilities in order to assess the system risk and thereby locally guarantee energy adequacy. The inclusion of power electronics reliability will aid to gain accurate and realistic results as it constitutes a fundamental part of renewable generators.

Understand and deal with the challenges of the existing physics-of-failure based method, which can lead to inaccurate lifetime predictions
As previously stated, numerous concerns are linked to the existing physics-of-failure based methods including the doubtfulness approach of extrapolating the accelerated test results to other usage conditions and also the assumption of only one existing failure mechanism. There is a need for methods, which no longer rely on static lifetime predictions and empirical models. This thesis will investigate if a reliability analysis based on physics-of-degradation, can be exploited. The physics-of-degradation approach relies on the information of condition monitoring, which enables the possibility of evaluating the current health state at any given time instead of basing the analysis on a static estimate.

Develop a monitoring concept that utilizes a health precursor, which can indicate the health state of entire converters
The existing monitoring methods are typically limited to one single type of component or an individual component, which is a severe limitation as the degradation is likely to occur on multiple components concurrently. It is therefore necessary to develop methods, which can indicate the health state of complete converters and account for the degradation of multiple power electronic components. Additionally, with the use of a unified health precursor, it is required to develop methods that can state the remaining useful life of power converters.

1.5.2 Study Limitations

The following assumptions, simplifications and limitations are part of the study:

- Due to the lack of available, real degradation data, a part of the data used in this study is chosen based on monitoring data from existing literature. This is not regarded as a severe issue as the framework and methodology can be readily adopted to available data and is basically generalized concepts.
- There is no direct one-to-one comparison of the system risk evaluation using the PoF based and the physics of degradation based method, as the physics-of-degradation based method is only applied to one single unit.
- Units are assumed to be in "as good as new" state at the time of termination of the repair process. Meaning a full converter replacement is assumed.

- Repair time is the same for all types of generators and is assumed to be a duration of 2 days.
- Parameter drift is only considered in the active power switches, the diodes and the capacitors. Power losses in filters and gate drivers are considered but assumed to be constant during the entirety of the device life-cycle.
- The degradation of the components is assumed to be uniform in each type of power electronic component meaning that they all reach the same level of degradation when they reach the defined end-of-life.

1.6 Thesis Outline

The thesis consists of two parts; a project summary and the selected publications, that are made throughout the Ph.D. study. In Fig.1.24, it is outlined, which publications constitute the contents of each respective chapter and the overall structure of the thesis.

Chapter 2 provides a comprehensive analysis on how the existing power electronics reliability concepts can be incorporated into the domain of power system reliability assessment methods. This includes the thermo-electro modelling of the power electronic components, as they are subjected to real-field mission profiles, and also the probabilistic analysis that support the reliability analysis of power converters. The failure tendencies of the generation units are then implemented into the power system domain analysis, by extending the conventional Markov process modelling concept. This enables the use of non-constant failure rates, which are characteristic for power converters. From Chapter 3 and onwards, alternative reliability assessment methods are presented, which exploits the concepts of physics of degradation and condition monitoring. Chapter 3 presents a method, in where the operating efficiency of the converter can be used as a health-state precursor and also proposes a concept, which utilizes the rate-of-change of the health-precursor, that can be harnessed to state the end-of-life. Chapter 4 proposes a framework on how to exploit the sensory information of the efficiency based health precursor to model how the degradation process evolves as time passes with the overall motive to continuously update the residual life distributions. The distributions can then be exploited to continuously reevaluate the risk-based decisions of power electronic systems. Chapter 5 presents a method, that utilizes data-driven concepts to detect when the end-of-life of power converters is reached based on the efficiency-based health-precursor. The method deals with the issues of the health-precursor being affected by its respective operating conditions. Finally, the project is concluded and further research perspectives are discussed.

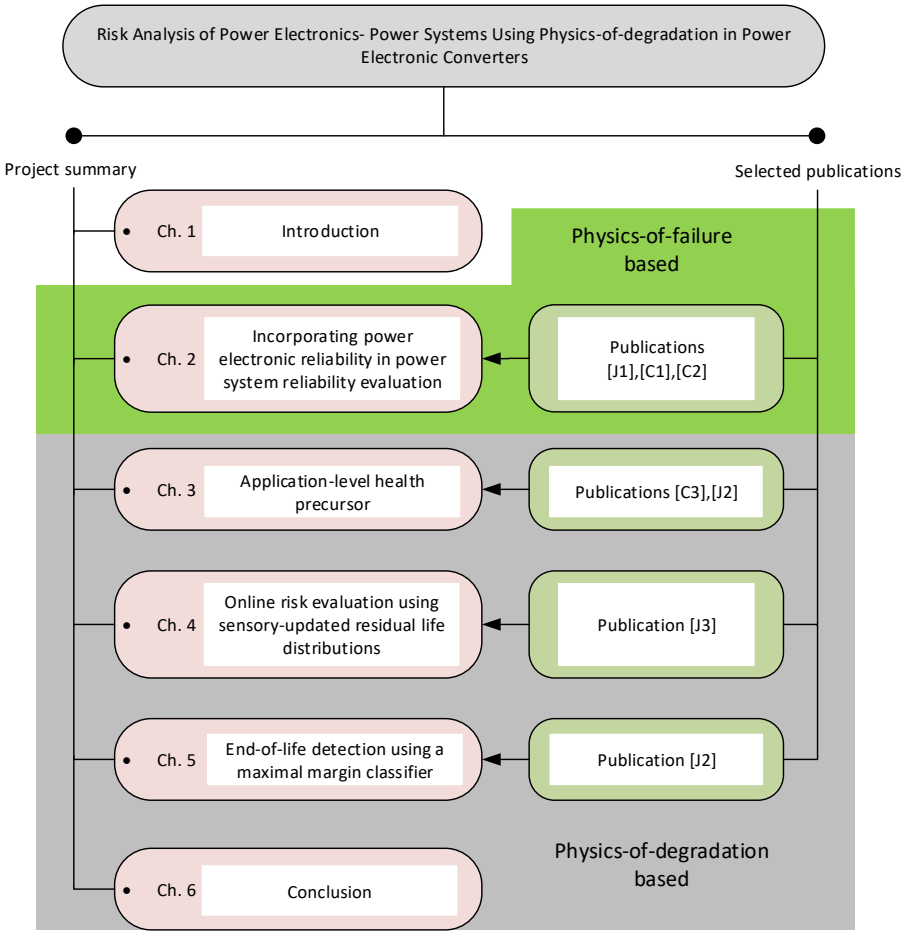

Fig. 1.24: The structure of the thesis and an overview of which publications constitute the contents of each respective chapter. The chapters with green background is physics-of-failure-based whereas the chapters with grey background is physics-of-degradation-based.

1.7 List of Publications

The selected research outcome of this Ph.D. project has been disseminated and published in the form of publications in conference proceedings and peer-reviewed journals. The selected publication list is presented below, where each publication is named Cx for conference proceedings and Jx for journal publications, where x is an abbreviation of "paper x". The paper abbreviation is also used throughout the thesis for citing and referring to the respective papers.

Publications in Peer-Reviewed Conferences

C1 M. V. Kjaer, Y. Yang, H. Wang and F. Blaabjerg, "Long-Term Climate Impact On IGBT Lifetime," 2020 22nd European Conference on Power Electronics and Applications (EPE'20 ECCE Europe), 2020, pp. P.1-P.10.

C2 M. V. Kjaer, H. Wang, Y. Yang and F. Blaabjerg, "Reliability Analysis of Power Electronic-based Power Systems," 2019 International Conference on Smart Energy Systems and Technologies (SEST), 2019, pp. 1-6.

C3 M. V. Kjaer, H. Wang and F. Blaabjerg, "Exploiting the Converter Efficiency as Application-level Health Estimation Precursor," 2021 IEEE 22nd Workshop on Control and Modelling of Power Electronics (COMPEL), 2021, pp. 1-8.

Publications in Peer-Reviewed Journals

J1 M. V. Kjaer, H. Wang and F. Blaabjerg, "Adequacy Evaluation of an Islanded Microgrid, Electronics 2021, vol. 10, pp. 2344-2370.

J2 M. V. Kjaer, H. Wang and F. Blaabjerg, "End-of-Life Detection of Power Electronic Converters by Exploiting an Application-Level Health Precursor," in IEEE Open Journal of Power Electronics, vol. 3, pp. 549-559, 2022.

J3 M. V. Kjaer, "Framework for Online Risk Evaluation of Power Converters Using Sensory-updated Residual Life Distributions," under preparation for an IEEE Journal.

Chapter 2

Incorporating power electronics reliability in power system reliability evaluation

This chapter covers the integration of the physics-based converter lifetime predictions into the reliability concepts of power systems. This specifically includes the non-exponential failure distributions that are characteristic of power converters and which are obtained from the device-level analysis. The concept of repair is introduced with the purpose of computing the state probabilities of the power electronic-based generation units which are required for the adequacy analysis of power systems. The chapter will conclude with some defined replacement policies based on not violating a specified risk of not supplying the system loads.

As the integration of renewable energy sources (RES) is gaining momentum, power electronics are becoming a substantial part of the power system. As a result, power electronics will significant influence the efficiency and cost of renewable-based generation systems. In addition, power converters are in the midst of frequent sources of failure, which, eventually, can result in increased downtime and maintenance-related cost [**J1**], [68].
The reliability of power electronic components depends on multiple factors, including the mechanical strength of the device, the applied electrical loading, the environmental condition that subjects the unit, and the applied switching and control schemes. All these factors are an inherent part of the

Physics-of-Failure (PoF) analysis, which is based on the knowledge of how the individual elements of power converters react to the subjected stressor and, in particular, how these stressors affect the wear-out and lifetime of power converters. However, the reliability analysis is restricted to the lifetime estimations of the power converter. This is a severe limitation with respect to performing optimal decision-making in terms of design, planning, operation, and maintenance scheduling of power converters operating in power systems. Furthermore, proper planning is basically not possible using solely the power electronic reliability analysis since the outcome of power electronic reliability analysis is a failure probability, which assumes instant repair. For the computation of the system risk, the state probability of the power electronic-based generation units is needed, which requires the use of power system reliability assessment concepts, and there is therefore a fundamental need to bridge the concepts of converter reliability with the assessment methods used to evaluate the reliability of power systems. In particular, the adequacy evaluation, i.e. the evaluation of sufficient generation capacity to satisfy the system demand, when taking into account the corrective and predictive maintenance of renewable-based generators **[J1]**. The system adequacy is evaluated using risk indices such as Loss of Load Expectation (LOLE) and Loss of Energy Expectation (LOEE) [69].

2.1 Methodology

The evaluation of power system adequacy can be divided into two separate tasks, which are to gain insight into the probability of generation outage and what consequence such outage will have on the ability of the system to perform in an adequate manner, as illustrated in Fig. 2.1. The two concepts will eventually be merged when the system risk is to be evaluated. However initially, the system is designed in a manner in which adequate operation is guaranteed in the case of not considering generator outage. The consequence of an outage of any respective generation is then analyzed by initially accounting for the field-dependent stress obtained via a mission profile translation, which also accounts for the energy conversion efficiency and the utilization limits of each respective renewable energy technology. The stress of electronic apparatus is primarily related to the temperature of both steady-state and cycling types, which changes accordingly to the applied loading, and it is therefore crucial to gain knowledge of the exact loading profile applied in the field **[J1]**,**[C2]**.

In order to obtain the probability of generation outage, it is required to perform mission profile-based device-level analysis of the power converters, which will provide the lifetime distribution of each respective converter-

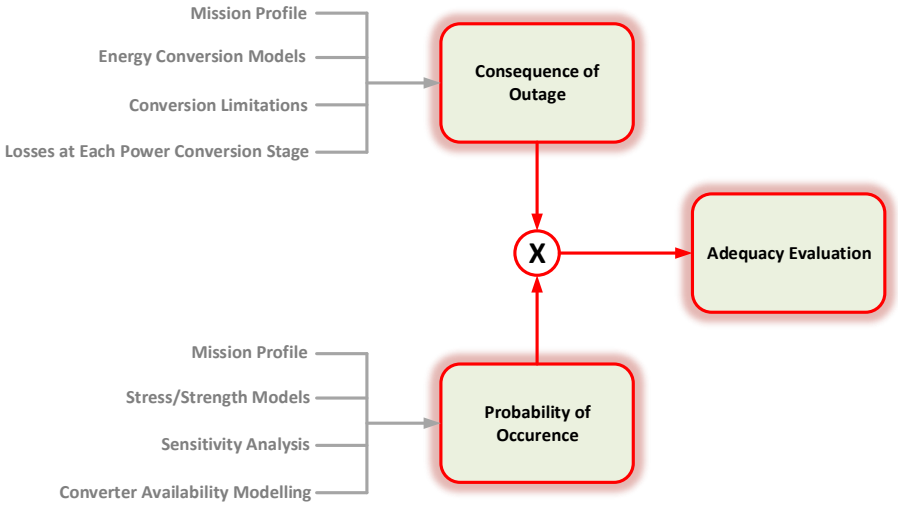

Fig. 2.1: Flowchart outlining the concepts included in order to evaluate power system adequacy [**J1**].

based generation unit. The reliability analysis of power converters is not the main focus of this chapter as it has already been thoroughly described in the existing literature. It will simply be outlined by means of a conceptual flowchart accompanied by brief explanations and the references needed for further study. The concept of repair is introduced, and the analysis is moved to the power system analysis domain, where some additional techniques needed to cope with the non-exponential failure distributions are introduced, which is indispensable when computing the state probabilities of power electronic-based generation units. Finally, a replacement policy is adopted, which guarantees that the system will not enter a state in which inadequate operation is at risk [**J1**]

2.2 Framework

In this section, the system, which will constitute the basis of the adequacy analysis, will be described along with some modifications of the system, in regards to how it was originally proposed, in order to make it suitable for standalone mode operation reliability assessment. The network as it was originally proposed can be found in [**C2**]. In addition, the section will state the annual load demand and the renewable-based generation capacity, which is based on measured real-field environmental data.

2.2.1 LV distribution network

A factual low-voltage benchmark system is formed and used for reliability studies based on fully renewable systems. The network model originates from the proposed CIGRE benchmark systems for network integration of renewable and distributed energy sources, which can be found in [70]. Unfortunately, the Cigre low-voltage (LV) residential network was not designed with the purpose of long-term reliability studies, but for frequency regulation in case of interruptions that will result in short-term islanding mode. In the originally proposed system, the main-source-of-supply during normal conditions was by means of a main feeder to the upstream network. So, because the primary energy supply was provided via the upstream network during normal operational mode, it led to a poor supply-and-demand ratio. Due to this supply and demand mismatch of the original network, it is not suitable for reliability studies during long-term islanding mode of operation since the main supply via the upstream network is no longer considered. As the primary purpose of this study is to conduct long-term adequacy studies, the original system is modified to suit this type of analysis, and its final form is shown in Fig. 2.2. The system consists of two dual-stage photovoltaic (PV) inverters, one rated at 4 kW and one rated at 3 kW, and a wind-based generation unit using a back-to-back two-level converter topology, which is rated at 5.5 kW. Additionally, a storage unit of 14 kWh is integrated in order to gain some degree of system flexibility by compensating for the system unbalance, which is a result of the intermittent energy production of the RES. By observing the system used for adequacy studies, presented in Fig. 2.2, it is evident that it differs from the one proposed in [70]. The overall purpose of the following sections is to outline which modifications were made in order to obtain a system suitable for long-term reliability evaluation when operating in islanded mode.

2.2.2 System design overview

In order to evaluate the consequences that are related to the occurrence of generation outage, the amount of grid-injected power supplied by each respective unit needs to be obtained by translating the real-field mission profiles. The available capacity profiles are attained by translating the environmental conditions into electrical energy, using the energy conversion models of the respective RES as well as their limitations in terms of the units energy yielding capabilities [71] ,**[J1]**. Additionally, it is also necessary to evaluate the conversion efficiency of the power electronic converters at each respective conversion stage. The concept is exemplified using the renewable technologies of the system shown in Fig. 2.3. In the case of wind-based generation, the wind speed is correlated to the mechanical power that is enforced to the

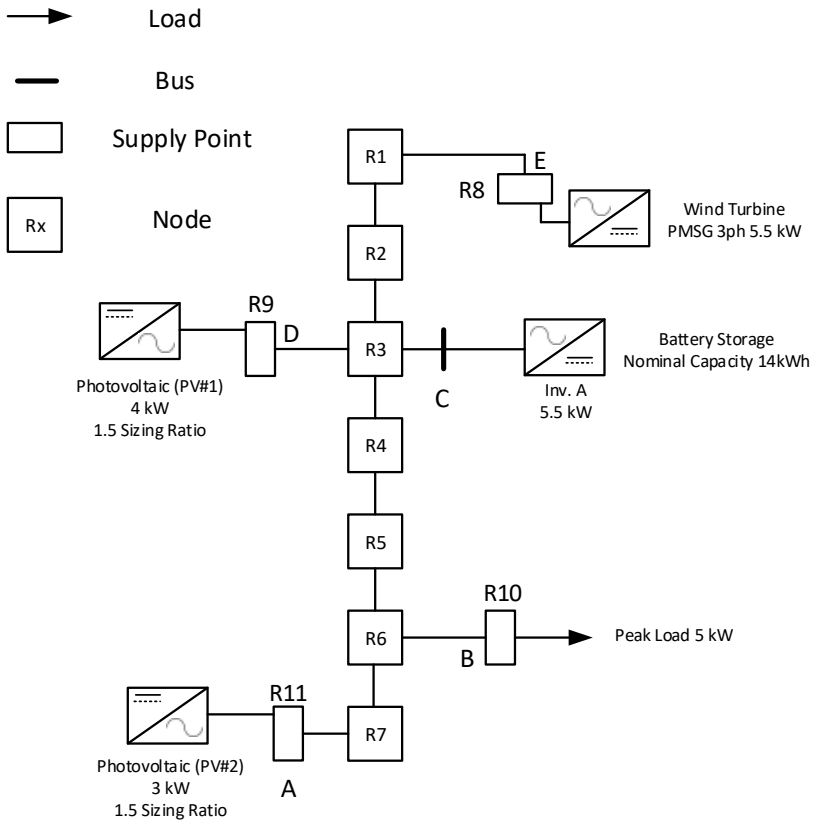

Fig. 2.2: Cigre LV distribution network used for adequacy studies [**J1**].

generator shaft by the following expression [72].

$$P_{mech} = \frac{1}{2}\rho A v^3 C_p \tag{2.1}$$

where v is the wind speed, ρ is the air density, A is the area swept by the turbine blades and C_p is the wind energy utilization coefficient, which expresses to which extent the turbine is able to exploit the wind energy. The wind energy utilization factor and similar relevant data on the wind turbine used in the study can be found in [73]. In extension to the utilization factor, the turbine is assigned an upper power saturation limit according to measurements provided by the manufacturer, which can also be found in the referred datasheet. Finally, a lower limit wind speed, e.g. the power needed to overcome the mechanical friction of the permanent magnet synchronous generator (PMSG), also commonly referred to as the slip-in wind speed, is assigned. The used machine parameters can be found in [74]. The machine

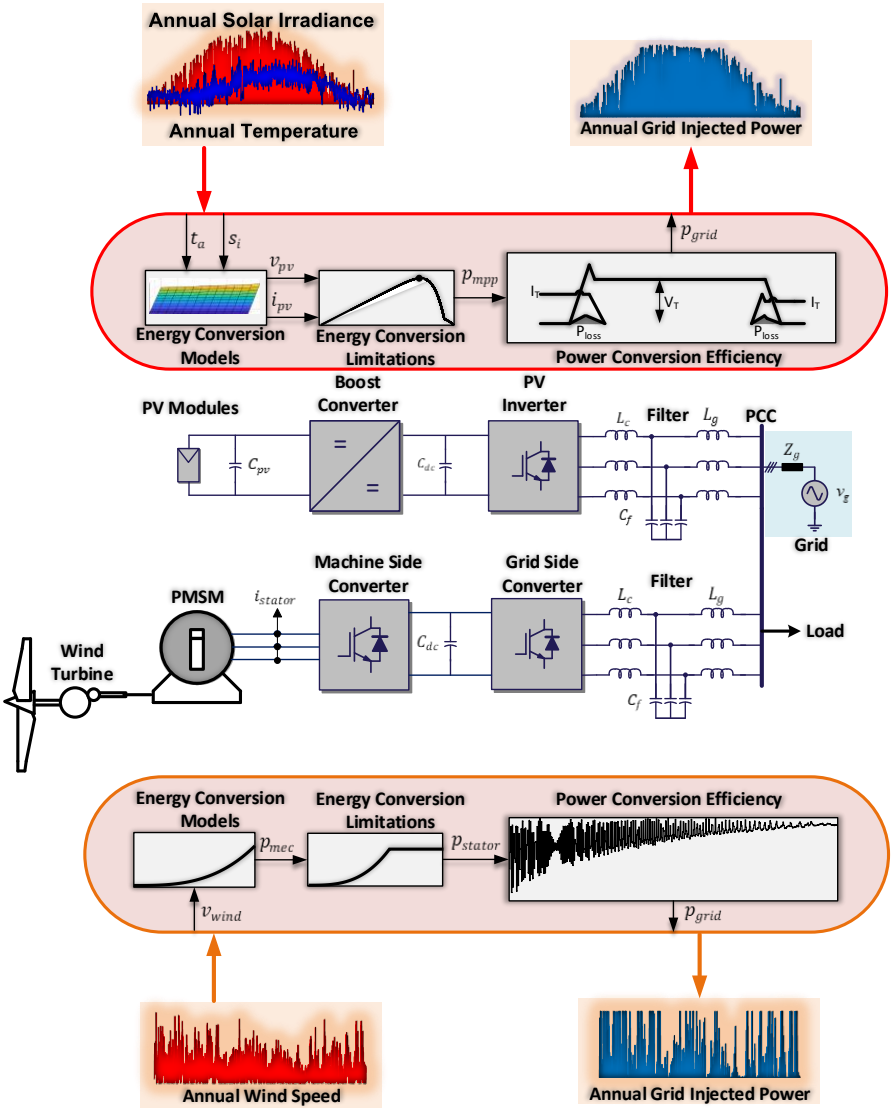

Fig. 2.3: Conceptual figure outlining the methodology used for obtaining the available generation capacity of the network presented in Fig. 2.2. The blue PV generator input curve denotes the annual ambient temperature and red input curve denotes the annual solar irradiance **[J1]**.

parameters are adapted in a full-scale Piecewise Linear Electrical Circuit Simulation (PLECS) simulation model that is controlled for each defined operating condition of the applied torque. The applied torque, which is sufficient to generate a power flow towards the grid, is noted as the resulting slip-in wind speed V_{min} needed for power generation.

In the case of solar-based generation units, the environmental profiles consist of solar irradiance and ambient temperature, for which some suitable operating conditions are defined in terms of different levels of the environmental parameters. Each respective entry in the defined operational interval maps a corresponding output power of the PV array, which is correlated by [75]

$$i = I_{ph}(G,T) - I_o(T)\left(e^{\frac{v+R_s i}{nN_s V_{th}(T)}} - 1\right) - \frac{v + R_s i}{R_p} \tag{2.2}$$

where I_{ph} is the photo-generated current, I_o is the dark saturation current of the PV module, R_s is the series resistance, n is the ideality factor, N_s is the number of series connected PV cells, V_{th} is the thermal voltage of a single cell and R_p is the shunt resistance. Regardless of renewable energy technology, the output power lookup tables are used to map the entire time series of annual mission profiles into annual output power profiles, as exemplified in the case of solar-based units in Fig. 2.4 **[C1]**. Finally, the maximum feed-in

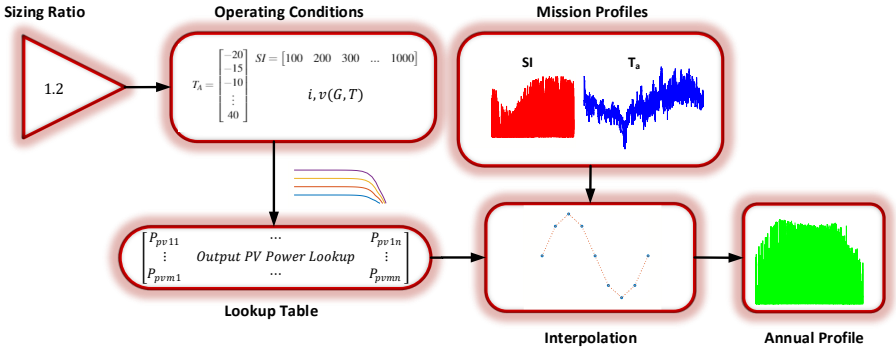

Fig. 2.4: The methodology used for obtaining the annual loading profiles. A sizing ratio between the rated output power of the PV array and the generation unit of 1.2 is used. The operation conditions are defined, and the corresponding output power is mapped. The annual output power of the PV array is then obtained using the mapped output power entries for interpolation of the annual mission profiles. T_a is the ambient temperature, SI is the solar irradiance, P_{pv} is the output power of the solar array **[C1]**.

power depends on the power generated by the respective energy source and the control algorithms abilities to extract the maximum amount of generated power. In the case of the solar-based units, this includes a perturb and observe (PO) algorithm used for maximum power point tracking (MPPT), as

shown in Fig. 2.5 **[C1]**. With the available annual power generated by the

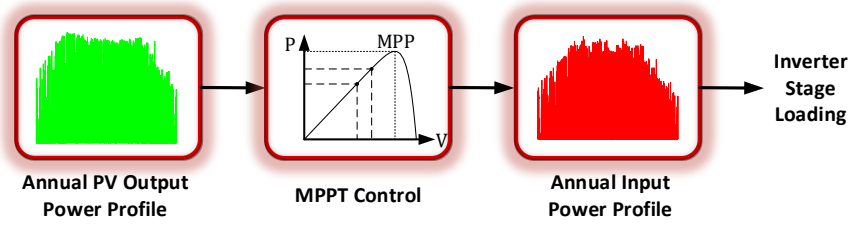

Fig. 2.5: The methodology used for obtaining the converter loading i.e., the net loading supplied to the DC link, which depends on the boost stage ability to extract the maximum available PV output power. V is the output voltage of the PV array, P is the output power and MPP is the point of maximum power output **[C1]**.

RES at hand, it is now relevant to determine the demand and storage capacity, which will guarantee that the system is well qualified for conducting an adequacy analysis.

2.2.3 Unit design

With the overall purpose of obtaining a system design qualified for standalone adequacy analysis, it is fundamental that the system is fully adequate when the generation units are in their normal operating conditions. This requirement can be met by ensuring a proper generation capacity and load demand ratio. In this study, it is chosen not to change the original proposed ratings of the generation units of the Cigre benchmark system and instead rescale the peak load to ensure a proper capacity/load ratio. A daily loading profile was also suggested by the Cigre task force, which can accompany studies of the system [70]. Data points of the proposed loading profile are extracted and fitted in order to generate a function which can replicate the nature of the data by means of a sum-of-sine function **[J1]**.

$$\sum_{i=1}^{n} a_i sin(b_i t + c_i) \tag{2.3}$$

The data along with the fitted function is shown in Fig. 2.6. The determination of the rescaled peak load value is carried out using a simple deterministic approach that is based on having a capacity/load ratio that results in a spinning reserve that equals the capacity of the largest generation unit, as conceptualized in [76].
In this particular case, the total rated generation capacity amounts to 12.5 kW, and the largest unit being the wind-based generator with a power rating of 5.5 kW. Assuming that the generation capacity and load demand are

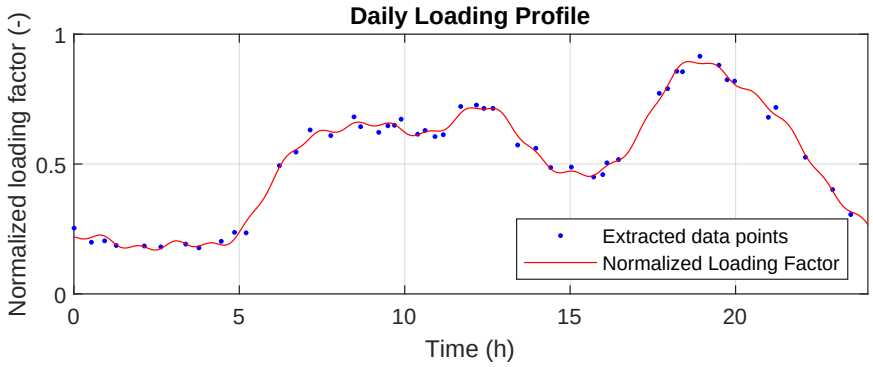

Fig. 2.6: Daily loading profile of the LV distribution network where 1 equals the rated peak load [**J2**].

equal and then adding the largest unit as the spinning reserve results in a capacity/load ratio of 1.44. The Largest Unit (LU) method was originally developed for fully-dispatchable generation units. It is therefore required to make some additional considerations that account for the intermittent generation that is a signature of this system. Each unit's respective capacity factor and load factor are considered with respect to the determination of the capacity/load ratio. The factors are simply the ratio of the actual annual energy production or demand and the units respective rated values. When considering the capacity factors while having the aim of retaining the 1.44 ratio of the total generation capacity and the load demand, the system rating values presented in Table 2.1 are obtained [**J1**].

Table 2.1: System ratings and their corresponding capacity/load factors [**J1**].

Wind Generation Unit Rated Power	5.5 kW
Wind Generation Unit Capacity Factor	0.497
PV Generation Unit #1 Rated Power	4 kW
PV Generation Unit #2 Rated Power	3 kW
PV Generation Units Capacity Factor	0.153
Rated Peak Load	5.1 kW
Load Factor	0.521

As it can be observed, Table 2.1 also presents the obtained capacity factors from the used mission profiles for the wind- and PV-based generators, which according to [77–79] coincide well with the historical data of real-field units. It should be noted that the units can be scaled in any desired manner as long as the ratio between the generation capacity and the load demand is main-

tained. Also, despite having an excess generation capacity in terms of ratings, the intermittent generation of the non-dispatchable units creates the need to advance the system flexibility through the implementation of a storage unit.

2.2.4 Storage unit

With the purpose of ensuring a proper power balance in the system by managing the surplus energy, which is not directly consumed by the load, a storage unit is implemented. Battery Energy Storage Systems (BESS) are deemed as being a promising solution due to their high degree of scalability and the continuous decrease in the cost of battery units [80, 81]. In order to ensure that the storage technology is attractive and the expansion of BESS integration in future microgrids, it is crucial to minimize the cost of stored energy. Minimizing the cost of stored energy eventually includes the task of determining the suitable nominal storage capacity which is sufficient to remove any possible energy deficiency in the system's power balance while ensuring that the unit is not oversized, as this would lead to unnecessary high costs. A means to gain knowledge of the optimal sizing of the storage unit is based on analysing the annual power balance to gain insights into the most probable charging and discharging cycle lengths. Based on the cycle lengths, the surplus and deficit distributions can be computed, and the needed storage unit can thereby be determined. Initially, the power balance of the power grid can be computed as [**J1**]

$$P_{balance}(t) = P_{wind}(t) + P_{pv1}(t) + P_{pv2}(t) - P_{load}(t) \tag{2.4}$$

where $P_{balance}(t)$ is the power balance of the system, $P_{wind}(t)$ is the power injected by the wind-based generator, $P_{pv1}(t)$ and $P_{pv2}(t)$ are the power injected by the two solar-based generation units and $P_{load}(t)$ is the load duration curve shown in Fig. 2.6. The resulting power balance is shown in Fig. 2.7. As it can be observed, there is a pronounced energy deficiency throughout the entire year, where the generation capacity of the RES cannot meet the residential demand of the microgrid.

The the power balance cycle lengths extraction is carried out using the Rainflow algorithm, which is thoroughly explained in [42]. From the cycle extraction, it is acknowledged that a share of 93% of all cycle lengths is included within a time span of three hours, compromising both the positive and negative valued cycles, i.e. the charging and discharging cycles. As a result, the power balance is reshaped into time intervals of three hours, and the distributions of the surplus as well as the deficit energy are computed, as shown in Fig 2.8 [**J1**]. As it can be observed in Fig. 2.8, a nominal storage capacity of 14 kWh will ensure that 89.3% of the surplus energy is stored. It can also be concluded that it will require a significant increase in storage

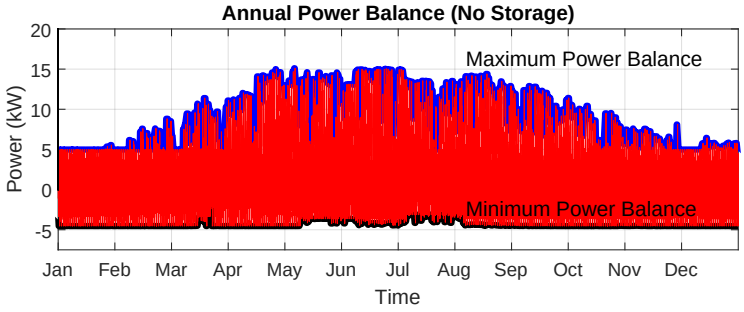

Fig. 2.7: The annual power balance of the system shown in Fig 2.2 with no storage implemented. The blue curve denotes the maximum power balance, whereas the black curve denotes the minimum power balance [**J1**].

.

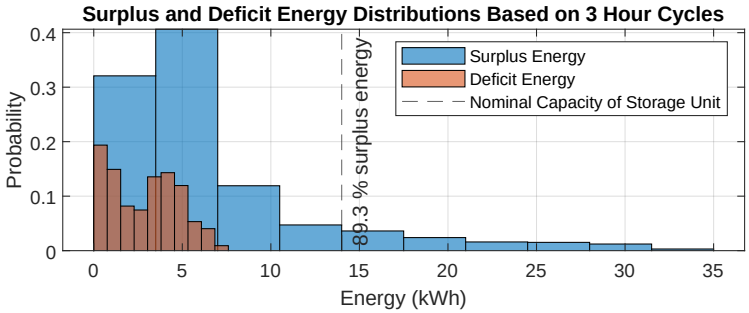

Fig. 2.8: The deficit and surplus energy distributions of the microgrid shown in Fig. 2.2 based on 3 hour cycles. [**J1**].

capacity to capture the remaining 10.7% and also, that the deficit energy at no time exceeds a value of 7.5 kWh. It can therefore be concluded that a further increase in the nominal storage capacity can lead to oversizing and an unnecessary increase in the cost of stored energy. It is worth noting that the critical parameter is the deficit energy since the converter control can reduce the power production, and therefore, the nominal storage capacity could be chosen only to cover the deficit energy. In order to guarantee a minimized cost in terms of long-term operation, it is fundamental that a compromise of nominal capacity, power capability, and lifetime is made. In terms of lifetime, there are some primary stressors, such as the depth of discharge, state-of-charge, and power capability, which all will influence the lifetime of the unit [82]. The ratings of the interfacing converter already fix the charging and discharging rates and will not be further analysed. Using an ad hoc approach when dealing with lithium-ion batteries, which states that a reasonable compromise between ensuring sufficient capacity and good battery

performance, is gained by choosing a nominal c-rate of one, i.e. 1C. A value of 1C indicates that the unit can transfer all of its stored energy within one hour. In addition, it should also be ensured that the unit is not operated at low state-of-charge (SOC) levels, which can compromise the power capability due to insufficient voltage levels. This is not expected to be of any concern in this particular case when observing Fig. 2.8, and considering that the nominal capacity is chosen well above the maximum levels of deficit energy and that there is an excess amount of annual surplus energy with respect to the amount of annual deficit energy. In [83], a correlation based on experimental data is developed between the cycle depth and the cycling capability. The results proved that as long as the unit is not operated at SOC levels below 50% of the full capacity, it would lead to the highest amount of lifetime in terms of cycling capability. Finally, it is required that the needed nominal capacity is available throughout the entire life-cycle of the unit, implying that it is needed to compensate for the ageing-phenomenon commonly referred to as capacity fade. A commonly used end-of-life criterion for batteries is the state when the capacity has decreased to 80 percent of its initial value because the rate-of-degradation tends to accelerate rapidly when it subceeds this value [84]. So with the purpose of gaining the ability to store a sufficient amount of energy that can remove all the deficit energy while also considering the stress and ageing mechanisms, the initial nominal storage capacity is required to satisfy the following constraint [**J1**].

$$C_{nominal,BOL} \cdot \Delta DOD \geq 1.25 E_{surplus} \tag{2.5}$$

where $C_{nominal,BOL}$ is the nominal capacity at the beginning-of-life, ΔDOD is the depth of discharge, which is shown to reduce to a factor of one, in [84], as long as the unit is not operated at SOC levels beneath 50%. $E_{surplus}$ is the capacity size chosen at 14 kWh. The factor of 1.25 compensates for the capacity fade that can be expected as the end-of-life state is reached, which in total amounts to a final value of 17.5 kWh of nominal capacity. Implementing the power capability limitations according to the converter rating and fixing the nominal capacity to 17.5 kWh results in the annual SOC profile presented in Fig 2.9 [**J1**]. As it can be observed from Fig. 2.9, the unit is mainly operated in the SOC region between 50% and 100% of full capacity, which, as previously mentioned, leads to a high cycle lifetime as a result of high-level discharge rates not being a common mode of operation. To gain insights into the system performance with the inclusion of the storage unit, the descending values of the SOC profile are extracted and added to the system power balance profile shown in Fig. 2.7. Adding the storage capacity results in the power balance profile shown in Fig. 2.10, where it can be observed that all presence of deficit energy is removed and the microgrid is therefore fully adequate during failure-free operation. The system is now well suited for analysing the impact of generation outages caused by converter failure,

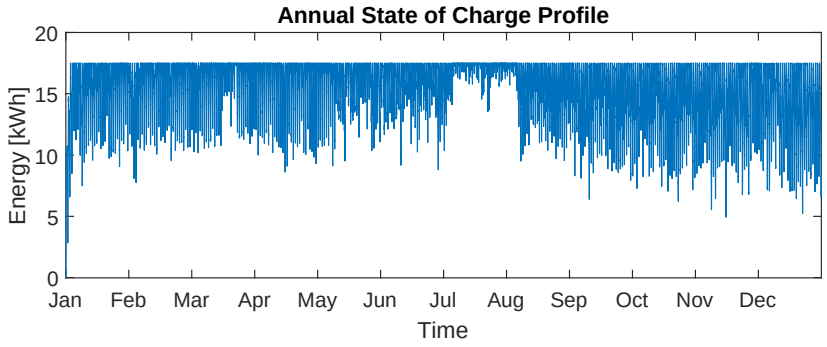

Fig. 2.9: The annual state-of-charge profile of the storage unit when considering the previously stated design considerations. **[J2]**.

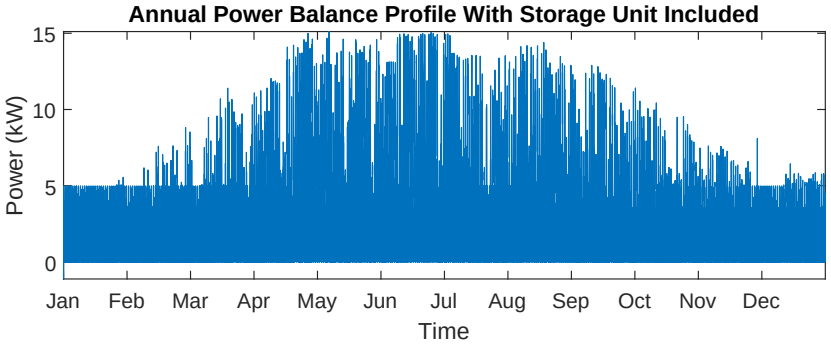

Fig. 2.10: The annual power balance of the microgrid when the designed storage capacity is included. **[J1]**.

which requires an in-depth reliability analysis.

2.3 Failure Distribution Modelling

As stated previously, the mission profile-based lifetime estimation is a comprehensive, multidisciplinary analysis, which has been thoroughly outlined in the existing literature [85–88]. The analysis will, therefore, only be outlined in terms of the essential steps accompanied by a graphical representation of the analysis flow, shown in Fig. 2.11.

2.3.1 Loading translation

Each of the respective power electronics components is subjected to various stressors. Among them are the temperature-related stressors, which are re-

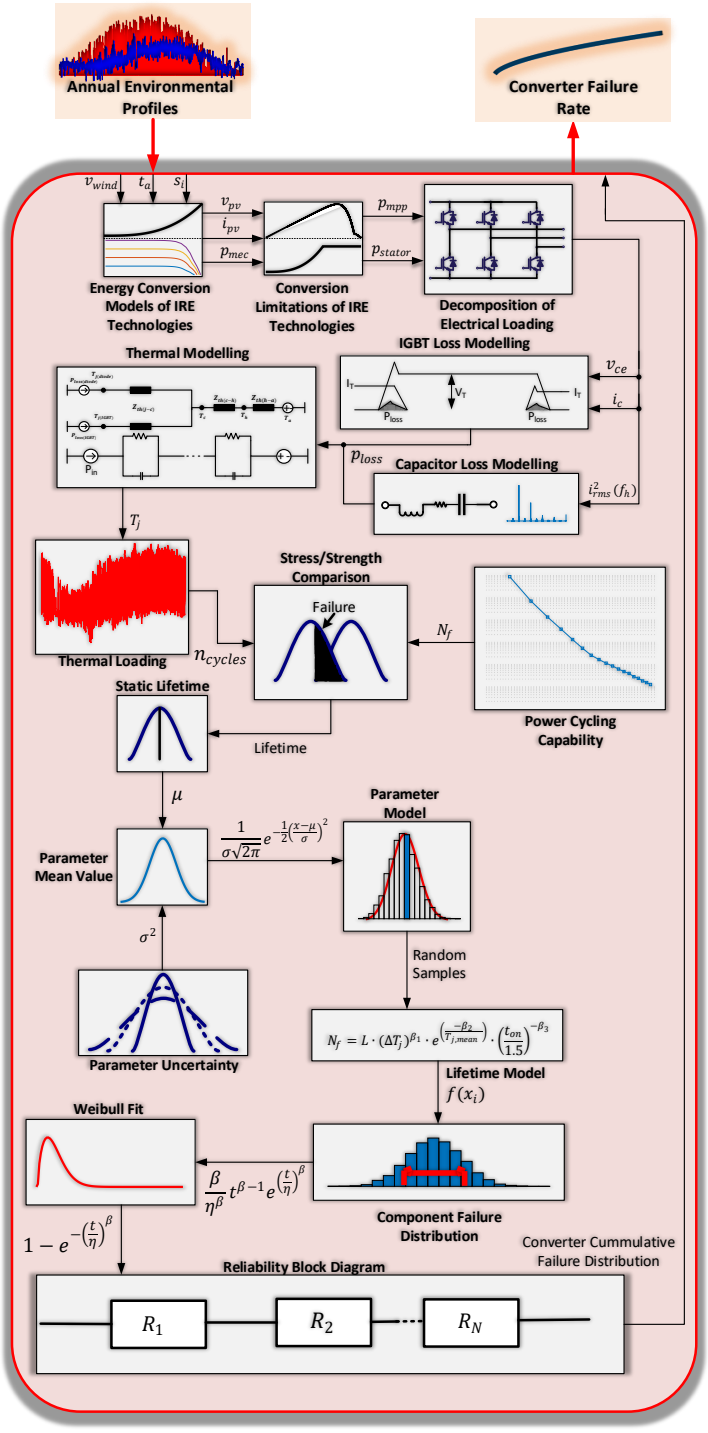

Fig. 2.11: The workflow needed to obtain the failure rates of power converters [**J1**].

garded as the central life-limiting factor, that can compromise the reliability of power electronic systems. Components such as semiconductors and capacitors are both influenced by the temperature subjected to each. In terms of semiconductors, the thermal stress can be classified as being the average junction temperature and the junction temperature variation, which is a result of the combination of the ambient temperature and the self-heating of the component, commonly referred to as power cycling [**J1**]. The wear-out of power converters results from changes in the component material, namely, the current variation causing the different elements to expand unevenly due to their different Coeffients-of-Thermal-Expansion (CTE). The mechanical stress will occur in accordance with the loading profile and will eventually lead to component failure, and it is therefore crucial that the real-field loading profiles are known. This includes obtaining the correct amount of power that can be utilized from the RES and translating it into the decomposed thermal loading subjecting the reliability-critical components. As previously mentioned, this is initiated by translating the environmental profiles into either electrical or mechanical loading using the energy conversion models of the respective RE technology. The final amount of power subjected to the converters is determined by factors such as the slip-in wind speed, the control algorithms ability to yield the power, etc.

The analysis is then moved to the component level by performing the modelling steps required to obtain the decomposed loading of each individual component. As shown in Fig 2.12, the loading stress of the components is influenced by numerous aspects. It requires circuit modelling in accordance with the power electronic topologies and the respective filter composition. In addition, the control strategy will dictate the current flow and how the stress is distributed, implying that the control scheme specification is an implicit part of obtaining the applied stress. Furthermore, the modulation technique and switching frequencies will influence the amount of dissipated losses and, indirectly, the subjected stress [**C2**]. In order to obtain the reliability metrics, the losses are characterized and applied to the respective thermal models, as shown in Fig. 2.13. In terms of the power modules, the junction temperature, i.e. the thermal loading for a given operation, is obtained using the models that describe the internal and external parts separately. The different layers of the module that connects the power chips to the casing are modeled using the Foster network, whereas the cooling components are modeled by means of the Cauer network [**C1**]. The models were presented and described in Section 1.2.3.2 and will therefore not be further elaborated. Unfortunately, with the use of a combination of these two distinct models, it is not possible to gain realistic junction temperatures due to the non-physical related thermal characteristic of the Foster model, which would be altered if combined with a Cauer model. An approach to overcome this issue is to divide the

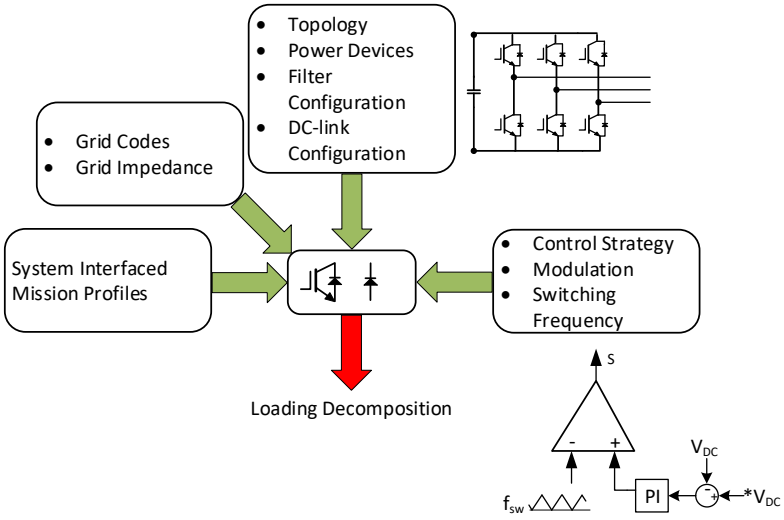

Fig. 2.12: Mission profile modelling factors needed to obtain the decomposed loading of the individual power electronic components [**C2**].

total thermal network into two parts, as shown in Fig. 2.14: one part, which will ensure that the right amount of power is applied to the cooling network by means of a low-pass filter, that is obtained by doing a Foster-to-Cauer transformation of the network representing the internal layers, as described in [43]. The adaption of the transform-based filter will guarantee that the correct casing temperature of the Foster network is obtained, which will then provide the correct junction temperature. Likewise, the power losses dissipated in the capacitors can be obtained by considering the ripple current, which is subjected to the Equivalent Series Resistance (ESR) of the capacitor. More in-depth details on the mission-profile translations and capacitors can be found in [47, 71, 87, 89, 90]. In the case of long-term analysis, some well-thought-out operating conditions are defined, and the resulting conduction losses and switching losses are inserted in look-up tables and assisted with a preferable interpolation method [**J1**].

2.3.2 Categorization of the thermal loading

Now that the thermal loading can be obtained for some specified operational profiles using the mission-profile translation methodology, it is now relevant to gain the stress information that excites the commonly known failure modes. In the case of power devices, the commonly identified failure mech-

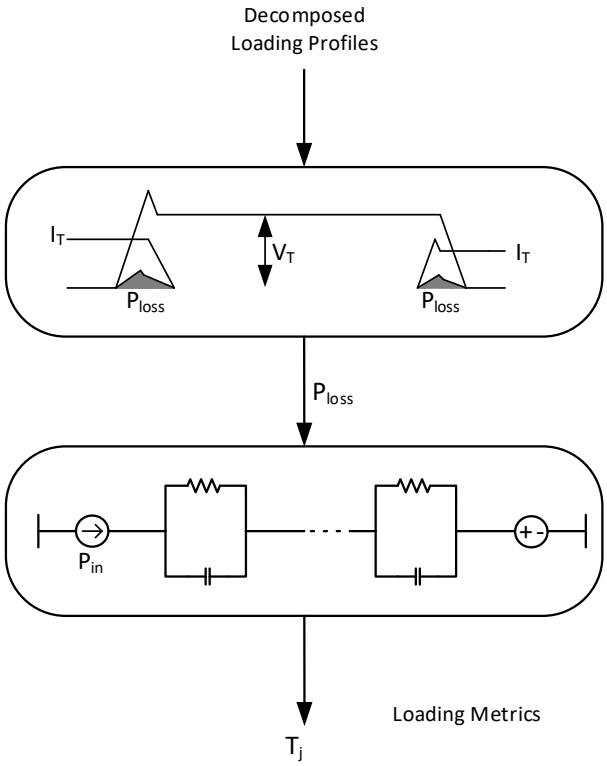

Fig. 2.13: Electro-thermal mission profile modelling used to obtain the loading metrics. I_T is the current conducted in the switch-on state, and V_T is the blocking voltage in the switch-off state. P_{loss} is the generated losses in the switch, which is supplied to the thermal network as the input power P_{in} and T_j is the obtained junction temperature. **[C3]**.

anisms are often an effect of the continuous variation of the thermal stress, which is subjected to the interconnections of the device and its external contacts. It is required that the cyclic behaviour of the thermal loading profile is extracted prior to applying it to the damage accumulation models in order to evaluate the likelihood of the occurrence of the particular failure mechanisms. The information needed to be processed is the number of cycles contained in the profile n_i, which has a specific cycle amplitude ΔT_j, a mean junction temperature $T_{j,mean}$, and a cycle duration t_{on} associated with each. This information is not readily available from the loading profile due to the irregular dynamical nature. In order to categorize the dynamical profile into the previously stated quantities, a counting algorithm is required, which is realized by the use of the Rainflow algorithm. The algorithm decomposes the irregular profile into a series of regular cycles and classifies them with respect to the cycle information, as shown in Fig. 2.15, which can then be

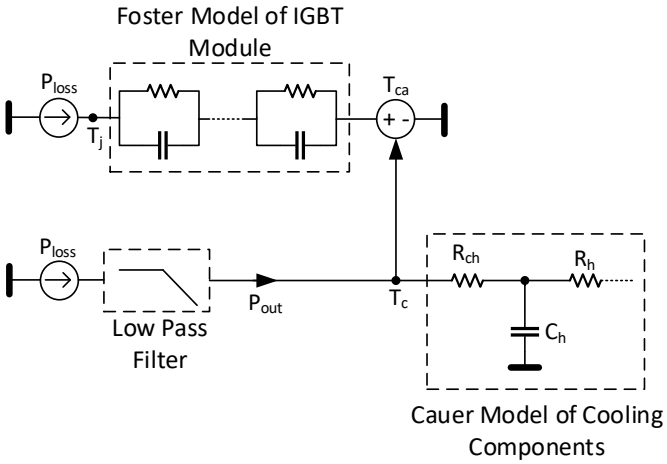

Fig. 2.14: A thermal network that can overcome the issue of combining the Foster and Cauer model by transforming the Foster-based model of the internal layers to a low pass filter, which ensures that the right amount of case temperature is added to the model of the internal layers. P_{loss} is the power loss subjected to the thermal network, P_{out} is the resulting power loss subjected to the Cauer-based model of the external cooling components, R_{ch} is the thermal resistance from case to heatsink, R_h is the thermal resistance of the heatsink, C_h is the thermal capacitance of the heatsink and T_{ca} is the temperature increase from ambient to case [**C1**].

directly applied to the strength models of the components [**C2**].

2.3.3 Strength models of the components

With the stress profiles decomposed, it is now relevant to model the strength of the power electronic components, i.e. their respective cycling capability. The lifetime is assessed by comparing the amount of applied stress with the component strength, as shown in Fig. 2.11. As stated in the introduction, field experience shows that power converters are among the critical system devices in terms of failure rate, lifetime, and maintenance cost, with several failure-inducing power electronic components [50, 91]. As a result of the power devices and capacitors being identified as the most failure-frequent and, thereby, life-limiting components of power converters, the reliability analysis of this Thesis is solely focused on those two types of components when considering the wear-out of the converters. The analytical strength model of the power devices, which describes the power cycling capabilities by relating the stress metrics with the number of cycles to failure, can be

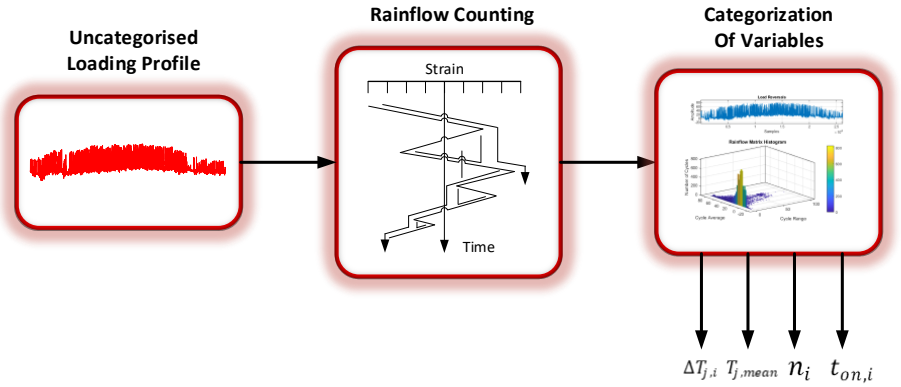

Fig. 2.15: Methodology to obtain categorized, discrete stress variables, which are directly applicable with the used strength model [**C1**].

expressed as [92]

$$N_f = \alpha(\Delta T_j)^{-n} \exp\left(\frac{E_a}{KT_{j,mean}}\right)\left(\frac{t_{on}}{1.5}\right)^{-\beta} \tag{2.6}$$

where the Coffin-Manson law relates the junction temperature cycling amplitude ΔT_j, the exponential Arrhenius term relates the mean junction temperature $T_{j.mean}$ and additionally, the cycle period t_{on} is added to account for the lifetime degrading effect of the cycle on-time. The strength model parameters α,n, and β are gathered through curve fitting the experimental power cycling curves presented in [93]. The lifetime prediction is based on the accumulation of damage, which is caused by each of the cycles, that is contained in the annual stress profile. A commonly used assumption of linear damage accumulation is used, also known as the Miner's rule, which can be expressed as [90]

$$A_D = \sum_{i=1}^{n} \frac{n_i}{N_{f,i}} \tag{2.7}$$

where n_i is the particular cycle of the i^{th} stress level and $N_{f,i}$ is the corresponding number-of-cycles-to-failure until the end-of-life is reached, for a given applied stress condition. When the accumulated damage reaches a value of one, the end-of-life state is reached, so if the value of the accumulated damage, caused by the annual profile, results in a fraction, the lifetime is obtained as the reciprocal value of the accumulated damage [**J1**].

In the case of capacitors, the central stress factors are the operating voltage V_o and the hotspot temperature T_h. By applying the annual stress profile

containing those stressors, the lifetime can be estimated using the following lifetime model [94]

$$L_f = L_0 \cdot \left(\frac{V}{V_o}\right)^{-p_1} \cdot 2^{\frac{T_o - T_h}{p_2}} \tag{2.8}$$

where L_0, V_o, V, T_o, and T_h are the rated lifetime, rated voltage, applied voltage, rated temperature, and hotspot temperature. In the case of electrolytic capacitors, the parameter p_1 is usually in the range of 3-5, whereas the p_2 parameter is commonly chosen to be at a value of 10 [94]. In the case of long-term operation, the Miner's rule is applied for damage accumulation

$$D = \sum_{i=1}^{n} \frac{l_i}{L_{f,i}} \tag{2.9}$$

where n_i is the specific cycle of the i^{th} stress level and $L_{f,i}$ is the corresponding number of cycles until the end-of-life.

2.3.4 Uncertainty implementation and Weibull analysis

Uncertainty aspects of the analysis need to be accounted for in order to make risk-informed decisions and make a realistic prediction that does not produce the same outcome regardless of different operating conditions and electrical parameters. The uncertainty is implemented by means of basing the component-level reliability assessment on the Monte Carlo simulation. This includes modelling of the lifetime model parameters and load stress parameters as distribution functions, including carefully chosen variance, that represents the impact caused by the respective uncertainties. The Monte Carlo simulation outcome is a distribution of the estimated lifetime, which is a more realistic lifetime measure, in contrast to the deterministic single-point estimations, as it is highly unlikely that a population of components will fail at an identical instant [**J1**]. In terms of the lifetime model parameters, static equivalents of the stress parameters are determined as the ones that will produce the same amount of number-of-cycles-to-failure, which was obtained by applying a given stress profile and which can be determined as

$$N_{f,i} = N_{f,static} = \alpha \cdot (\Delta T_{j,static})^{-n} \cdot e^{\left(\frac{E_a}{k_b \cdot T_{j,mean,static}}\right)} \cdot \left(\frac{T_{on,static}}{1.5}\right)^{\beta} \tag{2.10}$$

The lifetime model parameters α, n, and β are then modeled as distribution functions to account for varying testing conditions. The variance chosen for each of these parameters is based on the study [35]. The lifetime assessment is then executed as described in Section 2.3.3 for a population of samples that will represent the lifetime distribution. In terms of future usage uncertainty, a study was conducted on IGBT power modules from a leading

manufacture [95] in [**C1**], with the purpose of revealing the validity of basing the future usage conditions on the annual stress profile, that is used up to that point, by applying several years of mission profiles and conduct an uncertainty analysis similar to the one shown in Fig. 2.17. It proved that there was a significant difference in the single-point lifetime estimations from each of the subjected annual profiles, as shown in Fig. 2.16. The far right column

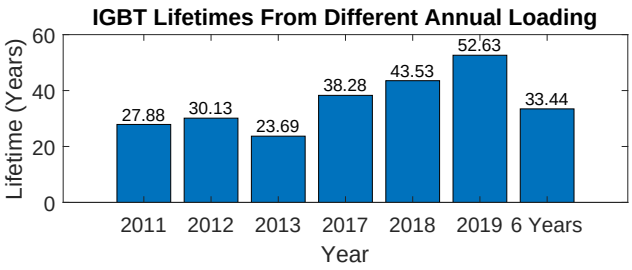

Fig. 2.16: The lifetimes obtained from each of the individual loading profiles causing a different amount of accumulated damage. The data originates from the AAU weather station and originates from the period of 2011-2019 [**C2**].

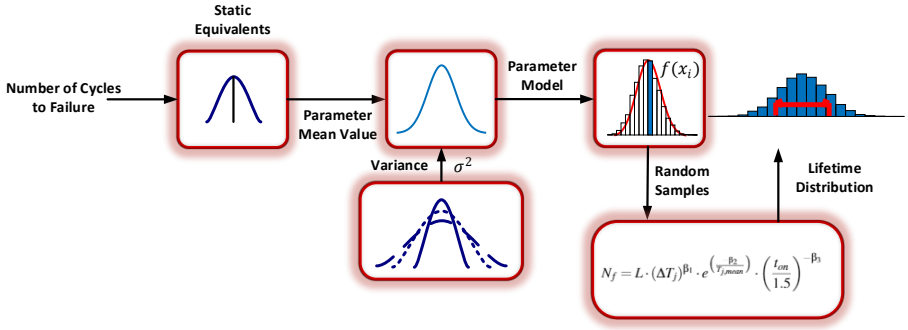

Fig. 2.17: Uncertainty implementation to obtain the lifetime distributions [**C1**].

shows the lifetime obtained when applying all six years of mission profiles, resulting in a more accurate lifetime prediction. However, the lifetime based on applying each of the annual profiles deviates as much as up to 57% with respect to the lifetime obtained when applying all six years of mission profiles [**C1**]. The Monte Carlo analysis is executed, and lifetime distributions are obtained by applying each annual profile separately while assuming the future usage remains the same throughout the entire life cycle. The Weibull parametric distribution function is fitted each of the respective lifetime yields,

which can be expressed as [33]

$$f(t) = \frac{\beta}{\eta^{\beta}} t^{\beta-1} \exp\left[-(\frac{t}{\eta})^{\beta}\right] \tag{2.11}$$

where β is the shape parameter, η is the scale parameter, corresponding to the point in time where 63.2% of the total population has failed. Using the obtained lifetime distributions, the reliability of the power modules can be expressed in terms of how large a percentage of the entire population has failed at the desired operational lifetime, which is, in contrast to the single-point estimation, a useful lifetime measure. In order to assess this measure of reliability, the Weibull Cumulative Distribution Function (CDF), also commonly referred to as the failure probability function, needs to be computed

$$F(t) = \int_0^t f(t)dt = 1 - \exp\left[-(\frac{t}{\eta})^{\beta}\right] \tag{2.12}$$

By use of Equation (2.12), the failure percentage of each respective estimation, which is based on one single annual profile, can be obtained at the desired operation life as shown in Fig. 2.18. At the desired operational lifetime of

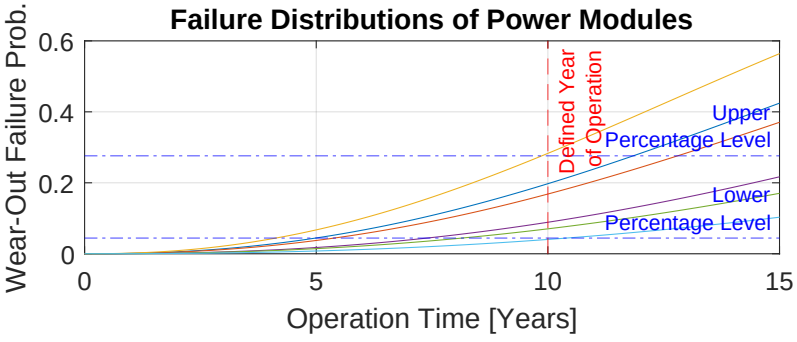

Fig. 2.18: The wear-out failure probability functions of the IGBT power modules when applying six different annual profiles [**C1**].

10 years, The upper and lower failure percentage boundaries are 27.6% and 4.4%, respectively. The significant difference in the failure proportion clearly demonstrates the lifetime of the IGBTs dependency on the environmental condition variation on a year-to-year basis, which is crucial to account for when estimating the lifetime of power converters. The lifetime estimation can still be based on a single year of mission profiles as long as the statistical uncertainty induced by the variation of climate conditions is accounted for by including some variance in the static stress parameters. The suitable amount of variance caused by the different annual profiles can be determined

by considering that each annual profile corresponds to a specific number of cycles-to-failure when evaluating the profiles by use of iteration. This difference in number-of-cycles-to-failure results in different sets of static stress parameters, that is obtained by use of Equation (2.10). The difference in the static stress parameters will dictate the amount of variance and the mean of the stress variable distribution by considering the extreme values and the overall mean, as exemplified in Fig. 2.19. From each respective stress profile,

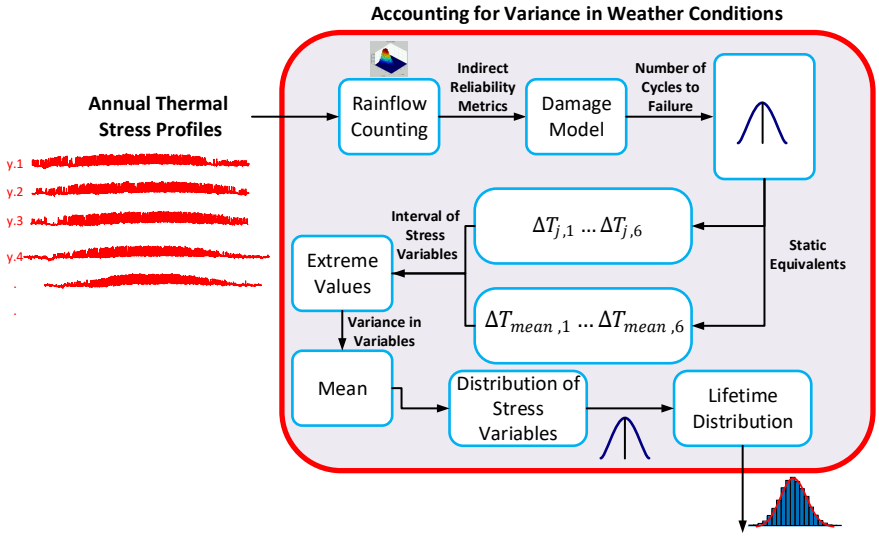

Fig. 2.19: Workflow needed for inclusion of the statistical future usage uncertainty caused by the annual variation of climate conditions. **[C1]**.

the resulting number of cycles-to-failure and the corresponding static values are summarized in Table 2.2

Using the values presented in Table 2.2 to compose the variance and mean of the stress variables, the models shown in Fig. 2.20 are obtained **[C1]**. When considering the actual system in question, an example of the results gained from the Monte Carlo-based uncertainty implementation that depicts a lifetime yield of a power device and a DC-capacitor operating in the wind-based generator presented in Fig. 2.3, is shown in Fig. 2.21. It can be observed in Fig. 2.21 that there is a significant spread in the failure distributions of the power devices when compared to the capacitors, in which the complete population is expected to fail within a time span of five years. This is also evident from the slope of each of their respective cumulative distribution functions, which clearly indicates the evolution of failure, where the rate-of-change of

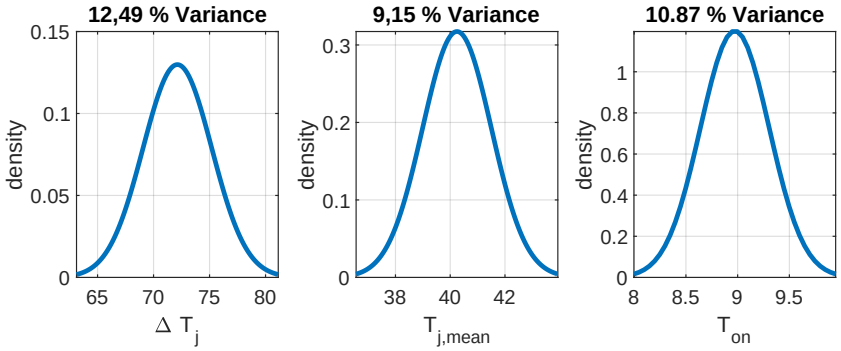

Fig. 2.20: The models of the stress parameters, which accounts for future usage uncertainty. The model variance is obtained from difference in static stress parameters gained by applying different annual mission profiles. **[C2]**.

capacitor failure is substantially higher. **[J1]**. The large distribution spread is mainly due to the variance of the lifetime model parameters α, n, and β in equation (2.6). The chosen model parameter variance is, as stated previously, based on the study [35], which is based on a large share of power cycling data. In particular, the temperature variation related Coffin-Manson parameter n shows to have a significant impact on the lifetime spread even at minor lifetime model parameter variance. The cumulative distribution function is once again useful as a reliability metric for stating an allowable failure percentage, which is commonly referred to as the B_x lifetime [33]. The obtained B_{10} lifetime for the power device and capacitor operating in the wind-based generator are 9.5 and 23 years, respectively, as shown in Fig. 2.21. Finally, it is necessary to combine each of the failure distributions of the power electronic components, which is subjected to the reliability analysis in order to gain the failure distribution of the full power electronic-based generation units, which

Table 2.2: Parameters used to include statistical uncertainty in the stress variables in order to take into account the difference in annual climate conditions obtained by using several years of mission profile data **[C1]**.

Static stress variables used to account for statistical uncertainty				
Year	N_f (Obtained from Iteration)	$\Delta T_{j,static}$	$T_{j,mean,static}$	$t_{on,static}$
2011	362020	79.53	41.78	8.67
2012	391880	79.63	42.57	9.64
2013	310840	81.13	43.93	8.82
2017	542700	68.61	38.12	8.36
2018	600040	68.94	38.04	8
2019	754780	63.12	36.56	9.95

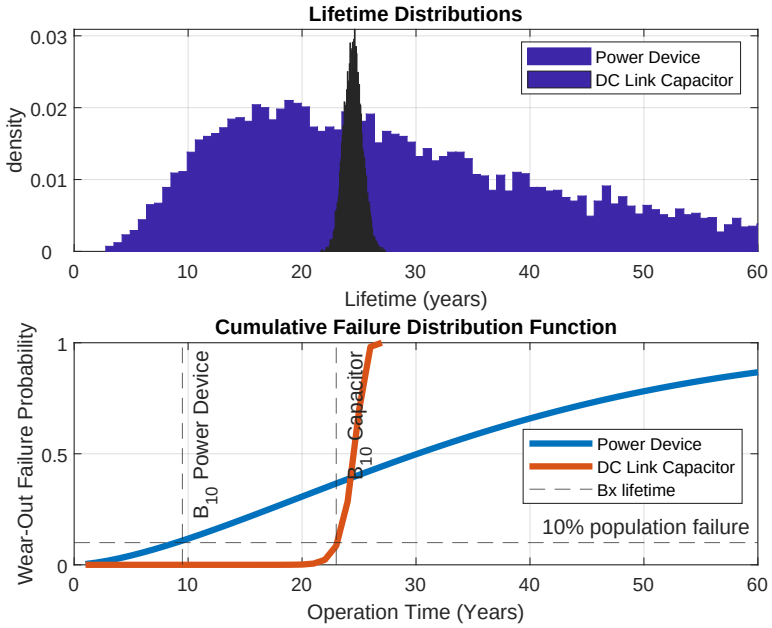

Fig. 2.21: Results obtained from the Monte Carlo-based uncertainty implementation show the lifetime distributions and cumulative distribution functions of a power device and a capacitor operating in the machine-side converter and the DC-link of the wind-based generation unit shown in Fig. 2.3 [**J1**].

consists of several power electronic components. The reliability of these systems is assessed by means of the Reliability Block Diagram (RBD), where the combination of each of the respective failure distributions, which provides the overall distribution, is dictated by how the individual component failure will influence the system's ability to remain operational despite of failure. In the case of a system containing n components, in which any single component failure will lead to overall system failure, the system is then organized as a series connection of the RBD [33]

$$R(t) = \prod_{i=1}^{n} R_i(t) \tag{2.13}$$

If, in contrast, the system only needs to rely on one of the systems components to remain operational, the RBD can be studied as having active parallel redundancy, in which the total reliability can be obtained as [33].

$$R = 1 - \prod_{i=1}^{n} (1 - R_i(t)) \tag{2.14}$$

With the overall failure distributions of the generation units, the failure rate can be calculated, which is an essential requirement when moving the reliability analysis into the domain of power systems. The failure rate is computed by use of the fitted Weibull shape and scale parameters of the generation unit failure distributions as [33].

$$\lambda(t) = \frac{f(t)}{R(t)} = \frac{\beta t^{\beta-1}}{\eta^{\beta}} \tag{2.15}$$

The obtained shape and scale parameters of every unit are presented in Table 2.3

Table 2.3: Weibull shape and scale parameter of each generation unit's failure distribution of the system shown in Fig. 2.2 **[J1]**

Wind Generation Unit	β = 1.57	and η = 5.28
PV Generation Unit #1	β = 1.85	and η = 7.72
PV Generation Unit #2	β = 2.12	and η = 11.82
Storage Unit	β = 1.44	and η = 8.32

2.4 Availability Modelling of Power Converters

One indispensable precondition of power systems is that they must stay operational at all times. This suggests that a fundamentally different approach needs to be taken as the analysis is moved into the domain of power systems relative to the one used for converter-level studies in Section 2.3. This is due to the principal difference in how repairable and non-repairable systems are analysed mathematically. None of the frequently used distributions practiced in the converter-level analysis is applicable in repairable systems as they assume instantaneous repair, which, in this case, is not a valid assumption **[J1]**. This implies that the system reliability modelling should be based on stochastic processes. In this particular case, the converters are assumed to be in an "as good as new state" at the time of termination of the repair process since the complete unit is replaced. This seems to be the most likely case considering the high cost of downtime in combination with the long and exhaustive overhaul process if any possible component defect needs localization and remedying. Furthermore, in the case of repairable systems, the "classic" definition of reliability can solely be rightfully used until the time of the first failure occurrence. Due to these issues, the reliability-equivalent used in connection with power systems, known as availability, is used, which is defined as the probability that the unit is available, i.e. the proportion within a finite time interval where the unit is available for operation [30]. The availability

of a unit is evaluated by using its failure rate λ, obtained in the previous section, and its repair rate μ. The steady-state availability in the case of constant transition rates can be calculated as [76]

$$A = \frac{\mu}{\lambda + \mu} \tag{2.16}$$

The stochastic nature of power system reliability can be modelled by use of the Markov approach but needs some additional modifications to cope with the non-constant failure rates that are a signature of power electronic converters [**J1**]. The non-constant failure rates that were obtained in Section 2.3 bring about non-stationary processes, meaning that the probability of transitioning from one state to another does not remain the same throughout the converter life-cycle [96, 97]. In contrast, the repair rates are assumed to be constant for the sake of simplicity and assume a repair time of two days due to the relatively effortless accessibility of converters operating in a residential area [**J1**]. In the case of offshore wind farms or units operating in remote areas in general, an extension of the repair time must be considered. In order to benefit with respect to accessing a solution when calculating the availability of the power electronic-based generation units, it is advantageous to construct a state-space diagram of the entire system. The state-space diagram summarizes all the states in which the system can reside in and how any transition among those states can occur. The inclusion of the state-space diagram is a crucial part of the reliability assessment, as it deciphers the knowledge of system operation into a mathematical model which can be exploited using Markov procedures. Acknowledging that each respective generation unit can reside in either a down or an operational state and that only one single event can occur during state transition, the state-space diagram shown in Fig. 2.22 is obtained based on the network shown in Fig. 2.2. It can be observed in Fig. 2.22 that every single unique state is defined and coupled by their respective failure and repair rates. The complexity of the diagrams increases rapidly as the number of units considered increases. The number of included states increases with the rate of 2^n for an n-converter system. This removes the possibility of obtaining analytical expressions that can describe the evolution of each state, simply because it will be impracticable and downright unmanageable for systems of this size and also taking into account that the used methodology is only useful if it is scaleable to larger systems. There are two ways to deal with this issue. One is to apply state truncation by neglecting those states which have a low probability of occurrence. The other solution, which is the one adopted in this study, is to exploit the stochastic transitional probability matrix to assess each respective state evolution as time passes, using each of the defined transition rates. The stochastic transitional probability matrix is limited to use in discrete Markov chains. Since this study is dealing with the transition rates of the power converters and not the transi-

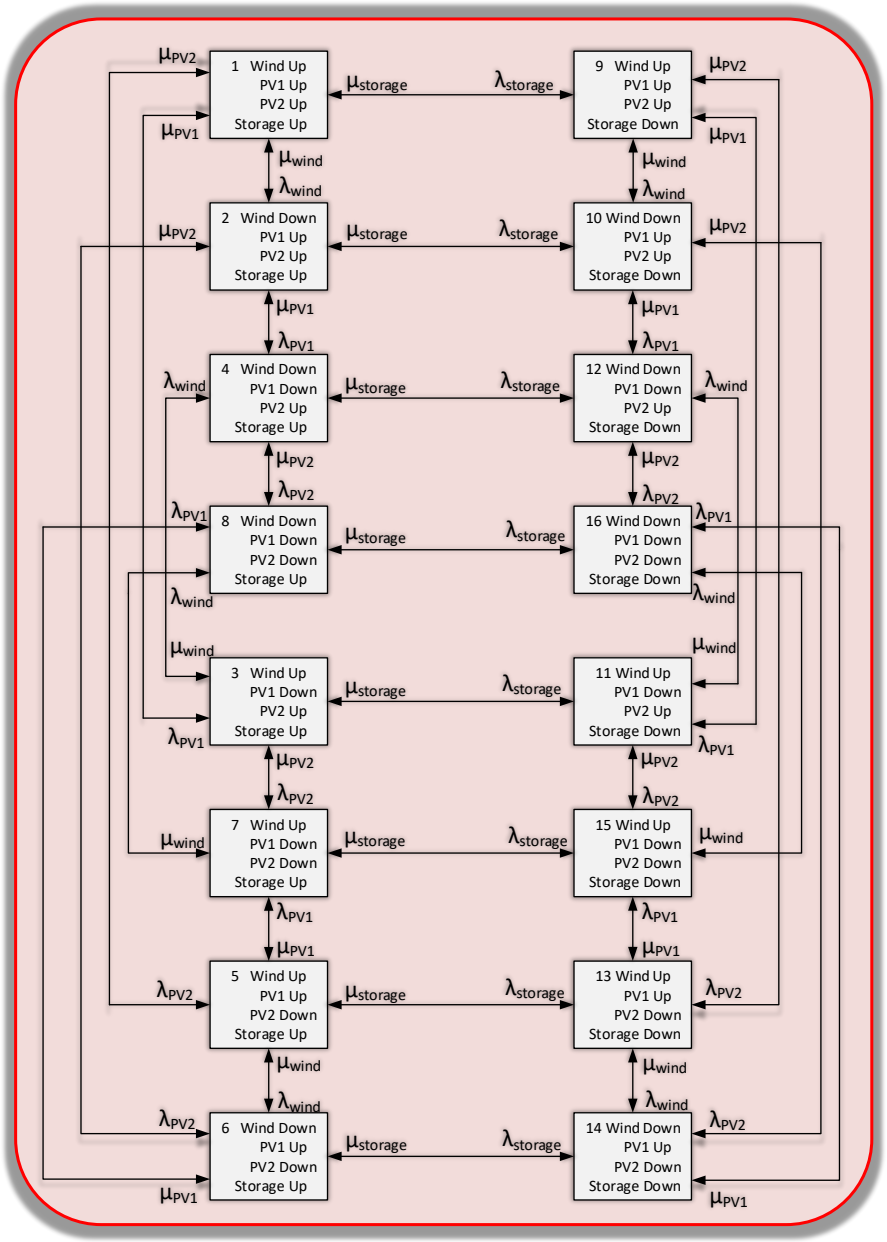

Fig. 2.22: State-space diagram showing each of the unique system states and related transition rates of the system shown in Fig. 2.2. As seen, each of the states is unique, with different units being in either the up state (operational) or the down state (in repair). λ is the failure rate that transits a unit being in its operational state to its failure state, and μ is the repair rate that transits a unit from its failed state to its operational state **[J1]**.

tion probabilities, it is needed to move from the continuous Markov process to the discrete Markov chains by defining an appropriate time increment Δt. When determining the time span of this interval, it is required to consider the fundamental assumption that realized the Markov approach to begin with, which is the limitation that only one event can occur during any unique state transition. This can be understood by observing the state transition from state one to state two in Fig. 2.22 and acknowledging that only one converter has changed its state of condition, i.e. from being in operational state to the down state. This suggests that the defined interval needs to be in accordance with the assumption of single-event state transition, meaning that it needs to be of sufficiently short duration, which will ensure that the occurrence of two or more events is highly unlikely. Due to this constraint, the discrete time increment was chosen to be of a duration of 1 hour, as it is highly that two or more converters will fail during that time span. Introducing this time increment results in the matrix entries take on discrete form as in (2.17), which facilitates the use of the stochastic transitional probability matrix shown in Equation 2.18 [**J1**]

$$p = \lambda \Delta t \tag{2.17}$$

$$P = \begin{bmatrix} P_{11} & P_{12} & P_{13} \dots & p_{1n} \\ P_{21} & P_{22} & P_{23} \dots & \vdots \\ P_{31} & P_{32} & P_{33} \dots & \vdots \\ \vdots & & \ddots & \\ p_{m1} & & & p_{mn} \end{bmatrix} \tag{2.18}$$

where the row entries denote the state from which the transition occurs, whereas the column entries denote the state to which the transition occurs to. The time evolution of the state probabilities is obtained by raising the stochastic probability matrix (2.18) to the power of the desired number of time increments by use of iteration [**J1**].

2.4.1 Coping with non-constant failure rates

As stated previously, the traditional Markov approach, which has been described up until now, can solely be employed to stationary processes, i.e. systems inhibiting constant failure rates. As described in connection with the uncertainty and Weibull analysis in Section 2.3.4, the outcome of that analysis proved to be non-exponential failure distributions and, thereby, non-constant failure rates. This suggest that supplementary modeling must be added to the previously described procedure. There are a considerable amount of existing procedures on how to cope with non-exponential distributions [98,99],

and the one applied in this study is based on splitting up the existing system states in order to gain a number of sub-states that are exponentially distributed [**J1**].

The principle of the following is to blueprint how the correct number of sub-states is obtained, how each of these sub-states should be composed, and lastly, which parameters should portray them. In the case of the power electronic-based generation units, the problem involves Weibull distributed failures with an increasing slope, i.e. $\beta \geq 1$. In the case of increasing slope, each of the existing states is partitioned into a number of series configured sub-states, which is outlined for the system state one in Fig. 2.23 [**J1**]. In addition to the partition of the system states, Fig. 2.23.b presents the bathtub curve, which is a superposition of each possible failure, that a power converter can encounter throughout its life cycle. The bathtub curve shows an introductory decreasing failure rate, commonly referred to as the infant mortality stage, an intermediate useful life stage, and the final wear-out stage. The stages that are treated in this study are the useful life and the wear-out stages, which exhibit either constant or increasing failure rates [**J1**]. The wear-out stage of the power converters is modeled by decomposing the failure transitions of each of the respective system states shown in Fig. 2.22 into some identical exponential distributed states with transition parameter ρ. The probability distribution function becomes the special Erlangian distribution in the case of equivalent states with state durations that can be described by exponentially distributed variables [96]. The special Erlangian distribution can be expressed as

$$f(t) = \frac{\rho(\rho t)^{\alpha-1} e^{-\rho t}}{(\alpha - 1)} \tag{2.19}$$

for which the rth moment is given by:

$$m_r = \frac{1}{\rho^r} \prod_{k=1}^{r} (\alpha + k + 1) \tag{2.20}$$

The decomposed state can be described by the two parameters α and ρ. Their respective values are determined by matching the first and second moments of the special Erlangian distribution with the analogous moments of the Weibull failure distributions of the power converters [**J1**]. The first and second moments of the special Erlangian distribution can be obtained by equating $r = 1$ and $r = 2$ in Equation (2.20), which results in the following

$$m_1 = \frac{\alpha}{\rho} \quad \text{and} \quad m_2 = \frac{\alpha(\alpha + 1)}{\rho^2} \tag{2.21}$$

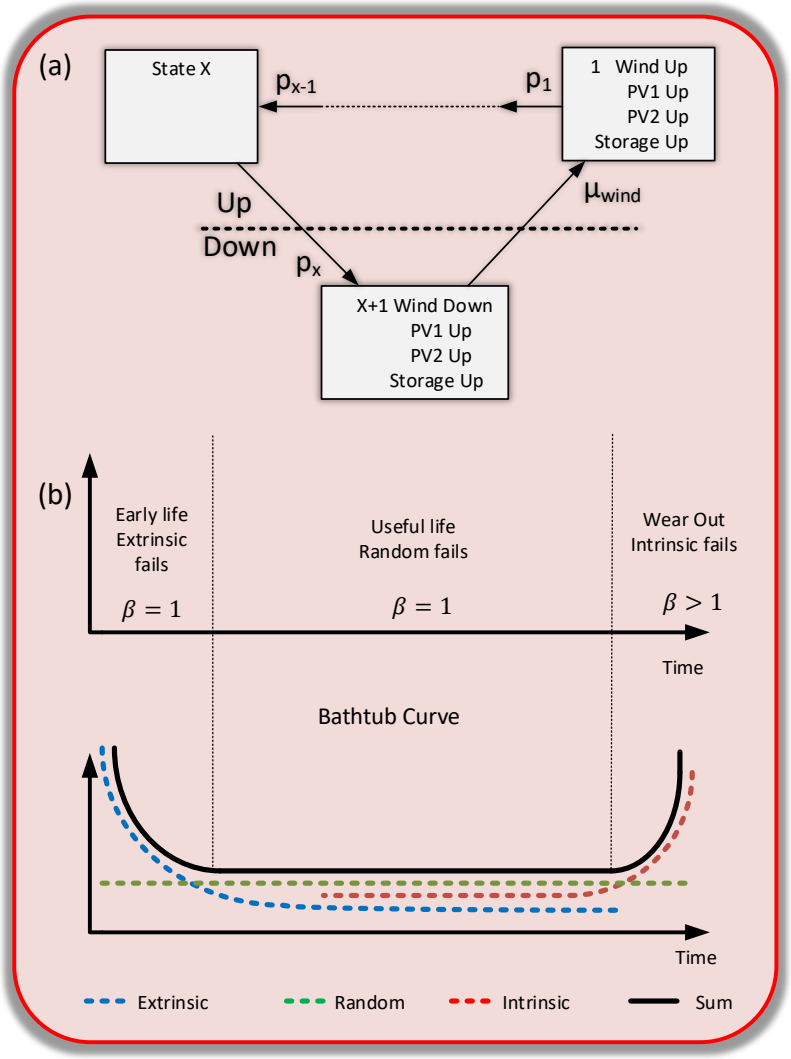

Fig. 2.23: (**a**) Decomposing the non-exponential distributed system state 1 from Fig. 2.22 into some series configured exponentially distributed states. (**b**) Bathtub curve outlining failure tendency of power converters throughout their entire life cycle. [**J1**].

Let M_1 and M_2 denote the first and second moments of the Weibull failure distributions and match the moments of the two distinct distributions as

$$m_1 - M_1 = 0 \quad \text{and} \quad m_2 - M_2 = 0 \tag{2.22}$$

Substitute the two expressions of the Erlangian moments in (2.21) into the expression matching the moments of each respective distribution in (2.22) and then isolating for α and ρ respectively, which leads to

$$\alpha = \frac{M_1^2}{M_2 - M_1^2} \quad \text{and} \quad \rho = \frac{M_1}{M_2 - M_1^2} \tag{2.23}$$

where α is the number of equivalent exponentially distributed states that are required to represent the behaviour of the original state, and ρ is the transition rate joining each of the exponentially distributed states. The two equivalent state parameters are now a direct function of the Weibull shape and scale parameters, as the Weibull moments can be expressed in terms of those as

$$M_r = \eta^r \cdot \Gamma\left(1 + \frac{r}{\beta}\right) \tag{2.24}$$

With the intent of evaluating the consequence of including the non-constant failure rates when assessing the state probabilities, the probability of all the converter-based generation units being in an operational state is computed using constant and non-constant failure rates and compared in Fig. 2.24. Where the constant failure rates is based on the static lifetime of the converters given as

$$\lambda_{constant} = (\text{Static lifetime})^{-1} \tag{2.25}$$

As it can be recognized in Fig. 2.24, the transient phase is substantially prolonged when using non-constant failure rates. Also, the use of constant failure rates will overestimate the system downtime during the first six months but severely underestimate the downtime during long-term operation and thereby falsely underestimate the system risk. Therefore, the risk evaluation of power electronic-based power systems using constant failure rates will not lead to realistic results and should be avoided. It should be noted that regardless of applying constant and non-constant transition rates, the state probabilities converge to the limiting values. This is an inherent characteristic of systems modelled by the use of the Markov method [96].

2.5 System Risk Evaluation and Maintenance Scheduling

This section intends to establish a replacement policy for the power converters that will guarantee adequate operation of the power electronic-based

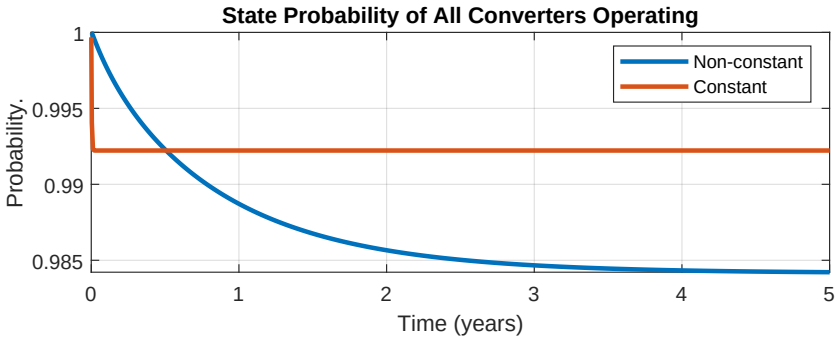

Fig. 2.24: Comparison of the state probability of all the converter-based generation units being operational using constant and non-constant failure rates [**J1**].

power system. The replacement policy is based on the definition of a risk limitation that is not allowed to be violated at any point in time. The definition of risk is the combination of the probability of the occurrence of a generation outage and the negative impact that an outage of such extent will produce [100]. Concerning the extent of an outage, the methodology used to obtain the generation capacity was presented in Section 2.2.2. The use of a risk criterion based on a specific quantitative measure is not practical. It is, therefore. rarely used due to the fact that a risk reduction does not come without some sort of related expense, and any changes should therefore be analyzed in terms of being cost-beneficial. Due to this ambiguous differentiation of acceptable from unacceptable risk with a specific quantitative measure, the risk is alternatively divided into areas of small risk, tolerable risk, and unacceptable risk. as illustrated in Fig. 2.25 [**J1**]. A further decrease from when operating in the tolerable risk area is only worthwhile if the reduction is practical and cost-beneficial, which is a complete analysis on its own terms and is out of the scope of this study. The index used to evaluate the system risk is appropriated as the Loss Of Load Expectation (LOLE), which can be expressed as

$$LOLE = \sum_{i=1}^{n} P_i(C_i - L_i) \tag{2.26}$$

where C_i is the generation capacity at time instant i, L_i is the load demand at time instant i, and P_i is the probability of a generation outage that will result in the corresponding measure of loss of load. Simply put, a specific capacity outage will commit to the system LOLE by a measure equal to the product of the probability of such a particular outage occurrence and the amount of time steps surpassed within the duration of the loss of load occurrence, if such an event would exist [**J1**].

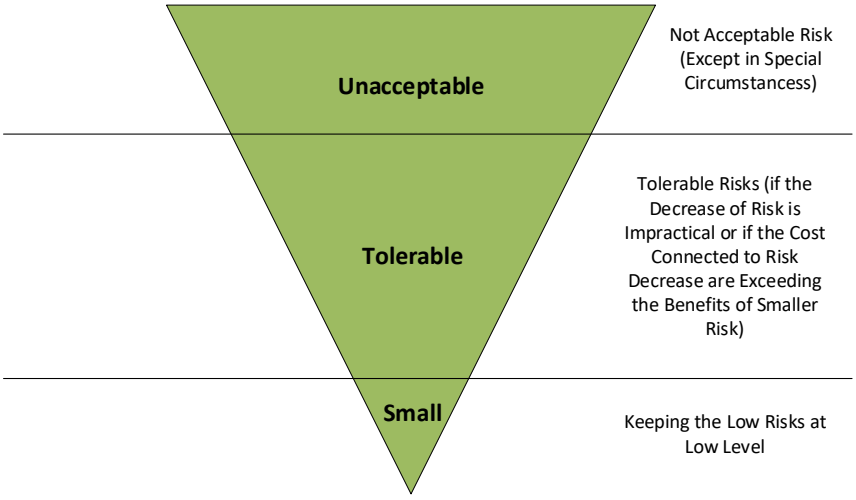

Fig. 2.25: Basing the risk criteria on zones of acceptable low risk, tolerable risk, and unacceptable risk in which, the preferred zone also should be chosen with a cost-benefit perspective [**J1**].

The most immediate approach to gain the system LOLE would be to compute the product of the overall converter unavailability and the discrepancy between the total generation capacity and the demand. However, the issue related to this is that this approach would not lead to authentic results since it is not accounted for how this unavailability is split among the respective units. Since they are not producing an equal amount of power, it would result in misleading risk rates. In contrast, each of the unique state probabilities needs to be studied along with their respective negative impact, i.e. loss of generation capacity. On the contrary, in this study, only four unique states are studied, which are the four single unit outage events, i.e. State 2, State 3, State 5, and State 9 in Fig. 2.22. This being due to the limiting state probability of two or more generation units being down concurrently is in the order of 10^{-6}. It does, therefore, not contribute to the system risk in any significance. It should be noted that incorrect results are also obtained if the risk assessment is obtained using the generation capacity distributions as well as the resolution of the generation, as this will not account for the uncertainty linked to the intermittent generation. Namely, it does not consider the generation at a specific point in time, which could be at a time when that specific outage does not cause any loss of load if the generation of this particular unit is not needed to make the system fully adequate. Preferable, each unique outage state should be modeled by means of the removal of the corresponding generation capacity profile from the system power balance and gaining

the total time span of when the loss of load occurs by the number of deficit samples and the profile resolution [**J1**].

The LOLE is calculated while a risk limit of 10 hours per year is favored, as this is commonly advised as being within what is thought of as constituting a reliable power supply and is adopted in the bulk of European countries, where the limit is stated somewhere in between 5 to 10 hours per year [101]. As the result will show, a 10-hour risk limit is a harsh requirement for a system of this type. It requires rather frequent converter maintenance, and the risk limits of conventional systems might not be the optimal solution for microgrids. However, by means of the methodology presented and the computation of Equation (4.14), the system risk is assessed, and the results are presented in Fig. 2.26. As it can be observed in Fig. 2.26, the risk increases

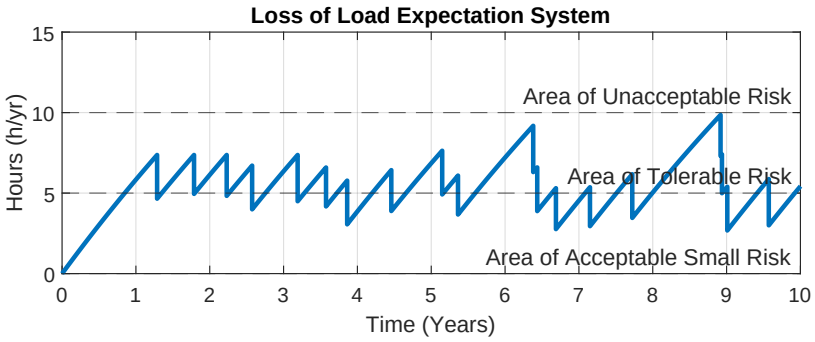

Fig. 2.26: The system risk response of losing the load, including unit replacements, in order to avoid violation of defined system risk limitations [**J1**].

as the probability of each of the converters entering the state-of-failure increases due to aging-related wear-out [**J1**]. This increasing failure probability influences the risk of not meeting the load demand. The system LOLE is the result of the contribution of each converter-based unit, and the replacement policy of each is based on ensuring that the total system risk does not violate the defined limitations. The resulting replacement policy of each respective converter is shown in Fig. 2.27, where it can be seen that their respective risk contribution is rebooted at the time of replacement, which prevents the risk of losing the system load from exceeding the defined limit of 10 hours per year [**J1**]. As a means to get some awareness of how much of the total energy demand is met when adopting the specific replacement policy, the energy index of reliability is calculated, which is given as [96]

$$EIR = 1 - LOEE_{normalized} = 1 - \sum_{k=1}^{n} \frac{E_k P_k}{E_{total}} \tag{2.27}$$

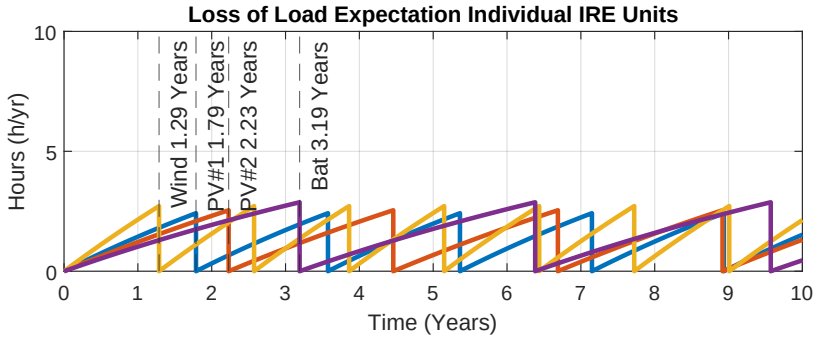

Fig. 2.27: Replacement policy of the power electronic converters that is needed in order to prevent the violation of the adopted system risk limitations **[J1]**.

where $LOEE_{normalized}$ is the loss of energy expectation normalized with respect to the total energy demand, which portrays the scale of the expected energy curtailed as a result of converter downtime and the total energy demand required to satisfy the load demand. When adopting the replacement policy presented in Fig. 2.27, the corresponding percentage of the load demand shown in Fig. 2.28 is met **[J1]**. It can be understood by observing Fig.

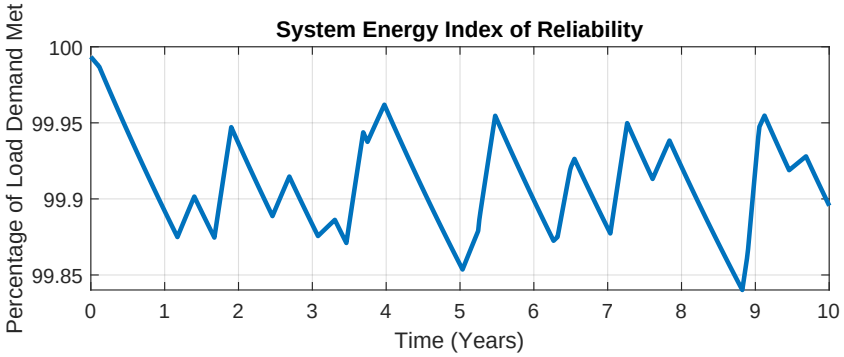

Fig. 2.28: The percentage of the probable total load demand met when adopting the replacement policy shown in Figure 2.27 **[J1]**.

2.28 that the probable proportion of the total energy demand that is not met will at no point in time exceed a value of 0.2 percent. However, from Fig. 2.27, it is quite apparent that the frequency of unit replacement is relatively high, which is partly an outcome of the stress/strength margins of the power electronic components that were used throughout the study. One method to gain an extension of the unit life cycle and, thereby, lower the replacement frequency for a specific application is to implement the design for reliabil-

ity feature. Despite this feature implementation being well out of this thesis scope, it is still worth proposing it as a useful feature. The central intention is reinforcing of the power electronic components in terms of the rated margins with respect to the expected usage conditions, which is applied throughout their operational lifespan. The reinforcement is imposed until a preferable converter replacement frequency is obtained, as outlined in Fig. 2.29. The

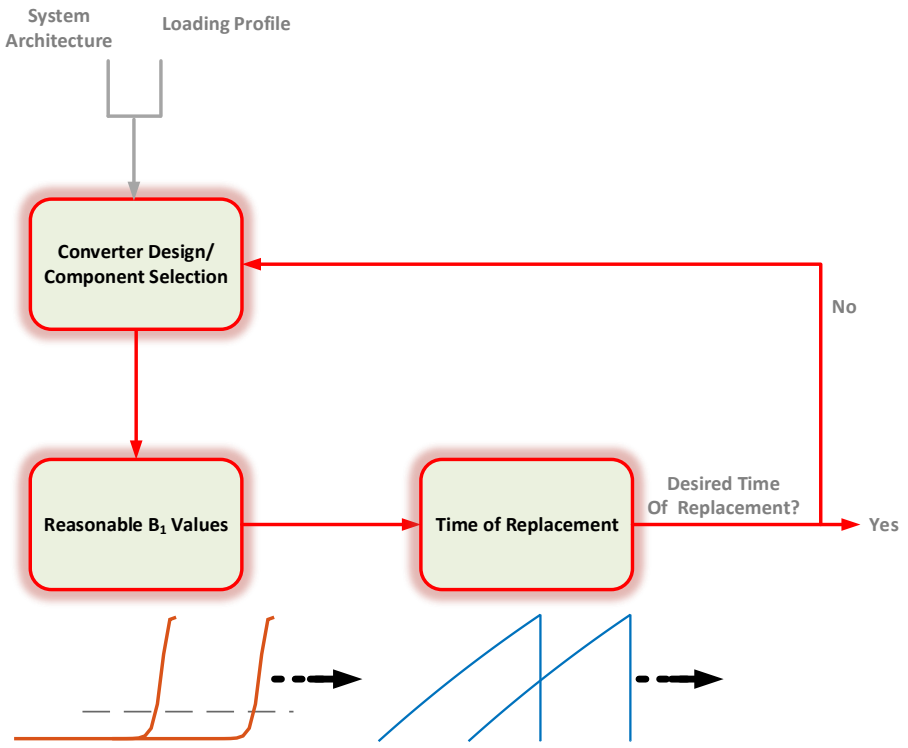

Fig. 2.29: Reducing the frequency of converter replacements by incorporating design for reliability features, where the power electronic components are reinforced until desired replacement frequency is obtained [**J1**].

reinforcements of the components can lead to a reduction in the replacement frequency without compromising a high system EIR. Finally, it is worth mentioning that the overall system reliability is never more reliable than its weakest link, and a reduction in the risk rates induced by the fragile units will be reflected in the replacement frequency of every unit contained in the system [**J1**].

2.6 Summary

Even though comprehensive research has been conducted on the subject of assessing the reliability of power converters, the existing studies do not bridge the gap needed to merge the reliability analysis of power converters with the assessment methods of power system reliability. This includes the extension of power electronics reliability concerning the repair and availability evaluation concept. Availability is a central quantification in power system reliability assessment. However, due to the non-exponential failure distributions that are an inherent tendency of power converters, the conventional availability modelling methods are not directly applicable.

In this chapter, a practice was proposed that expands the existing methods of power electronics reliability, which enables the study of them when they are operated within power systems. This included a routine that deals with the issue of the non-exponential failure distribution without adding any significant complexity, as it uses typical Markov process modelling. In the existing reliability studies on converter systems, the reliability block diagram is used to associate the failure distributions of the respective components. These methods are based on the fundamental assumption that the repair process is instant, which does not comply well with reality. The repair process was taken into account, and the concept of availability of the generation units was presented. The availability modelling of systems containing units that do not display identical and constant failure rates becomes a severely exhaustive process.

This chapter presented a method that discretized the continuous Markov process by introducing a time step wherein the probability of two or more state transitions is highly unlikely and which transforms the problem into one that can be solved using the Markov chain methods. One of the key features of Markov chains is the use of the stochastic transitional matrix, which exhibits clear computational advantages relative to the use of analytical expressions. Alternatives such as semi-Markov processes require the computation of complicated convolution integrals. The methods used in relation to the Markov process are not very well suited in regards to scale the analysis to include more than a few units. The stochastic transitional matrix can be used with ease when scaling up the system as this simply requires an addition in matrix dimensions, in contrast to solving large systems of equations that result in large and rather complex expressions. Finally, a method on how to utilize the system risk of losing its load to base the replacement policy of the power converter-based generation units was presented, which can be utilized to maintain a reliable and adequate power supply.

Chapter 3

Application-level Health Precursor in Power Converters

As a result of the uncertainty associated with the lifetime predictions of power converters, namely the uncertainty introduced by the extrapolation of the accelerated test results to real-field usage conditions, the failure distributions might end up having a variance of relatively many years. Due to this significant variance, the prediction of individual units tends to lack an acceptable amount of precision that can guarantee accurate risk rates, which, in the worst case, can lead to improper operation of power systems. In recent years, the reliability studies of power electronics have witnessed a rise in output which advocates for physics-of-degradation-based procedures, which benefit from variations in the electro-thermal parameters by using them as health precursors. However, the existing monitoring procedures are limited to the consideration of single components. Due to the impracticability of monitoring multiple components simultaneously, there is an indispensable need for procedures which are capable of monitoring the health state of power converters in their entirety. In this chapter, a proposed procedure exploits the converter operating efficiency for monitoring the occurrence of multiple component parameter drifts, which can be applied as an application-level health precursor with the possibility of gaining precision when stating the operational lifetime of power converters. Finally, the trends of the degradation progression of the power electronic components are analysed and used for indicate when the converter end-of-life is reached.

As described in Chapter 2, the state-of-the-art lifetime estimations of power

converters is based on empirical failure fatigue models which portray how some specified applied stress influences particular materials to induce the critical failure modes [102]. Numerous well-supported concerns are associated with these commonly practiced prediction procedures, particularly determining the useful life of the components based on the extrapolation of accelerated test results to real-field usage conditions. The extrapolation of the test results is a significant source of uncertainty, as testing conditions are often limited to covering a few unique loading conditions, which differs significantly from authentic application use [**C3**]. The loading profiles seen within renewable generation greatly fluctuate and inhibit a extensive array of gradients and cycle amplitudes [37]. A means to eliminate the uncertainty, to a certain degree, is to adopt the physics-of-degradation-based methods, which make use of wear-related alternations of the electro-thermal parameters as an indication of the health state of power electronic components. The parameter alternation is induced by changes in the material that occur at the interconnection-level, which enables the use of them as indicators of the degree of component degradation. The commonly used health state indicators in power devices compromise the on-state saturation voltage and the junction-to-case thermal resistance. The monitoring of the indicators can be used to assess the amount of consumed life by comparing the acquired data with models that inform of the trivial degradation trends [103]. The presence of uncertainty is then dictated by the amount of degradation variation recorded in a population of components, but this is not considered as being a severe issue in connection with physics-of-degradation-based methods, as the use of in situ monitoring enables the continuous reevaluation of the particular degradation event. The overall procedure of continuously updating the residual life distributions is illustrated in Fig. 3.1 [**C3**]. It summarizes the fact that all the components will not degrade at an identical rate and mode of behaviour, which leads to prediction uncertainty. Nevertheless, as time progresses, the degradation trend of any unique case will become increasingly transparent as the defined degradation limit is approached and the residual useful life can be stated with progressive precision. The end-of-life (EOL) criterion, i.e. the defined degradation limit, is chosen by reckoning a certain degradation margin with respect to the component destruct limit

The current physics-of-degradation-based lifetime predictions are limited to cover one single type of component or a single individual component [41, 54, 64]. Considering of the application level, the degradation will most likely take place on collective components altogether due to the occurrence of diverse types of parameter shifts, which all contribute to the complete converter degradation. It will undoubtedly be an exhaustive process, if not downright impossible, to monitor each single component functioning in the power converter. It is, therefore, beneficial if the health status of the entirety of the

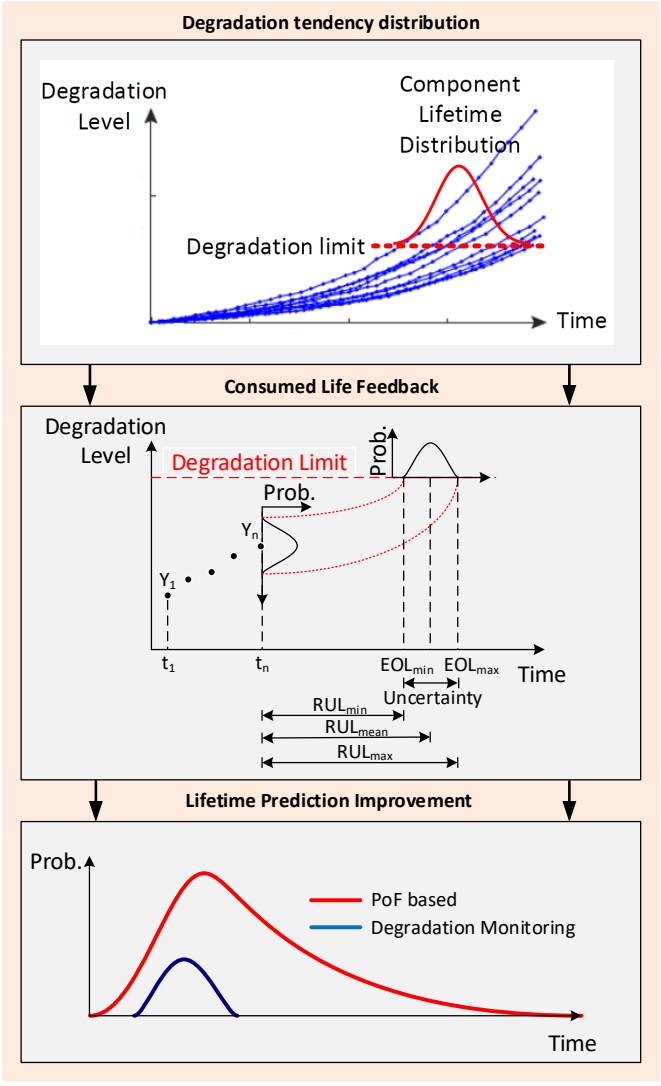

Fig. 3.1: Lowering the amount of variance within the lifetime distributions by continuously evaluating the component degradation while concurrently reconsidering the residual useful life. Y_i is the monitored signal, RUL_x is the remaining useful life and EOL_x is the time when the unit reaches end-of-life **[C3]**.

converter is monitored by the use of converter-level signal measurements. This chapter proposes a method that makes use of the converter efficiency as a health state precursor, which can lead to improved precision when stating the useful life of any unique power converter. Subsequently, an end-of-life criterion that is founded on the rate-of-change is presented. The criterion can be used for maintenance scheduling of power converters in a considerable assortment of applications and thereby help to raise the asset availability as a result of lowering the downtime and no-faults found maintenance [**C3**].

3.1 Application Level Health Precursor Framework

With the aim of clarifying the usefulness of the proposed method used for health assessment, each successive step required to carry out the analysis is granted in the form of a case study throughout the entirety of the analysis. The study is founded on the 4 kW solar-based generation unit labelled PV#1 in Fig. 2.2, in which the power processing is accomplished using a dual-stage PV inverter, as presented in Fig. 3.2 [**J1**]. The inverter embodies three over-

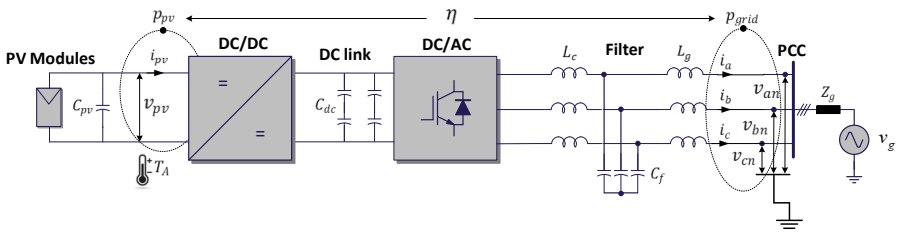

Fig. 3.2: A solar-based generation unit rated at 4 kVA is used for the case study in the degradation-related studies throughout this Thesis. η denotes the efficiency when considering the power losses that occur between the noted input power p_{pv} and the output power p_{grid} [**J1**].

all stages, which each further embodies congregations of multitude power electronic components [**C3**]. The specific types of components in which parameter shifts are considered are the active power switches, the power diodes, and the DC-link capacitors. The adopted allowed individual parameter shifts are defined based on the existing studies of component degradation [63]. The general consensus of these studies is that the parameter shifts correspond to a 20% increase in the on-state voltage and forward voltage of active power devices and power diodes, respectively. When the values exceed the specified limits, the respective components are considered to lose the ability of their primarily function. Further parameter shifts will start to occur at a rapidly increasing pace until the imminent state of abrupt failure occurs. The DC-link capacitors are assigned an allowable ESR increase of 300% before reaching their defined end-of-life state, which conforms with the literature [47].

The number of components that complete each stage of power conversion, including each respective parameter drift limitations, are outlined in Table 3.1 [**C3**]. The converter input power p_{pv} and the instantaneous synchronous

Table 3.1: The number of considered power electronic components at each conversion stage and their respective assigned parameter shifts when reaching EOL [**C3**]

Component type	Boost	DC link	Inverter
Power Switches (20 % increase in $V_{CE,on}$)	1 unit	-	6 units
Power Diodes (20 % increase in V_F)	1 unit	-	6 units
Capacitors (300 % increase in ESR)	-	4 units	-

reference frame AC output power are simulated and noted for the case of non-degraded components. Subsequently, identical simulations are carried out but with small increments of parameter shifts, i.e. increasing amount of degradation, until their respective degradation limits are reached, with the purpose of inspecting if any detectable decrease in conversion efficiency will occur, which could lead to further analysis, which in fact was the case.

3.1.1 Methodology

With the observation of a detectable efficiency change of the unit at hand, in the event of simultaneously occurring parameter shifts, the procedure on assessing when the end-of-life of the unit is reached is now relevant to define, as presented in Fig. 3.3 [**C3**]. First, the efficiency needs to be characterized for each defined operating and health state condition, which will provide the ability to compute the instantaneous, expected efficiency regardless of the environmental and operating conditions subjecting the unit. Then, by use of the familiarity of the typical degradation models, some distinctive degradation bounds can be stated, which in combination with the present operating condition, ensures that the bounds are sorted according to that specific condition. The degradation bounds are continuously compared with in situ efficiency monitoring, and the fraction of sample points that intersect the bounds are compared with those of the preceding 30-day interval. When the rate-of-change of the number of sample points that intersects the bounds reach a defined upper limit that is established based on the awareness of the typical degradation tendency, the planning personnel will be informed, as the instant for maintenance action has arrived. Each of the successive steps will be detailed in the following sections.

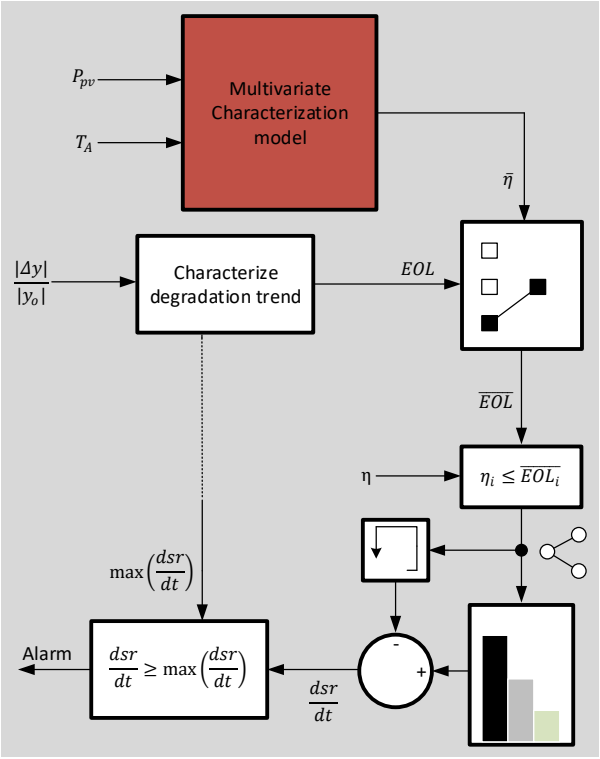

Fig. 3.3: A flowchart that outlines how to evaluate when power converter units end-of-life state is reached, based on share-rate of observations that intersects the defined degradation bounds. P_{pv} is the input power, T_A is the ambient temperature, Δy is the relative change in efficiency, y_o is the efficiency using non-degraded components, $\overline{EOL}$ is the expected efficiency, n_i is the measured efficiency sample points, sr is the rate of change of sample points being within the defined degradation bounds, i.e. acceptable, linear and non-linear degradation bound **[C3]**.

3.2 Converter Characterization Modelling

In this section, the aspects that indirectly permit operating efficiency as a health precursor are briefly characterized. The central theme is to take advantage of the fact that the power conversion will turn less efficient as the power electronic components degrade, and an end-of-life criterion can be defined based on the degraded efficiency. There are numerous aspects that impact the operating efficiency of the PV inverter, and with the omission of the degradation-related aspects, these aspects are considered as external aspects that are required to be described so that the specific efficiency change that is purely due to the degradation can be obtained and exploited for health-state monitoring purposes **[C3]**. The remaining external aspects that affect the efficiency comprises the loading and the operational temperatures of the

considered components, as outlined in Fig. 3.4. The frequently used wear-

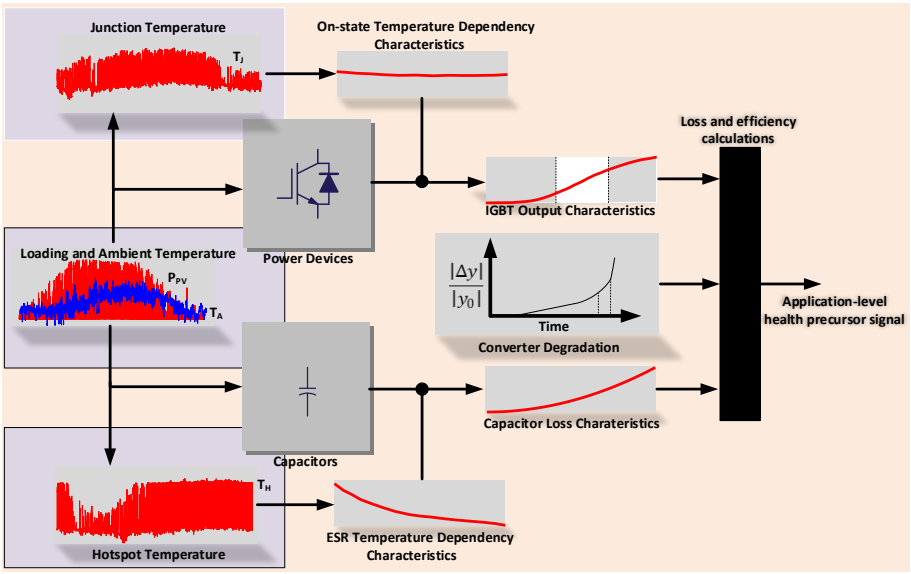

Fig. 3.4: A flowchart that outlines the characterization model of Fig. 3.3 for the active power devices and the capacitors in order to gain the health and operational dependent efficiency of the PV-converter.

out signals of the active and passive power devices, i.e., the on-state voltage and forward voltage, will both affect the dissipated losses. The examined power loss P_{Loss} can be segregated into the following six classes; the switching loss P_{SW} and the conduction loss P_{Cond}, which are both produced by the passive and active power devices, the ESR losses P_{ESR} of the DC-link and AC filtering capacitors, the gate charge losses P_{Gate}, and the magnetic copper loss P_{Copp} of the filter inductors [**J2**]. In this study, it is assumed that the passive and active power devices, as well as the DC-link capacitors, i.e. the conversion stages, are exclusively subjected to parameter drift, implying that the mentioned components are solely responsible for lowering of efficiency. The remaining losses, apart from the iron losses of the magnetics, are treated but are assumed to remain the same for the duration of the entire life-cycle of the converter. Fig. 3.5 outlines the classification of the power loss components, where the use of red color designates the components for which the occurrence of parameter drift is studied. The mathematical relationship between the power loss components, which are presented in Fig. 3.5 forms the following expression [**J2**].

$$\begin{aligned} P_{Loss} &= P_{Gate} + P_{SW} + P_{ohm} \\ &= P_{Gate} + P_{SW} + P_{Cf} + P_{Copp} + P_{Cond} \end{aligned} \tag{3.1}$$

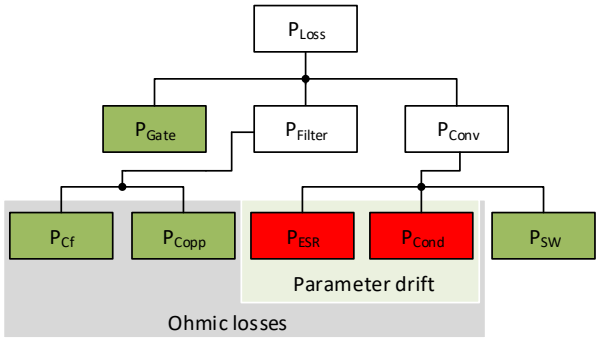

Fig. 3.5: Power loss classification, where the red color denotes the components considered for parameter drift as the components degrade. P_{Conv} is the total loss at the conversion stage that comprise the losses of the ESR in the DC-link capacitors P_{ESR}, the conduction losses of the power diodes and active power devices P_{cond} and the switching losses P_{SW}. P_{Filter} is the total loss dissipated in the AC filters, and P_{Cf} debits the combined losses caused by the ESR damping resistance of the filter capacitors. The copper losses of the filter inductors are denoted P_{copp}. Finally, P_{Gate} comprises the gate losses of the gate driver circuit **[J2]**.

where the ohmic losses P_{ohm} is originated in the power circuit and are proportionate to the squared RMS current. It is split among the respective losses of the ESR P_{ESR} and the damping resistance P_{Cf}, the copper loss P_{Copp} and the conduction loss P_{Cond}.

In the case of active power devices, the losses exhibit multivariable dependency, including load current, junction temperature, and on-state voltage, which can be described as **[C3]**.

$$P_{loss} = f(I_c, V_{CE,on}, T_J) \tag{3.2}$$

This multivariable dependency also implies that a single-valued threshold based on the efficiency reduction is of no use. Initially, the output characteristics are summarized for units being in their "out-of-box state," i.e., perfectly healthy units, according to the data of the manufacturers. Subsequently, the component-level health condition indicators are regulated in terms of the slight incremental increase until the defined degradation boundaries, which are listed in Table 3.1, are fulfilled **[J2]**. Concerning the non-ageing aspects that affect the efficiency, the output characteristics of the active power devices and power diodes are shown in Fig. 3.6. As it can be understood from observing Figs. 3.6(a) and 3.6(b), some of the distinct domains display practically linear relationships, but also some that are highly non-linear. The particular domains will affect the operating efficiency to different degrees, such as the domain that demonstrate an almost linear proportional relationship will be unresponsive to any load transitions. Unfortunately, the load circumstances

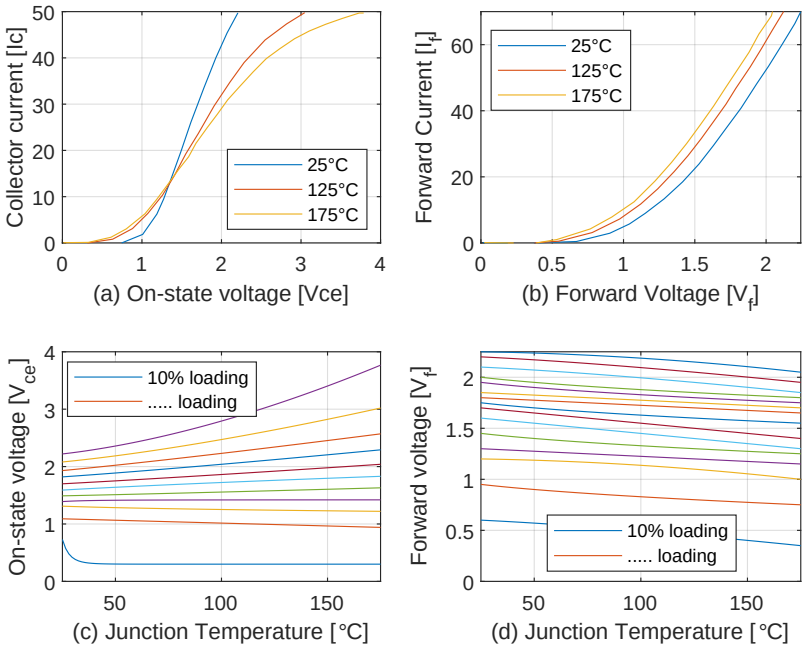

Fig. 3.6: The output characteristics of the active switches and the power diodes blueprints the efficiency dependence on the loading and the temperature. The temperature dependency is given for 25, 125, and 175 degrees, whereas the loading dependency is shown from ten percent to full load in steps of ten percent. (a): output characteristics of the active switches. (b): output characteristics of the power diodes. (c): The on-state voltage dependence on temperature. (d): The forward voltage dependence on temperature. **[J2]**.

within renewable generation are of high variety, which implies that the loading influence on the efficiency needs to be portrayed due to the fact that the operating conditions will both be governed in the linear and non-linear tendency domains **[C3]**. In Fig. 3.7, a typical load distribution that subjects the solar unit is presented. This particular load distribution is obtained when the unit used for the case study is exposed to some annual environmental settings collected from the Aalborg University weather data logger. It is quite obvious when inspecting Fig. 3.7, that the unit will function in its full range of operation modes, and despite the chosen design margins, the switches will function in one of the two high or low-loading domains, that display the highly non-linear relationship **[C3]**. The loading of the unit can be obtained using the solar irradiance and ambient temperatures confined in the environmental profiles by the correlation presented in Equation 2.2 in Chapter 2. As a result of the multivariable dependency of the power devices, the output characteristics are mapped by means of a 3D lookup table, as illustrated in Fig. 3.8, where I_C announce the localized loading and T_J is the device tem-

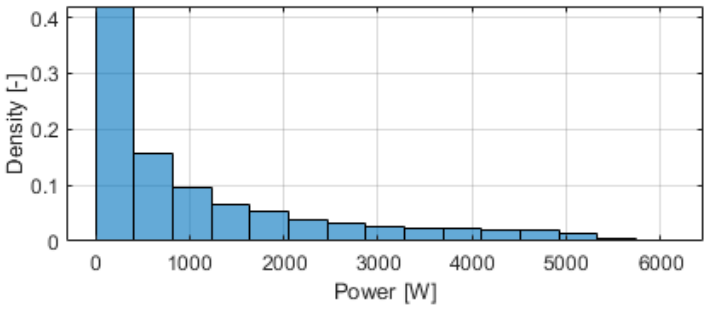

Fig. 3.7: The obtained PV array output power distribution when subjected to an annual mission profile collected at the Aalborg University weather station **[C3]**.

perature. The applied loading is subsequently decomposed into the distinct

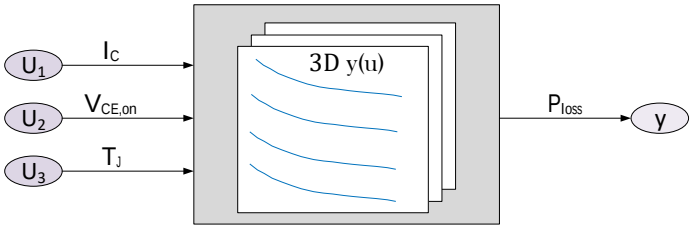

Fig. 3.8: 3D lookup table used to map the output characteristics of the active power devices of the DC/DC and DC/AC stage converter **[J2]**.

component loadings by means of a developed full-scale PLECS simulation model, and from the enforced loading stress and the ambient temperatures of the time series mission profile, the device junction temperature can be acquired by the use of **[C3]**.

$$T_J = P_{Loss}(IGBT) \cdot Z_{th(j-c)} + (P_{Loss}(IGBT) + P_{Loss}(Diode)) \cdot Z_{th(c-a)} + T_A \quad (3.3)$$

where $Z_{th(j-c)}$ announce the thermal impedance of the power module whereas $Z_{th(c-a)}$ announce the thermal impedance of the external cooling network. As outlined in Section 2.3, the models of the external and internal parts of the module differ from each other, i.e., the model of the internal layers is strictly created based on the measured thermal responses, which is described by a Foster type network. By the use of the Foster model, each of the internal module layers is described by a parallel configuration of the thermal resistance and the thermal capacitance that portray the transient temperature attributes **[C3]**. In contrast, the external network's thermal impedance is

modeled using a Cauer network. For righteous and credible use of Equation 3.3, the complete thermal tendency must be described by use of one single network of uniform type, which is not the default case. The connection of the external Cauer-type network with the internal Foster-type network would alter the thermal characteristics of the internal layers and therefore lead to incorrect thermal stress **[C3]**. This issue can be resolved by executing a Foster-to-Cauer transformation of the thermal parameters representing the internal layers or alternatively by applying the dual-network described in Section 2.3. The thermal parameters of the internal layers and the thermal grease are provided in the particular manufacturer datasheet. In contrast, the thermal impedance of the heatsink is decided based on application requirements, in particular, the maximum desired junction temperature. It is worth recognizing that an identical methodology applies to the case of power diodes, where the forward characteristics are also summarized by means of lookup tables.

When considering the usage-related degradation of the electrolytic DC-link capacitors and their respective contribution to the reduction in the converter performance, the long-term alternation of the ESR will influence the dissipated losses, which can be calculated as

$$P_{Loss,cap} = ESR(T, f) \cdot I^2_{RMS}(f) \tag{3.4}$$

where $I^2_{RMS}(f)$ announce the RMS value of the ripple current components and T denotes the hotspot temperature of the capacitor. It is obvious from the expression that the capacitors display a polynomial loss trend, as shown in Fig. 3.9, which implies a distinct sensitivity to the applied loading, which is therefore required to be portrayed. Another evident fact, when observing ex-

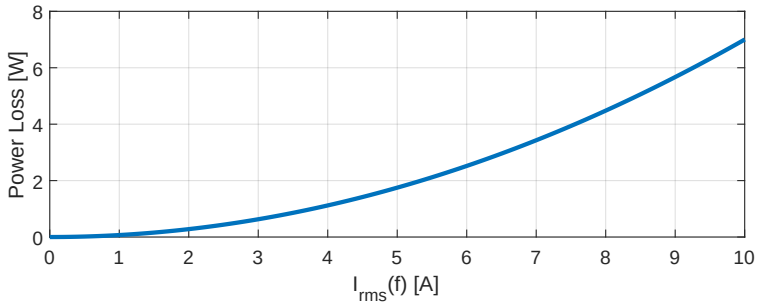

Fig. 3.9: The polynomial loss development of the capacitor **[C3]**.

pression (3.4), is that the ESR does involve some temperature and frequency reliance, which are presented in Fig. 3.10(a) and Fig. 3.10(b) respectively. As shown in Fig. 3.10(a), the ESR exhibits a decreasing trend as the frequency

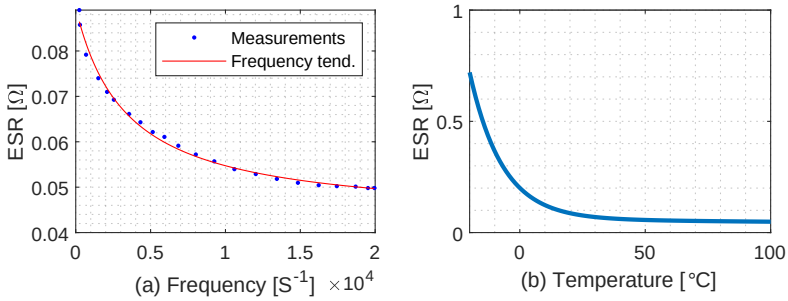

Fig. 3.10: (a) and (b): Adaption of the respective frequency and temperature dependency of the equivalent series resistance in the studied DC-link capacitors, which both exhibit a decreasing tendency as the frequency and temperature is increasing **[J2]**.

increases. This decrease in the ESR value is even more evident with the increase in temperature, as seen in Fig. 3.10(b), which depicts an approximately generalized trend for electrolytic capacitors. The temperature data originates from [104], but is normalized and adapted to the particular capacitor used for the case study by means of arranging the normalized trend so it has the same ESR value at 25 degrees as the one listed in the datasheet of the specific capacitor used for the case study **[C3]**. Still, these distinct reliances are accounted for due to their influence on the extent of dissipated losses in the DC-link capacitors. In respect to the frequency reliance implementation when computing the power loss, the ripple current components are extracted using an FFT analysis, in which the predominant components are proven to be multiples of the practiced switching frequency and the matching sidebands, for this particular case, that makes use of active switches on both the input and output side of the DC-link. Lastly, the hotspot temperature of the capacitors can be obtained by use of the acquired power loss and thermal resistance as **[C3]**

$$T_h = T_A + \sum_{i=1}^{n} [ESR(f_i, T_i) \cdot I_{RMS}^2(f_i)] \cdot R_{th} \tag{3.5}$$

where T_h is the hotspot temperature, T_A is the ambient temperature, and R_{th} is the thermal resistance, which can be split into two different contributions as given **[C1]**

$$R_{th} = R_{th(h-c)} + R_{th(c-a)} \tag{3.6}$$

where $R_{th(h-c)}$ represents the thermal resistance from the hotspot to the case, whereas $R_{th(c-a)}$ represents the thermal resistance from the case to the ambient and for which numerical values can be found in [104] for a large variety of

capacitors. It should be noted that the thermal capacitance is not accounted for when computing the thermal stress of the capacitors. This is regarded as being entirely legitimate because electrolytic capacitors exhibit some relatively large thermal time constants when considering the sampling frequency of the ordinarily used mission profiles. There are, therefore, no issues with respect to catching all the temperature information [105].

It might seem like an exhaustive process to map all the loss characteristics that include several reliances. However, in fact, each of these reliances is associated, e.g. the aspects that affect the losses, such as the temperature and degradation influence, can be accounted for by altering the on-state voltage. Furthermore, as it can be understood by observing Fig. 3.4, every single tendency can be trailed back as being a function of the applied loading P_{pv}, and the ambient temperature T_A, which means that those two variables are solely required as model inputs [**C3**].

To get a sense of to which degree the degradation influences the component losses and at which share each unique parameter influences the lowering of the efficiency, a power loss breakdown will now be studied. The electrical parameters that characterize the AC filter and the gate driver circuit are provided in Table 3.2, and the results of the power loss breakdown are revealed in Fig. 3.11 [**J2**]. As it can be understood by inspecting Fig. 3.11, the conduc-

Table 3.2: The electrical parameters of the AC side filter and the gate driver, which influence the power loss of the converter [**J2**].

Power rating	P_{rated}	4 kW
Switching frequency	f_{sw}	10 kHz
Filter resistance	R_f	0.2 Ω
Filter resistance (grid side)	R_{fg}	0.1 Ω
Damping resistance	R_d	1 Ω
Total gate charge	Q_g	0.395 μC

tion losses of the power devices answers for the greater part of the efficiency alternation by being responsible for roughly one-third of the total power loss that the converter generates in its degraded state. This one-third share is on the larger side of a 7% addition of its respective share in relation to its share in the non-degraded state [**J2**]. Furthermore, the power loss involvement, due to the degradation of the DC-link capacitors do, also demonstrate a considerable shift by even exceeding a duplication of its engagement in the overall power loss. Lastly, the wear-affiliated degradation is modelled by means of adding an incremental enlargement of the ESR until it attains the defined parameter shift limit criterion given in Table 3.1 [**J1**].

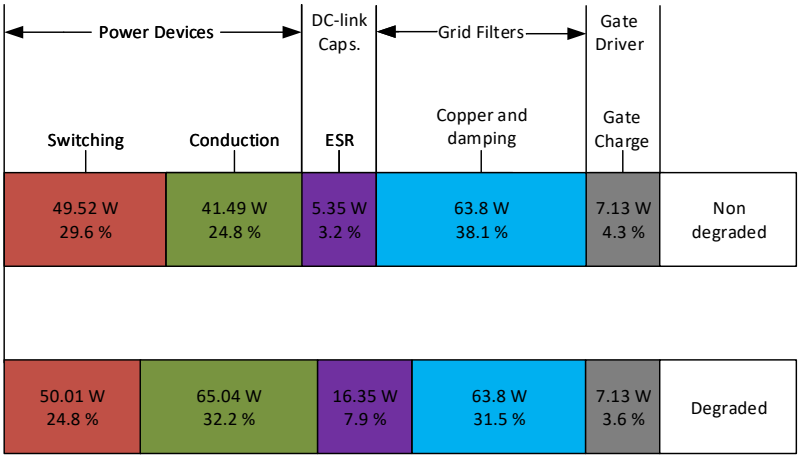

Fig. 3.11: Power loss breakdown for the non-degraded and degraded states of the components considered for parameter drift. The power loss breakdown is conducted at 6 kW, 10 kHz operation [**J2**].

Attributed to the loss portrayal and degradation modelling, the long-term efficiency response can be evaluated based on real-field mission profiles as a means to imitate realistic operational usage [**J2**]. Moreover, independent of which conditions enforce the unit, the efficiency can be acquired for any given health state, as illustrated in Fig. 3.12, where one distinct operating condition is proved to result in two different efficiency responses due to diverse health states [**J2**]. The earned possibility of gaining the efficiency response regardless of operating condition and health state permits the option of creating multifaceted datasets required for the design of the condition monitoring algorithms [**J2**].

3.3 End-of-life detection

The primary intention of this section is to demonstrate how the trends of the converter degradation can be practiced for the definition of an end-of-life criterion and then expand this knowledge to gain a procedure which indicates when the converter enters its end-of-life state. At first, data that chronicles the evolution of the respective component parameter shift of the $V_{CE,on}$ and the ESR are gathered and presented. Both types of component data exhibit exponentially increasing trends as degradation occurs, which can be modelled by simple data-fitted functions and exploited in the following studies. The $V_{CE,on}$ is normalized and presented in Fig. 3.13 [**C3**]. It is worth mentioning that due to the inadequate sample size required to rightfully conduct the

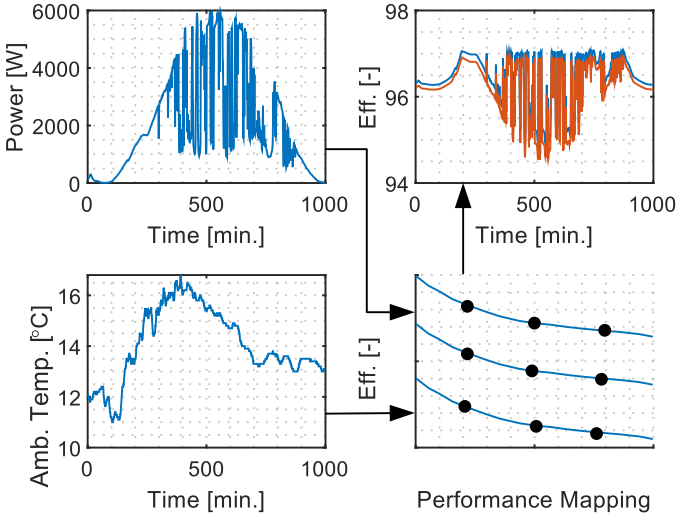

Fig. 3.12: Enabling the computation of long-term efficiency responses using performance mapping of each operating and health condition. Two different efficiency responses are shown in the top right plot, where the blue curve designates the efficiency response of a healthy unit, and the red curve designates the efficiency response of a degraded unit. The two upper and lower left side plots designate the conditions that subject the unit, which are the same for the healthy and degraded case [**J2**].

presented procedure, some common failure distributions of power devices and capacitors were developed and used as an aid in conducting the study. The single actual collected degradation data of each respective component will serve as the B_1 values of the multi-sample time-of-failure distributions. This is done by associating the respective B_1 values of the power devices and the capacitors with the insights in their distributions' specific, frequently acquired shape factors. These respective shape factors are gained from the existing research [53,88] and is known to have a value of 3 and 4, respectively. Making the assumption by employing these shape factors results in the distributions shown in Fig. 3.14, that details a certain amount of variance, which these components exhibit in terms of when a population reaches their respective degradation limits [**C3**]. With the intention of creating some realistic degradation data, 15 random values are extracted from each of the distributions shown in Fig. 3.14 in order to gather some useful sample variance of the time-to-failure according to the defined end-of-life criteria [**C3**]. Also, a variance in the order of 20% is admitted at each progressing time step of the matching degradation functions. This continuously included randomness guarantees that the degradation tendencies vary throughout the entire life span and not only at their respective times of reaching the defined degradation limit. In other words, it prevents a degradation data representation of 15

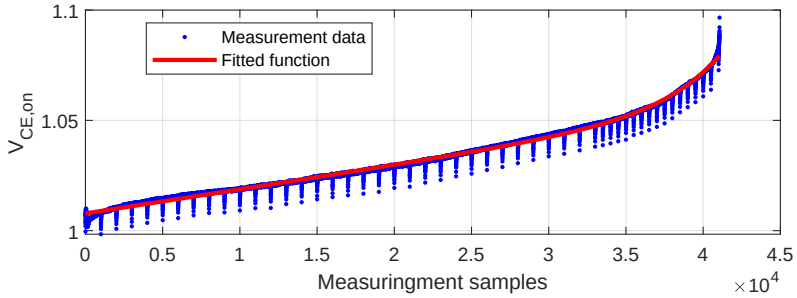

Fig. 3.13: Experimental data outlining the normalized tendency of $V_{CE,on}$ as the power device degrades **[C3]**.

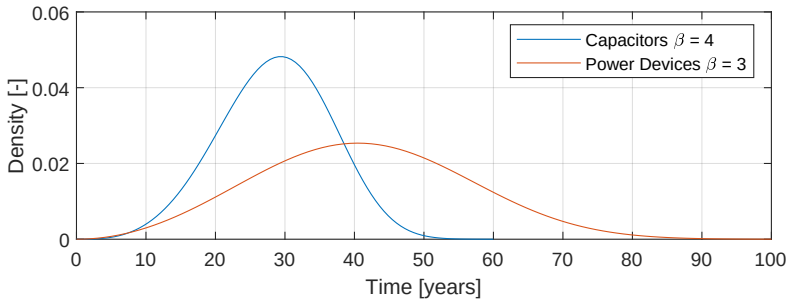

Fig. 3.14: Failure distributions rooted in the shape factors from actual studies and are assumed to have a B_1 of approximately ten years each. These are computed in order to get some time-to-failure variance and thereby obtain some realistic degradation data **[C3]**.

equally shaped curves with only their time-to-failure differing. The resulting sample of the degradation functions of the on-state voltage is shown in Fig. 3.15 **[C3]**. The exact same methodology is practiced in order to develop samples of the degradation functions of the ESR of the DC-link capacitors, and from each of these populations of degradation functions, a mean degradation trend and a corresponding confidence interval are computed. The confidence interval relies upon the sample spread and the sample size, as exemplified in Fig. 3.16 **[C3]**. This mean degradation trend in association with the characterization model is used as a foundation for stating some constrained converter degradation bounds, which will eventually help reveal the converter health state. First, the first-order derivative of the average degradation curve is computed to gain insight into how large a share of the entire parameter shift takes place at a linear development, which constitutes a domain where the efficiency alters linearly. This domain naturally needs to be quantified in terms of confidence intervals, as the proportion of the total efficiency change

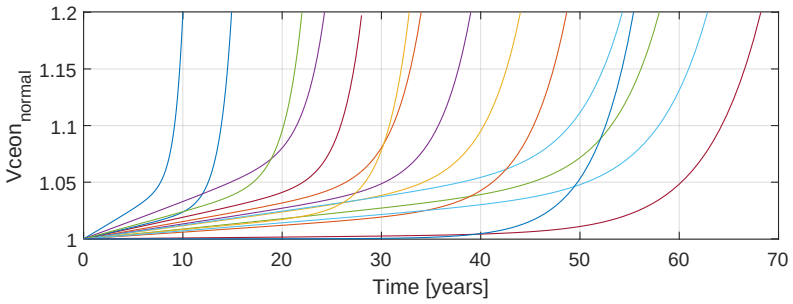

Fig. 3.15: Degradation functions that are obtained based on a single case of experimental data, for which a β value of 3 and random continuous function variance is assumed to characterize the degradation tendency of multiple units **[C3]**.

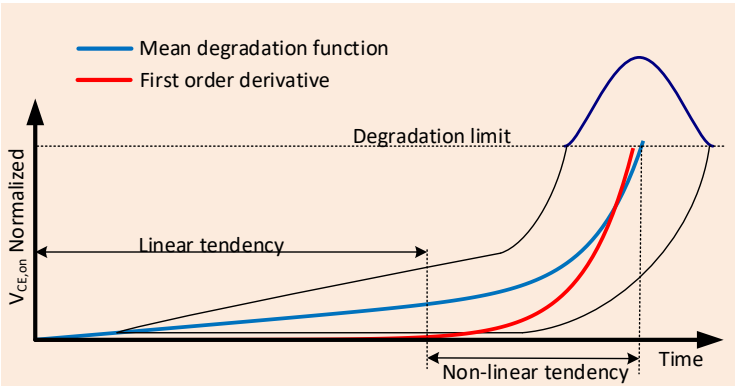

Fig. 3.16: The mean degradation tendency, including the distinct regions, which can be characterized by the difference in the pace of deviation with respect to the initial parameter value of the on-state voltage of an IGBT **[C3]**.

that occurs in the linear domain differs from sample to sample. The width of the confidence interval depends on the number of accessible degradation functions, i.e. the larger the sample size, the narrower the resulting bound can be gained, and the confidence bounds will align more with the defined degradation bound as exemplified in Fig. 3.17 **[C3]**. Fig. 3.17 shows the rough efficiency change admissible for each loading condition, where the green-to-red boundary separates the safe operational area and the end-of-life area. Still, the efficiency shift obtained through the characterization assumes that the components experience the same amount of degradation, which causes a specific efficiency change. This assumption will be more authentic in cases of high sample sizes due to the relatively higher confidence **[C3]**.

Finally, the combination of the mapped data information gathered through

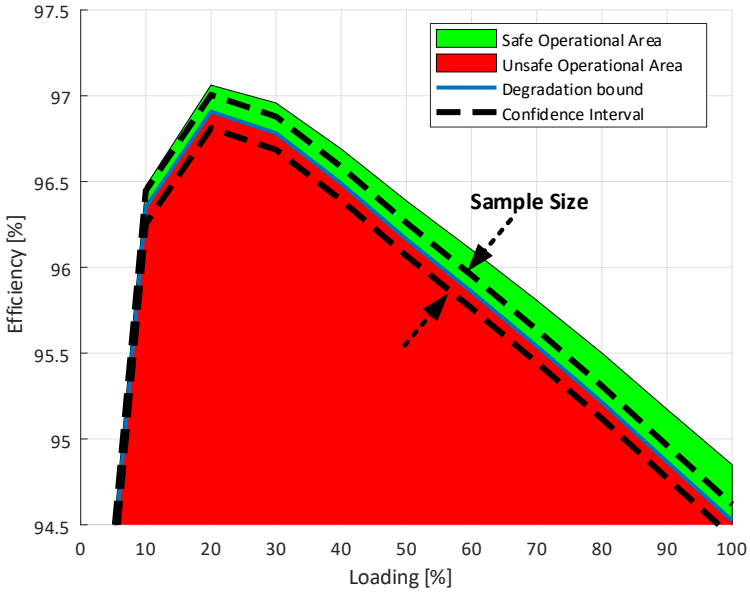

Fig. 3.17: The safe operational area of the PV system shown in 3.2 and its dependence on sample size in terms of locating the confidence bounds closer to the degradation bound illustrated by the arrows pointing towards the degradation bound [**C3**].

the characterization and the obtained typical degradation trend will serve as the basis for choosing the degradation bounds presented in Fig. 3.18 [**C3**]. It shows the instantaneous efficiency when the converter is subjected to the daily loading profile that is shown in Fig. 3.19, along with the linear degradation bound and the end-of-life bound [**C3**]. It can also be understood by observing Fig. 3.18 that the assigned bounds continuously accommodate the subjected loading and environmental conditions, which is enabled by characterizing the PV converter efficiency for a set of input power and ambient temperature as illustrated in 3.12. In Fig. 3.18, the non-degraded efficiency response, with supplementary white noise, is modelled with the intention to mimic a genuine monitored signal. The coinciding bounds are rooted in the typical degradation trends presented in Fig. 3.16 [**C3**]. The region bound that represents the linear deviation from the initial parameter shift is based on the extent of parameter drift that has occurred when the mean degradation curve, i.e. the blue curve, passes the point where it no longer diverges from its initial value at a linear rate. This specific linear range is selected based on when a noticeable change in the first-order derivative of the mean degradation curve, i.e. the red curve, is observed. Once more, it is important to note that as a result of the unavoidable difference in when the linear deviation ends for a population of units, it is required to include a matching confidence level

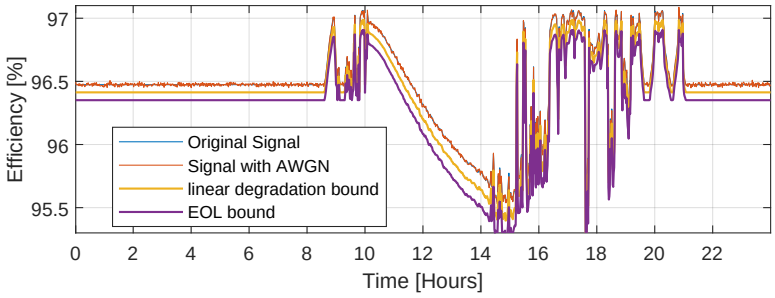

Fig. 3.18: The non-degraded instantaneous efficiency response and its corresponding degradation bounds that are constituted on the basis of the mean degradation tendency. AGWN is additive Gaussian white noise that is added to the efficiency signal in order to mimic genuine monitored signals **[C3]**.

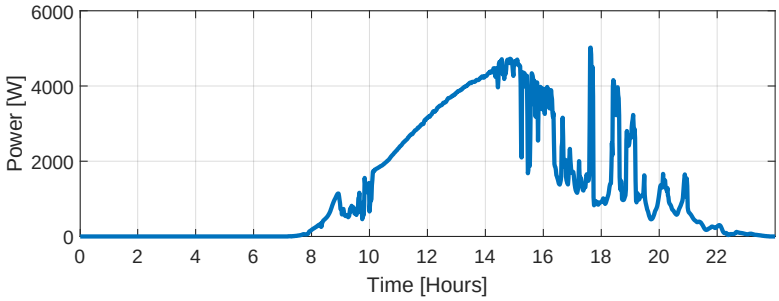

Fig. 3.19: The instantaneous power profile, which results in the corresponding efficiency response that is presented in Fig. 3.18 **[C3]**.

of, e.g. confidence of 95% **[C3]**. The specified end-of-life bound resembles the state where the converter reaches its degradation restraint based on the combined component degradation. It is also worth noting that an efficiency offset value is assigned strictly during no-load conditions as this prevents the monitored signal from reaching the level of the end-of-life bound at this specific operating condition. This is regarded as preferable with respect to the computational load required with the removal of all observed data instants at the no-load condition afterward.

As a result of being concerned with the noisy monitoring signals, it would be non-optimal to establish the present efficiency-based health state based on absolute values. Alternatively, the contribution of samples surpassing the

bounds is used for end-of-life detection as

$$\sum_{i=1}^{n} \eta_i \leq E\bar{O}L_i \tag{3.7}$$

where n denotes the extent of monitored samples collected during a 30-day interval, η_i is the sample value of the monitored efficiency, and EOL_i is the sample value of the ith expected degradation bound. The division of the sample proportions within each region is sorted as presented in Fig. 3.20 [**C3**]. The previous 30 days sample separation is compared with the present 30

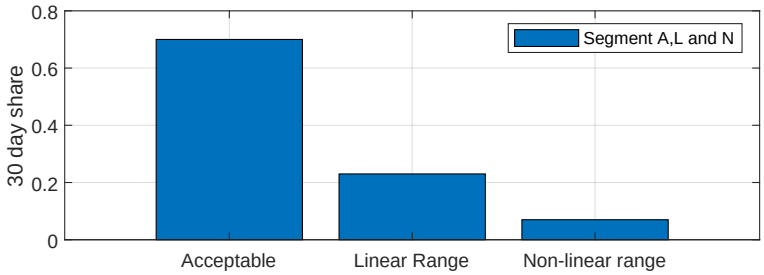

Fig. 3.20: Bar plot depicting a random amount of sample proportions, which are situated within each of the regions, that is confined by the defined degradation bounds [**C3**].

days, and at the time when the share rate sr of sample proportions conforms with the specified maximum rate-of-change, the end-of-life state is reached. The maximum rate-of-change of degradation is chosen based on insights into how much the health indicator is expected to change when considering the first-order derivatives of the component degradation trend functions when they reach their defined limit. The rate-of-change of efficiency can be linked to a certain amount of change in the percentage of samples contained in the non-linear range bar of Fig. 3.20 compared to the prior 30-day monitoring period. The end-of-life criterion can be expressed as

$$\frac{dsr}{dt} \geq max\left(\frac{dsr}{dt}\right) \tag{3.8}$$

When this change in sample proportions crossing the end-of-life bound is reached, the maintenance personnel will be alerted. This alert notification signifies that the time of unit replacement has arrived, with the intention of preventing an induced system risk in case of unit downtime. It is worth mentioning that it is required to apply correction factors to the sample proportions when applying the presented procedure. This is due to the unevenness in the allowable efficiency change depending on the different loading subjecting the unit, which is shown by the difference in the width of the green area

in Fig. 3.17. Furthermore, due to the variability of the seasonal loading, i.e. the available solar power, the mean difference between the monitored signal and the defined bounds will differ, which will influence the share of sample proportions that surpasses the bounds. Therefore, the exclusion of correcting for the variation in the applied conditions can result in either an over or under-estimation of the current health state of the unit. Therefore, it is highly recommended that their influence is weighted using the loading conditions distribution of the past 30 days. Ultimately, the procedure presented here can be improved when merged with the methodologies presented in the following chapters. Still, this chapter has its high relevance as the efficiency characterization modelling presented in this chapter is the entire foundation that enables the methodologies presented in the following chapters.

3.4 Summary

Extensive work has been conducted in the pursuit of estimating the lifetime of power electronic converters when they are exposed to application-dependent mission profiles. However, the methodologies used in the current studies involve a fair amount of uncertainties that result in the outcome being stated in terms of a distribution that exhibits a variance of several years. The primary cause of uncertainty is associated with the procedure of basing the failure fatigue models on extrapolating the accelerated test results to different usage conditions. The issue with this is that the actual application usage profiles are highly varying, which is in stark contrast to the accelerated tests, which are often executed at a few distinct constant loading conditions. As a result of significant distribution spread, the lifetime prediction eventually ends up having inadequate accuracy when predicting failures of unique units.

In order to achieve some reduction in the prediction uncertainty, the incorporation of physics-of-degradation-based methods seems promising as they can assess the current state of the unit by taking advantage of the drift in the electro-thermal parameters associated with the degradation occurrence. The severe limitation of the existing physics-of-degradation-based useful life predictions is that they are limited to cover only single components. It would most certainly be tedious, if not impossible, to monitor every single component present in power converters. It is therefore fundamental to gain an application-level health precursor. This chapter has presented a procedure in which the operating efficiency is exploited in order to indicate the present health state of the unified converter. The procedure exploits the combination of the awareness of the impact of the usage and environmental conditions on the instantaneous efficiency and the average degradation tendencies.

The merging of these two distinct models permits the opportunity to define some degradation bounds that can guarantee safe operation and which are adjusted to the actual conditions that impose the unit. Lastly, a procedure was introduced which uses the rate-of-change of the monitored samples that surpasses the defined end-of-life bound, with the intention of detecting the end-of-life state with more confidence. Combining this method with the methodologies concerning dynamical useful life estimations and absolute value end-of-life detection presented in the subsequent chapters can lead to a decrease in the prediction uncertainty. This is due to the increasing transparency of a particular degradation event, which will distinguish itself from the remaining population degradation patterns as time passes and the end-of-life state is imminent. Lowering the amount of uncertainty associated with lifetime predictions will help to advance the system availability by preventing failure-related downtime and no-fault-found maintenance. The methodologies of the subsequent chapters build upon the content presented in this chapter.

Chapter 4

Online Risk Evaluation Using Sensor-based Updated Residual Life Distributions

An efficient method to overcome the issues mentioned in Chapter 3, which are related to the PoF methodology, is the utilization of the condition monitoring procedures. This enables the exploitation of the fact that a degradation curve uniformly contains more information than one single-point end-of-life prediction measure gained through an empirical lifetime model [41]. As explained in Chapter 3, the incoming sensor data of condition indicators can be practiced in relation to conduct reliability strategic decision-making in order to gain improvements in fields such as maintenance operation. This can aid in reducing the LCOE, which is due to maintenance and operation costs. As previously mentioned, the occurrence of interruptions causing unforeseen downtime is often costly, as this results in energy not being distributed [10].

The following Chapter builds upon the efficiency-based application-level condition signal presented in Chapter 3, indicating the health state of the converter presented in Fig. 3.2. The continuous data stream of the condition sensor is then used to accurately model how the degradation process evolves with time, with the main functionality of continuously updating the residual life distributions. These distributions are then used to provide the needed information to the operation and planning personnel, which can continuously update the risk-based decisions, which is the basis of replacement policies and maintenance management in power electronic-based generation systems. The method proposed in this Chapter can aid in reducing the arranged maintenance and extend the maintenance cycles and thereby preserve

efficiency timely repair in contrast to the existing risk evaluation procedures, that is based solely on static predictions.

4.1 Online Risk Evaluation Framework

In this Section, the framework of the method, which is able to continuously evaluate the risk of losing the load promoted by power electronic-based generation units, is presented. The method merges the distinct sensory data of power converters and the degradation trends of a population of units in an effort to evaluate the degradation process of a single unique unit. By the use of this method, the ability to process the residual life distributions at each single collected sensor-data sample is gained. The Weibull distribution parameters can be estimated from the gained distributions, which is a requirement, when evaluating the risk. The study is a continuation of the content presented in Chapter 3, and it is based on the case using the solar-based generation unit shown in Fig. 3.2, which makes use of the power devices found in [106] and the capacitors found in [107]. Analogues to the previous chapter, the considered component parameter shift involves the capacitors, the active power devices, and diodes. The power losses associated with these occurring parameter shifts are once again leveraged with the purpose of estimating the health state of the converter as its operating efficiency decreases as the aging process evolves.

The framework that is used in association with this method, is illustrated in Fig. 4.1, which consists of three main parts. These parts include the modelling and loss characterization presented in Section 3.2. It also includes the identification of the valuable features of the raw signal which acquires the physical transformation that takes place as the converter degrades. Appropriate models can be established based on the identified features using the common patterns that govern the specific sensor-data feature. Specifically, this comprises the determination of a suitable model and subsequently applying sets of historical degradation data to gain the prior parameters, i.e. the first iteration of the degradation model parameters. The models can then be utilized to estimate how the degradation evolves and later assess the degradation evolution as the converter-specific sensor data arrives. The methodology utilizes a stochastic degradation model that can compute and continuously reevaluate the residual life distributions of partially degraded converters. This makes the procedure a vital tool in relation to the support of risk-based decision-making, which is the foundation of maintenance management, including converter replacement policies.

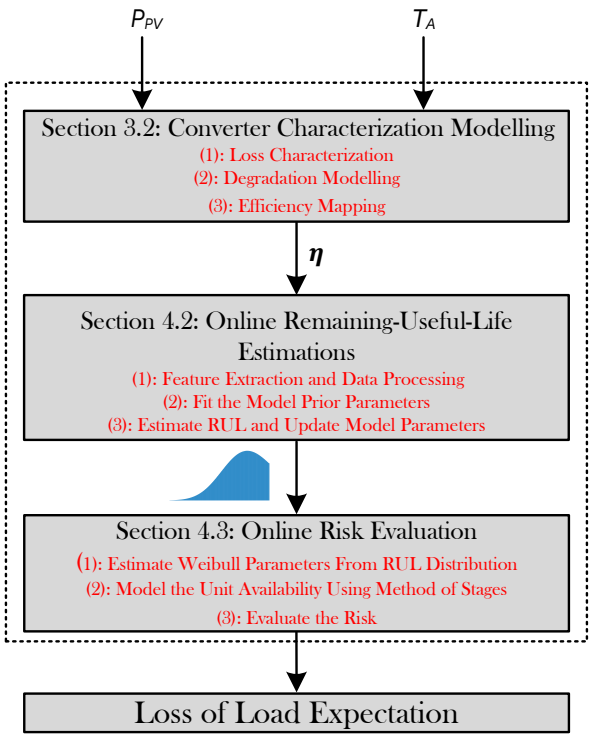

Fig. 4.1: Framework associated with the proposed evaluation method and the involved sections presented in this Chapter. The system used in this Chapter is the PV-based generation unit shown in Fig. 3.2, where P_{pv} is the input power that subjects the unit. T_a is the ambient temperature surrounding the unit and η is the efficiency when considering the input power P_{pv} and output power P_{grid} in Fig. 3.2**[J3]**.

4.2 Online Remaining-useful-life Estimations

In the following Section, the fact that the power conversion becomes increasingly inefficient as the power converter degrade will be utilized to estimate the residual life distributions during the physical transition that follows the degradation until the efficiency decrease reaches a predetermined lower boundary. For this purpose, a parametric model is used, which can take advantage of the sensor data gathered from online condition monitoring that permits the real-time calculation of the residual life distributions. In addition, real collected measurement data of appearing component parameter drifts are used to gain knowledge of to which degree and at what pace the lowering of the efficiency develops, with the intention to obtain a genuine long-term degradation process that is able to be observed by the converter health precursor mechanism. The long-term degradation process is illus-

trated in Fig. 4.2, where the individual degradation events of the ESR and the $V_{CE,on}$ is shown in Fig. 4.2.a and Fig. 4.2.b respectively. The resulting

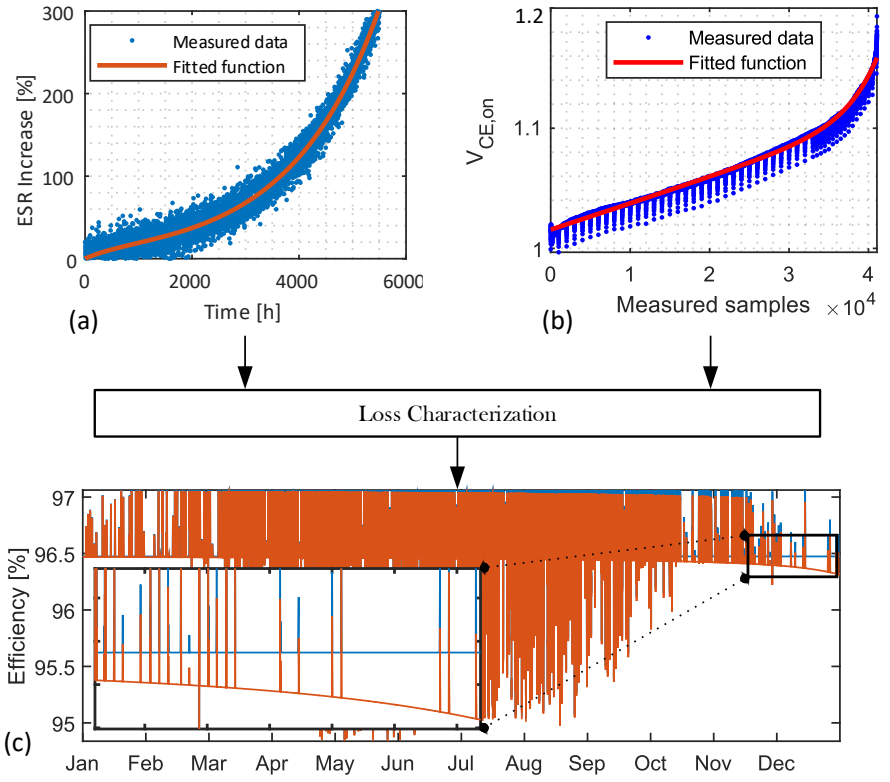

Fig. 4.2: The methodology used to gain the long-term degradation response in terms of a decrease in the operating efficiency. (a): is the ESR degradation trend replicated using the data from [108]. (b): is the experimental $V_{CE,on}$ degradation trend data, which originates from own labaratory. (c): is the efficiency signal of a non-degraded unit (blue) and the obtained degraded signal (red) when applying the shown degradation processes to the components listed in Table 3.1 when operating in the system shown in Fig. 3.2 **[J3]**.

long-term efficiency response is shown in Fig. 4.2.c, in which the time-frame of the final wear-out stage close to the point where the degradation threshold is reached is magnified with the purpose of displaying the inequality amid the non-degraded (blue) and the degraded signal (red) as the rate-of-change of degradation advance. It is worth noting that the degradation development is sped up in this case. Hence, it takes place within the time span of a single year, for the reason being to avoid the burden of displaying the large share of data that is necessary to cover the entire lifespan in a single plot. It is altogether evident from Fig. 4.2.c that the efficiency is highly varying as a result of the variation in the applied loading, which implies, that the raw efficiency

measurement signal must be processed before it can be used as a health precursor. The processing involves the extraction of the appropriate signal feature capable of capturing the physical change that appears as the converter ages and simultaneously is able to remove the impact of the loading. By observing the upper-right plot in Fig. 3.12, which presents the efficiency signals at two distinct levels of degradation, it can be observed that the peak efficiency value within the thousand minutes time-frame differs between the two distinct efficiency signals. This suggests that the peak value can be a competent signal attribute in regards to differentiate between the different levels of degradation and is, therefore, suitable in terms of degradation modelling. The peak efficiency is calculated in half-week time windows, which amounts to 5040 samples, using the data presented in Fig. 4.2.c. It can be recognized by examining Fig. 4.3.a that the extraction of the peak efficiency yields an exponentially descending degradation trend. It should be noted that the component degradation trends shown in Fig. 4.2 are seen. However, now it is assumed that it takes approximately 11 years or 140 months to reach their defined degradation threshold. This assumption is made because both cases originate from accelerated tests and not real-field usage. A 10-15 years life-cycle is not unusual for these types of components operating in two-level PV-inverters. For maximum usage of the feature data in terms of RUL prediction, the peak efficiency is rescaled using the $min - max$ normalization, which forces the range of the data to lie within $[0, 1]$ and which can be expressed as **[J3]**

$$\eta'_{peak,i} = \frac{\eta_{peak,i} - min(\eta_{peak})}{max(\eta_{peak}) - min(\eta_{peak})} \tag{4.1}$$

where $\eta'_{peak,i}$ is the ith normalized peak efficiency value. It is noteworthy to mention that the broader the data window used for computation of the peak value is, the better the true degradation trend will be reflected in the feature data. More specifically, it is critical that the peak point of the loading/efficiency curve is present in each of the respective intervals wherein the peak efficiency is computed. This is generally not an issue as this point is reached at about 40% of the rated power, but during wintertime, there can be subsequent days consisting of solely low loading settings. This is also apparent in the peak efficiency signals shown in Fig.4.3.a, where some following values are higher than the preceding ones. Overall, a few of those cases will not obscure the general trend of the resulting model. Nevertheless, if required, this issue can be dealt with by extending the sample interval for computation of the peak efficiency to one or maybe even several weeks. This will considerably advance the probability of encountering the loading setting that results in the peak load/efficiency point. In addition, it will not reduce the robustness of the method to extend the sampling window due to

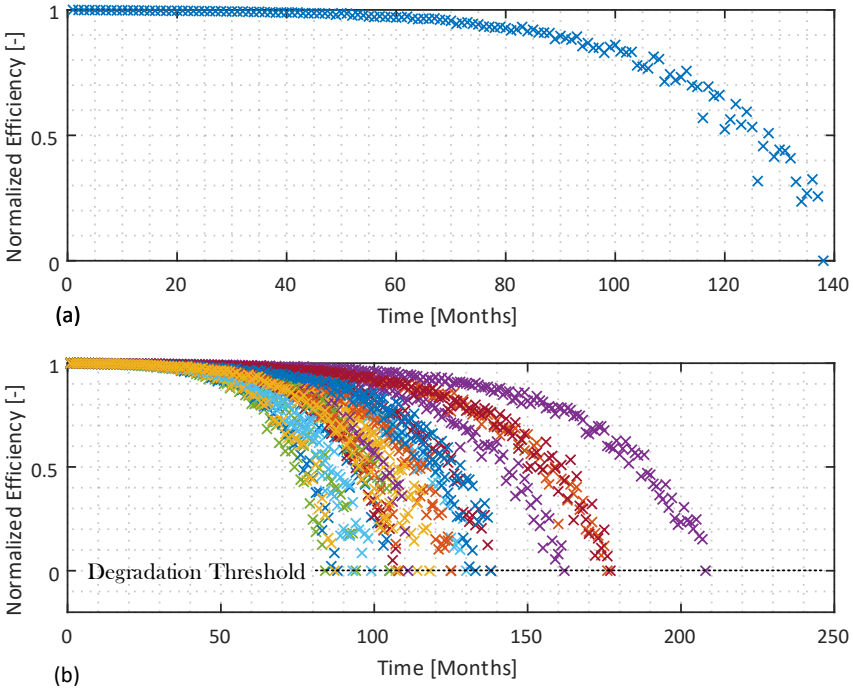

Fig. 4.3: (a): The degradation trend obtained using the peak efficiency, within intervals of half a week, using the degraded efficiency data shown in Fig. 4.2.c. (b): Population-wide dataset used to train the degradation model where each color denotes a specific degradation process and where each of the unique processes is obtained by adding random variance to the signal shown in Fig. 4.3 [**J3**].

the degradation process being relatively slow, and a considerable change in the health indicators is not expected on a week-to-week basis [**J3**]. Finally, a population-wide set of degradation signals is shown in Fig. 4.3.b. This dataset is created in a similar fashion that was described in Section 5, which includes the adding of some random variance to the original signal shown in Fig. 4.3.a, in order to emulate a real dataset, that can be used to form the basis of a degradation model, i.e. fit the prior model parameters, that will be updated as data from the test converter arrives.

The model used in this study is capable of taking advantage of the monitored degradation signals and using the data for the computation of the RUL in real time. The degradation model is characterized as being a stochastic process where $\{s(t), t > 0\}$ and it portrays the signal amplitude until it reaches its predetermined threshold value. As stated previously, the efficiency degradation trend of the converter exhibits exponentially descending characteristics

during the physical transition that the degradation causes. In order to model that specific signal pattern, the following is defined [**J3**].

$$S(t) = h(\phi, \theta, t) + \epsilon(t) \tag{4.2}$$

The model presented in (4.2) comprises the deterministic parameter ϕ and the stochastic parameter θ. The deterministic parameter describes the constant signal value equal to the primary degradation value, i.e. the peak efficiency value for a converter in an "as good as new" condition. The stochastic parameter follows a distribution and takes into account the variation among the distinct degradation processes of every single unit shown in Fig. 4.3.b. In addition, the signal noise is accounted for by the random variable $\epsilon(t)$, which is a normally distributed stochastic variable. Due to the generality of the degradation trend of the converter, the model presented in [103] is used in this study, which can be expressed as

$$S(t_i) = \phi + \theta e^{(\beta t_i + \epsilon(t_i) - \frac{\sigma^2}{2})} \tag{4.3}$$

where ϕ is the deterministic parameter, θ and β are the random variables, and ϵ is the normally distributed random noise variable with a mean value of 0 and a variance of σ^2 and t_i is the discrete-time measurements. By reason of gaining some mathematical convenience, the natural logarithmic function is employed on Equation (4.3), which leads to A_i, which is described as [**J3**]

$$A(t_i) = ln(S(t_i) - \phi) = ln\theta + \beta t_i + \epsilon(t_i) - \frac{\sigma^2}{2} \tag{4.4}$$

Now, let $A_i = A(t_i)$ and let $\theta' = ln(\theta - \sigma^2/2)$, then Equation (4.4) can be written as follows [109]

$$A_i = \theta' + \beta t_i + \epsilon(t_i) \tag{4.5}$$

The prior distribution of the model parameters is determined by considering the population of degradation patterns shown in Fig. 4.3.b. When the prior parameter distribution has been acquired, the initial converter RUL estimate can be assessed, and consecutive model updates are obtained using the efficiency sensor signal of the converter subjected to monitoring, from which the RUL can be re-evaluated.

The updating mechanism utilizes the last recorded data observation of the health precursor A_i collected during either the current or latest data sample. The procedure is established on the theory of Bayesian inference, which utilizes the conditional distribution of the degradation signal provided the current model parameters $f(A_i|\theta', \beta)$, which is normally distributed with zero mean and the variance of σ^2. The process also weighs in the prior parameter distributions that constitute a joint distribution, which is assumed to follow

a bivariate normal distribution $\pi(\theta', \beta)$ **[J3]**. The combined information gathered from the prior distribution and the current degradation signal sample is used to calculate the posterior joint distribution of the model parameters, from which a reevaluated estimation of the RUL can be computed as outlined in Fig. 4.4. The posterior model parameter distribution exhibit direct

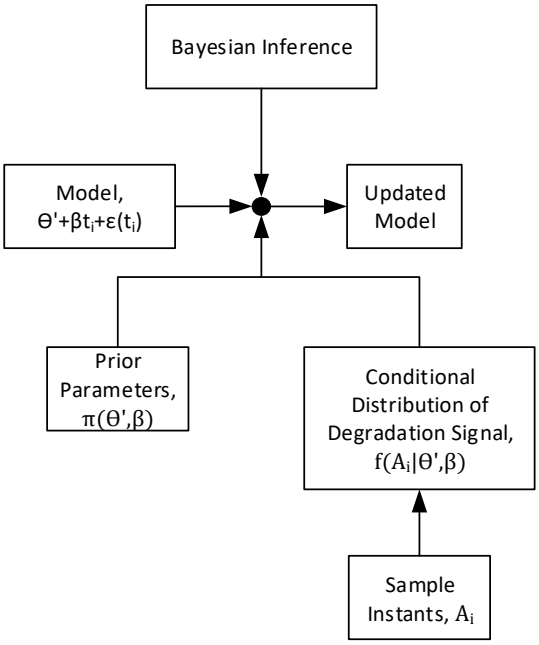

Fig. 4.4: The modelling updating mechanism is based on the theory of Bayesian inference. The posterior model parameters are obtained using a combination of the prior parameters and the conditional probability of the measured signal when given the current model parameters, also known as the likelihood function [110] **[J3]**.

proportionality to the prior model parameter distributions and the last data instant of the degradation signal A_i, which can be expressed as

$$p(\theta', \beta | A_i) \propto f(A_i | \theta', \beta) \pi(\theta', \beta) \tag{4.6}$$

The posterior parameter distributions can be expressed as a standard bivariate normal distribution in terms of its respective means $(\mu_{\theta'}, \mu_\beta)$, variances $(\sigma_{\theta'}, \sigma_\beta)$ and the correlation parameter ρ [109]

$$\pi(\theta', \beta) = \frac{1}{2\pi\sigma_{\theta'}^2\sigma_\beta^2\sqrt{1-\rho^2}} exp\left\{ \frac{-1}{2(1-\rho^2)} \left[\frac{(\theta' - \mu_{\theta'})^2}{\sigma_{\theta'}^2} - \frac{2\rho(\theta' - \mu_{\theta'})(\beta - \mu_\beta)}{\sigma_{\theta'}\sigma_\beta} + \frac{(\beta - \mu_\beta)^2}{\sigma_\beta^2} \right] \right\} \tag{4.7}$$

The posterior distribution of the model parameters is then the enabling information that leads to reevaluated estimates of the RUL distribution of the partially degraded converter, shown in Fig. 3.2. First, a degradation threshold T needs to be established, which in this specific case is determined based on the resulting efficiency change, which is a direct result of the component parameter drifts listed in Table 3.1. As mentioned earlier, this threshold value of the efficiency that designates the end-of-life is normalized to equal the value of zero **[J3]**. Now, let E stand for the RUL, then the primary goal is to approximate when $A(t+E) = T$, i.e. when the efficiency reaches its threshold value. This is fulfilled by examining the conditional cumulative distribution function (CDF) of the residual life E provided the most recent sample observation A_i

$$\begin{aligned} F_E|A_i(t) = P\{E \leq t|A_i\} = P\{A(t+t_i) \geq T|A_i\} \\ = 1 - P\{A(t+t_i) \leq T|A_i\} = \Phi(g(t)) \end{aligned} \quad (4.8)$$

where Φ is the CDF and $g(t)$ is the residual life distribution function. Essentially, the CDF of the RUL dependens on the probability that the monitored signal A_i is larger than the assigned threshold value T at the time $t + t_i$. Unfortunately, as the CDF is defined at this point, the residual life E domain can include non-positive values, which is not a realistic outcome. To deal with this issue, the conditional CDF is required to be limited, or specifically, it needs to be constrained to only include positive values $E \geq 0$. The constrained CDF can be written as [111]

$$P\{E \leq t|A_i, E \geq 0\} \quad = \quad \frac{P\{0 \leq E \leq t|A_i\}}{P\{E \geq 0|A_i\}} \quad = \quad \frac{\Phi(g(t)) - \Phi(g(0))}{1 - \Phi(g(0))} \quad (4.9)$$

which essentially truncates the CDF covering the entire domain of E, so it only covers the positive valued domain of E. The convenient measure of the RUL is the probability density function, and thus, the derivative of Equation (4.9) with respect to t is computed so that the PDF can be acquired as

$$f_{E|A_i, E\geq 0}(t) = \frac{\phi(g(t))g'(t)}{1 - \Phi(g(0))} \quad (4.10)$$

where $\phi(.)$ is the PDF of a standard normal random variable. A detailed explanation of the degradation model and the corresponding math linked to the updating procedure can be found in [112–114]. This study does not include any further analysis of which particular distribution the resulting RUL outcome resembles, but as demonstrated in Section 4.3, the distributions can be well estimated by the use of the dual-parameter Weibull fit. Fig. 4.5 blueprints the modelling process scheme, which includes the prior model, that is computed using the initial set of parameters obtained from

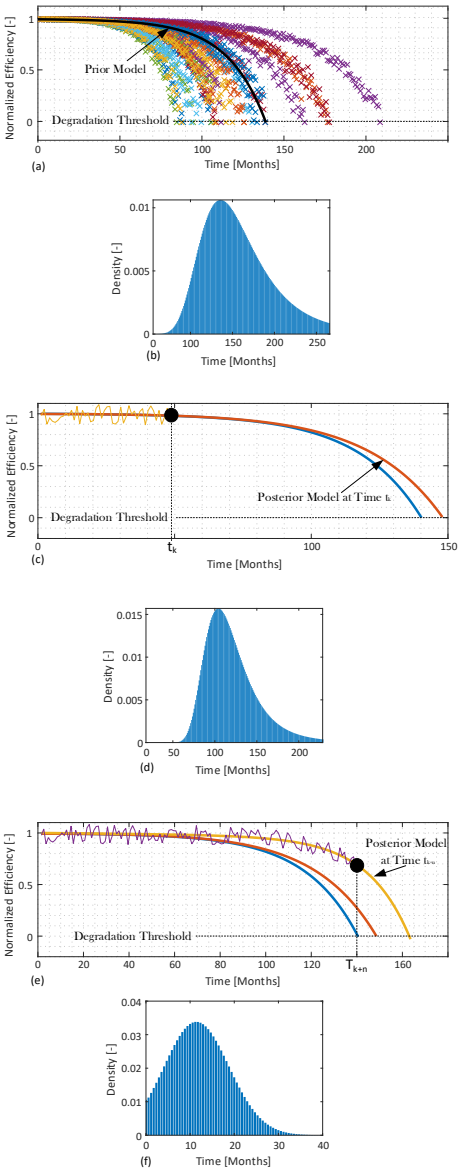

Fig. 4.5: The updating mechanism of the degradation modelling-based on the measured stream of data from the monitored converter and the corresponding RUL distributions. (a): the population of degradation history and the resulting prior model (black) based on the degradation history. (b): the initial residual life estimate based on the prior model parameters. (c): a posterior model (red) calculated at time $t = 48$ months into operation, which prolongs the total useful life compared to the prior estimate (blue). (d): the residual life distribution based on the posterior model calculated at time $t = 48$ months of operation. (e): posterior model calculated at time $t = 140$ months of operation, which again differs from the previous models. (f): the residual life distribution based on the model calculated at time $t = 140$ months, which has significantly less distribution spread compared to the previous estimates due to increased certainty in the degradation path [**J3**].

the population-wide degradation history presented in Fig. 4.3.(b). Using the prior model, the first residual life estimate is made as shown in Fig. 4.5(b), and it is clear, when observing the data, that there is a significant amount of variance in the predicted output. This is a result of being in such an early stage in the series of evaluations, meaning that at this point, the future degradation path of the test converter is uncertain and could resemble any of the cases in the historical degradation data shown in Fig. 4.5(a). As time passes, the model parameters are renewed, and the corresponding residual life is reevaluated [**J3**]. Fig. 4.5(c) displays an updated posterior model at time $t = 48$ months of operation. It distinctively exhibits that the posterior model differs from the prior model based on the parameters obtained at the initial stage. This is a result of the decrease of the sensor signal amplitude being somewhat less pronounced at this point than initially expected. The subsequent estimate can be interpreted superior as the test device's specific degradation path is becoming increasingly transparent. Using the posterior model, the residual life distribution at time $t = 48$ months can be computed as presented in Fig. 4.5(d), and despite this estimate having a prolonged total predicted lifetime, the reevaluated remaining life has been lowered due to the increase in consumed life. Lastly, a new update is computed at the converter wear-out stage, which details the accelerating decrease of the monitored signal value at time $t = 140$ months as depicted in Fig. 4.5(e). Once again, the total life expectancy has been prolonged with respect to previous estimations based on the increased degradation data availability at that point in time. Once more, the matching residual life distribution is computed and shown in Fig. 4.5(f), which exposes the true strength of the methodology as the distribution variance has been significantly reduced, and the RUL can therefore be acquired with comparatively high precision [**J3**].

The complete progression of the RUL prediction procedure, as data becomes continuously available, is presented in Fig. 4.6. As it can be observed in Fig. 4.6, the procedure is not initiated before the change in health indicator signal exceeds a predetermined slope, i.e. a slope detection mechanism based on when the descent of the last collected sample in respect to the previous one exceeds a certain value. It is suitable to choose this slope detection in a manner that causes the inherent signal noise to be inadequate to execute the RUL calculations and thereby ensures that some significant degradation needs to take place, which reduces the computational demand. It is also evident from Fig.4.6 that there is a considerable contraction of the width of the confidence bounds as the degradation progresses towards the end-of-life stage. With that considerable decrease in the width of the confidence bounds, a relatively accurate estimate can be given at a time of high relevance, i.e. near the end-of-life state [**J3**].

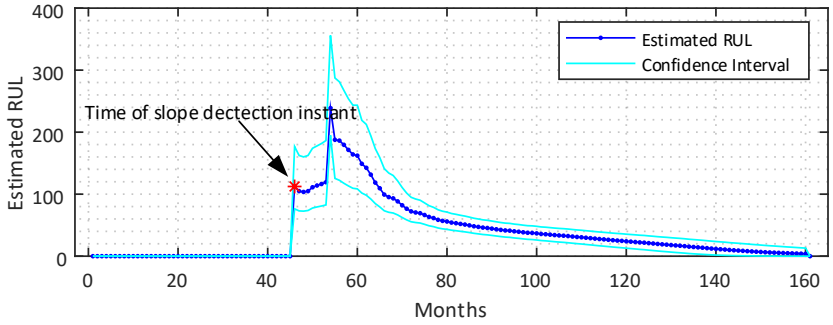

Fig. 4.6: The evolution of the RUL computations with the corresponding 95% confidence intervals [**J3**].

The development of the degradation model parameters trajectories, which is a direct outcome of the degradation trend of the converter subjected to monitoring, is presented in Fig. 4.7. The parameter values shows a radi-

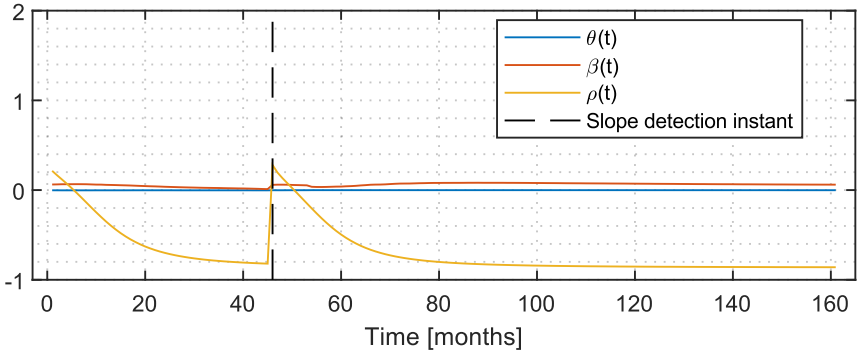

Fig. 4.7: The evolution of the model parameters as the degradation process takes place [**J3**].

cal change immediately after detecting a sufficient degradation slope in the data. In the course of time, the parameter values are likely to converge as the specific degradation pattern gets increasingly apparent. In this case, the absolute values might not appear to show any significant change, which is a consequence of the data being normalized, which forces the output range to be within $[0, 1]$, which is a relatively low extent of output values. Actually, θ does decline while β grows simultaneously, which leads to a descending output value when considering the model presented in Equation (4.3). Their various changes are also reflected in the ρ parameter change, which designates the correlation between θ and β. Now that the RUL estimations are obtained, it is now appropriate to connect those with the theory of power

system risk evaluations [**J3**].

4.3 Risk Evaluation Using Efficiency-based Remaining-useful-life Estimations

In the course of this Section, a technique that can be used to estimate the Weibull parameters of the residual life distributions obtained in the prior Section is given. The Weibull distribution function is a parametric function of two parameters, which can represent an extensive range of distributions and thereby proves itself to be quite powerful in regards to gaining the availability of the device subjected to monitoring, which is fundamental when assessing the risk, that the particular unit causes. The initial step of the procedure is to estimate the histogram of the residual life distributions, which in turn can be used for fitting the Weibull parameters that are needed for the computation of time-varying availability of the converter-based unit.

The outcome of the RUL predictions comes in the form of the remaining life values t_k and the matching probability density values p_k. It will now be convenient to form the histograms using the RUL output data, from where the Weibull parameters can be fitted, which are the enabling metrics used for the risk assessment [**J3**]. The residual life output can be sorted into $n-1$ bins in the shape of $[t_{k-1}\,,\,t_k]$ having the bin boundaries of $t_1, t_2, ..., t_n$. With the purpose of establishing the RUL-based histograms, the probability density values of X that are affiliated with the bins $B_k = [t_{k-1}\,,\,t_k]$ are used, which can be obtained as

$$p_k = P(X \in B_k) = \int_{t_{k-1}}^{t_k} f(t)dt = F(t_k) - F(t_{k-1}) \tag{4.11}$$

where f is the density function of the RUL output and F is the matching cumulative distribution function. These probability values are readily available from the RUL output, and in order to gain the histograms, the probability values are divided by the particular bin widths as [115]

$$\hat{f}(x) = \frac{p_k}{t_k - t_{k-1}} \quad for\, x \in (t_{k-1}, t_k) \tag{4.12}$$

Numerically, this is accomplished using a vector containing observable instants X_{hist} of the disposed intervals in the frequency of observations t_k. Then, to gain the observation instants of the midpoint of the histogram bins, a moving average function is applied to the current and prior time instants, i.e. t_k and t_{k-1} while disregarding the final value to gain a vector equal to the length of the vector that holds the density values P. The relative frequency

of observations p_k conforms with the PDF of the latent Weibull distribution of discrete data observations of X_{hist}. Random realizations of X_{hist} are sampled using the density values as weights [116], and the Weibull distribution function is then fitted the sampling yield, which leads to an estimate of the needed distribution parameters β and η. The Weibull distribution function is given as expressed in Equation (2.11) [33]. By use of the acquired Weibull function parameters, the converter failure rate can be determined, which is a necessity in order to calculate the availability. At first, a validation of the estimated Weibull distribution object is given, which is fulfilled by examining how well a computed distribution object resembles the authentic RUL data output at a given time t. A comparison is given in Fig. 4.8 at time $t = 75$ months of preoccupied life **[J3]**. As it can be appreciated by inspecting Fig.

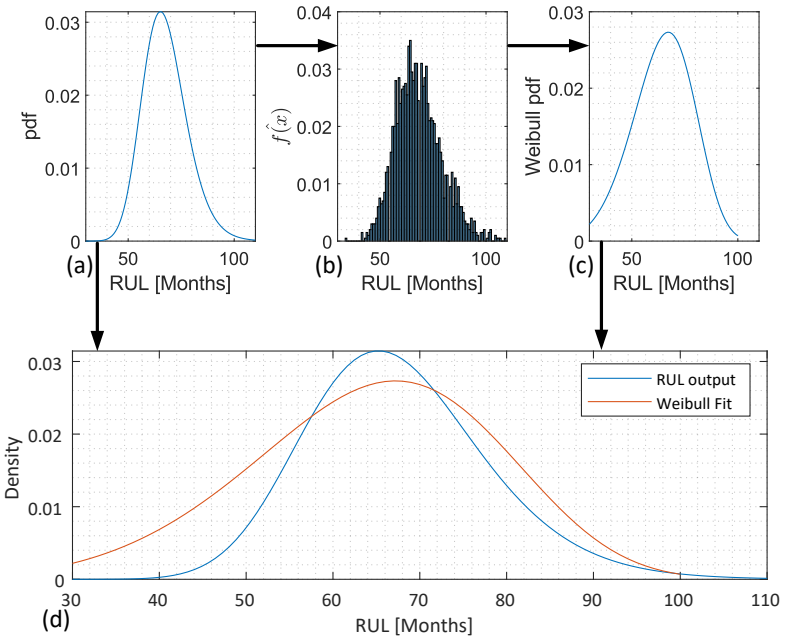

Fig. 4.8: The validation of the estimated Weibull probability distribution object. (a): the original RUL output data. (b): the resulting sampling yield gained through random sampling. (c): The resulting Weibull fit distribution function. (d): A direct comparison of the original RUL output and the Weibull fit generated distribution function **[J3]**.

4.8.(b), the approach of random sampling the RUL estimation output using the authentic probabilities as weights attain a good outcome in terms of regenerating the authentic RUL output, that is shown in Fig. 4.8.(a). In contrast, the operation of actually fitting the sample yield is not accomplished to the same successful degree. The obtained Weibull fit is given in Fig. 4.8.(c) and a head-on comparison of the authentic RUL output and the Weibull fit is given

in Fig. 4.8.(d), where it is evident that the Weibull fit differs somewhat from the original data [**J3**]. With the intention of examining if this discrepancy will have any critical influence on future availability computations, a comparison of the failure rate and the reliability function of the respective sample yield and the Weibull fitted function is made. The comparison is shown in Fig. 4.9.(a) and Fig. 4.9.(b) respectively. As it can be appreciated by studying Fig.

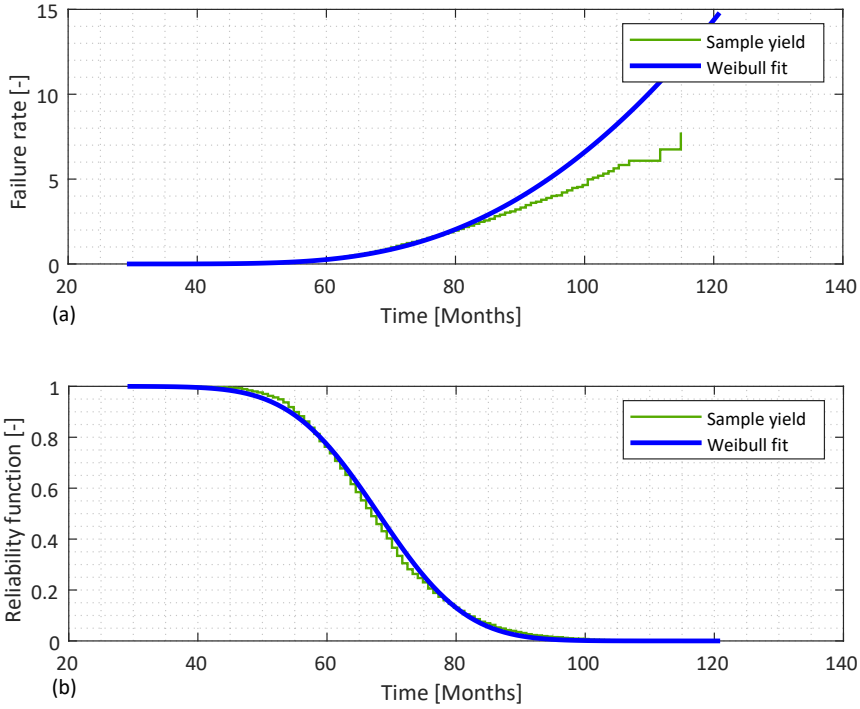

Fig. 4.9: Examining the impact of the fit deviation on the failure rate and the reliability of the RUL output. (a): Failure rate comparison.(b): Reliability comparison [**J3**].

4.9.(a), the failure rate of the Weibull fit do reproduce the data perfectly up until the RUL prediction time of 85 months, where the Weibull fit starts to exaggerate the failure rate of the data, which would lead to a conservative availability prediction. In contrast, if attention is moved to Fig. 4.9.(b), it can be understood that the reliability function of the Weibull fit does replicate the data quite well and also contemplate that at the RUL time of $t = 85$ months, the reliability can be observed to be at a value of ≈ 0.05, implying that just five percent of the data remains within the RUL time frame of $t = 85$ months and the highest estimate of the end-of-life, which is the time-frame where the failure rate of the Weibull fit is exaggerating the data [**J3**]. Rooted on this information, the fit is found suitable for portraying the RUL data.

The real potential of the procedure, which renews the failure distribution as the degradation path becomes increasingly prominent, is that the data update also influences the risk assessment. This is mainly due to the changing distribution outcome, leading to differing failure rates. For example, in Fig. 4.10, the failure rate is obtained by the use of different RUL estimates at times with different extents of consumed life. In the conventional PoF-

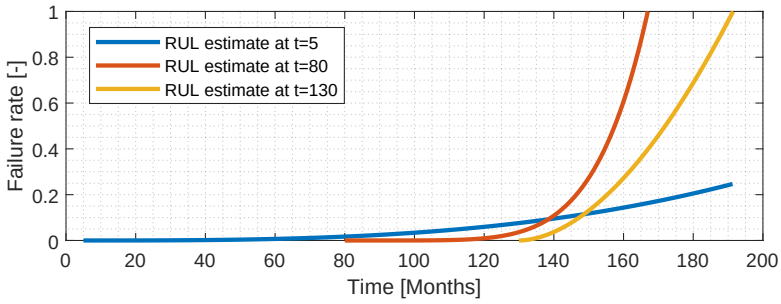

Fig. 4.10: Comparing failure rates that are obtained from RUL distributions, which is estimated at different times throughout the operational life of the converter **[J3]**.

based analysis, the failure distributions are often gained at one specific time using one year of loading as the input data, meaning a static evaluation is made one year into the operational life. This is a relatively early estimate to conduct when the future usage is literally uncertain and therefore assumes that future usage is the same as the one experienced up until that one year of operation, which can be a source of inaccuracy. For this case, the early estimate at $t = 5$ months bears little resemblance to the estimates conducted well into the converter's useful life as a result of the degradation deviation from what was initially expected. The gathering of reevaluated failure rates is an apparent superiority when seizing the awareness of the unit availability as this is a direct function of the failure rate as shown in the expression of time-variant availability [1]

$$A(t) = \frac{\mu}{\lambda + \mu} + \frac{\lambda}{\lambda + \mu} e^{-(\lambda+\mu)t} \tag{4.13}$$

where λ is the failure rate and μ is the repair rate. The availability can be comprehended as being the state probability of being in a healthy operational state in some forthcoming time t. As it can be noticed by putting the attention on Fig. 4.10, the obtained failure rates are non-constant due to the failures not being exponentially distributed. Equation (4.13) does only hold for cases with constant failure rates, and therefore, the methodology proposed in Section 2.4.1 needs to be enforced **[J3]**. The method of obtaining a

sufficient number of sub-states that indeed are exponentially distributed is simply revived by using the flowchart shown in Fig. 4.11. For a rigorous explanation of the procedure, revisit Section 2.4.1.

Subsequent to the execution of the procedure of the state partition, the

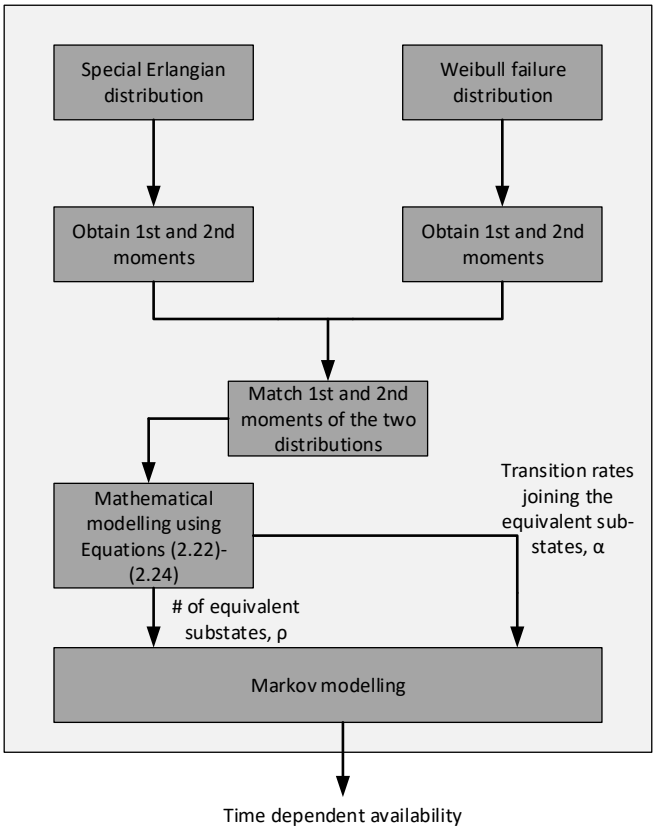

Fig. 4.11: The procedure needed to model the availability of generation units with non-exponential failure distributions [**J3**].

possible and expected deviation of the availability of the unit, obtained at different times of operational life, is examined. The availability is obtained at $t = 5$ months and $t = 130$ months due to the serious distinction between the two individual failure distributions. The assessed Weibull parameters belonging to the failure distribution at $t = 5$ months of consumed life is a scale parameter of $\eta_5 = 99.17$ and a shape parameter of $\beta_5 = 4.24$, while the obtained parameters of the failure distribution at time $t = 130$ months of

consumed life is a scale parameter of $\eta_{130} = 20.79$ and a shape parameter of $\beta_{130} = 2.8$ **[J3]**. Employing the gained parameters to the theory given in Section 2.4 and Section 2.4.1 led to an availability state composed of 14 sub-states, where each is interlinked by a transition rate of $\lambda_5 = 0.1567$ for the estimate made at $t = 5$ months. Regarding the availability assessment at $t = 130$ months of consumed life, it resulted in an availability state comprised of 7 sub-states connected by a transition rate of $\lambda_{130} = 0.3623$. Adopting the acquired states and transition rates in combination with a presumed repair rate amounting to four days in each case led to the time-varying availability responses presented in Fig. 4.12. As depicted in Fig. 4.12, there is a pronounced

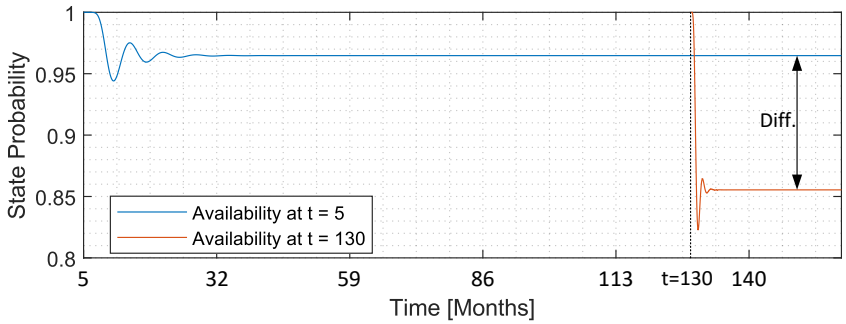

Fig. 4.12: A comparison of the availability computed from the respective RUL estimations at $t = 5$ months and $t = 130$ months of consumed life **[J3]**.

difference in the limiting state availability, i.e. the steady state availability of each estimate made at different amounts of consumed life. The steady-state availability acquired at $t = 5$ months of consumed life is 0.965, while it only adds up to 0.855 when computed at $t = 130$ months of consumed life. This is a demonstration that the proposed method excels the traditional procedures, that is founded on a single year of loading profiles and assumes those conditions throughout the operational life of the device **[J3]**. Employing the proposed procedure secures that the failure probability is reassessed as the consumed life develops, and it will therefore advance the accuracy in regards to the quantification of the risk the specific unit induces to the system. This can be appreciated by noticing the risk index that classifies the amount of loss-of-load that is likely to occur when considering downtime associated with failure, which was first introduced in Section 2.5 but is reintroduced for convenience and which can be expressed as [1]

$$LOLE = \sum_{i=1}^{n} P_i(C_i - L_i) \tag{4.14}$$

where C_i is the available generation capacity at time instant i, L_i is the load demand at time i, and P_i is the probability of generation outage, resulting

in a particular loss-of-load. The commonly used term in connection with failure probability is unavailability, that is (1−availability). As demonstrated, the consecutive availability is much different when computed at different times of consumed life, which introduces the different likelihood of the risk of losing the load. Using the suggested procedure can then result in an advancement in regard to the risk analysis of converter-based generation units. Using the procedure can therefore lead to higher precision when establishing the maintenance scheduling and, by that, lessen the unit downtime and reduce the levelized-cost-of-energy [**J3**].

4.4 Summary

Considering the fragility of power electronic components, they can be the main cause of changing the cost of generation in an unfavorable direction by inducting a risk of not meeting the load demand. The state-of-the-art reliability evaluation procedures of power electronics, which form the risk-based operation and planning determination, is established using the PoF concepts. One genuine disadvantage of applying the PoF-based concepts is the commonly made assumption of the forthcoming usage being identical to the one experienced up until the time of evaluation, which often amounts to a single-year usage profile, and by the use of that estimate, the useful life of the device. The uncertainties are later regarded, which causes the prediction quantification to be in the shape of a failure frequency distribution that includes a specific extent of variance. There are great concerns related to this procedure, including the establishment of the prediction on one isolated failure mechanism, which is an oversimplified and improbable assumption. Furthermore, the persistent use of Miner's rule that abstain from giving reason for the existence of non-linear damage accumulation during the degradation event. Lastly, the failure fatigue model is generated by the extrapolation of accelerated test results to real-field conditions which is widely regarded as the dominant origin of inaccuracy.

The study in this chapter sought to enhance the accuracy and make more accurate risk evaluations. This is realized by making use of the operating efficiency and using it as a feedback health indicator signal that is able to communicate how the degradation progresses as the converter's operational life advances as time progress and then exploit this data to reevaluate the remaining useful life throughout the entire life cycle of the converter. At first, signal processing was done by separating the peak efficiency within half-week intervals, as this demonstrated to be useful for categorizing the health condition as the degradation of the converter takes place.

A stochastic degradation model fused with an updating system founded on the Bayesian inference theory is used to frequently compute the remaining useful life distributions as the converter age. The procedure was demonstrated to be efficient as it led to a reduction in the distribution spread as the degradation path of the device became progressively clear. As a result of this reduction in distribution spread, it was possible to state the residual life with relatively high accuracy, especially during the time frame where the converter entered its wear-out stage. A procedure was presented that was able to estimate the RUL distribution and represent them using the Weibull distribution parameters. Using these parameters, the availability could be obtained at different levels of consumed life, which is in opposition to the conventionally used procedures, which estimate the risk in the beginning phase of the operational life cycle. The study demonstrated that there was a pronounced difference in failure probability from the beginning phase computations versus the reassessed computations gathered at a later stage. This is an indication of this procedure being superior relative to the traditional risk assessment procedures as a result of making sure that the failure probability is reassessed during the entirety of the useful operational life contra a static prediction measure. Applying the presented procedure can, for that reason, cause an enhancement in regards to risk assessments of power converter-based generation units. It can therefore improve the accuracy of maintenance scheduling which can result in a decrease of failure-caused downtime and, thereby, a decrease in the levelized-cost-of-energy.

Chapter 5

End-of-life Detection Using a Maximal Margin Classifier

The two previous chapters have sought to deal with the issues that were outlined in Chapter 1 by making use of procedures that are grounded in prognostics and health management methodologies, in which long-term changes of the electro-thermal parameters are utilized for indication of the components health-state. As previously stated, the power electronic component degradation will naturally materialize in the material and at the interconnection-level, and these changes govern the electro-thermal parameters. As a result, the parameters can indirectly convey the progressive component wear-out and, by that, be employed to determine the present component health status [54]. The traditional indicators cover the increase of the forward voltage of active switches and diodes as well as the thermal resistance of power devices. The alternation of the forward voltage is affected by temperature, gate oxide integrity, metalization reconstruction, and the condition of the electrical connections, particularly bond wire fatigue and, in the worst case, bond wire lift-off from the chip. A consistent and stable increase is an implication of the surface metalization impacting the ohmic resistance. In contrast, abrupt extreme escalation of the voltage drop can be observed during bond wire lift-off. This is a consequence of the matter of the residual bond wires being required to carry an extra load [55–59, 117]. Furthermore, the assessment of the thermal resistance can be drawn on to indicate the degradation in the form of occurring ceramic cracks that lower the power module's capability to conduct heat that arises in the power device and further onto the heat sink [55, 60, 61].

Based upon the present research, it is plain to apprehend that the gain from utilizing these health indicators is quite significant and that they are also

quite powerful in regards to covering multiple failure mechanisms, which is lacking and is one of the insufficiencies in the existing PoF-based methods. The major drawback is, as previously stated, that the PHM-based methods only cover the monitoring of single components [54, 62, 64, 65].

This chapter builds upon Chapter 3, which presented a procedure that gains benefit from the operating efficiency for use as a collective health indicator of the whole converter, which permits the evaluation of the health of the entire unit and thereby detect when it has reached its end-of-life state. This can help to advance the precision when evaluating the lifetime of the unique power electronic-based generation units.

Nevertheless, in regards to ensure that this procedure is functional in the matter of detecting when the end-of-life state is realized, a decisive maximum level of allowed degradation needs to be characterized, The central concern that needs to be dealt with when taking advantage of the operating efficiency, is the loading dependency. As a result of this dependency, a particular discrete threshold will not be useful since it will lead to a number of coinciding efficiency outcomes for contrasting levels of degradation. Therefore, this chapter proposes a procedure, that adopts a binary supervised classifier, that constructs a safe operational area and efficiently establishes a non-linear end-of-life boundary accommodating any given loading condition. The efficiency-founded end-of-life detection procedure can be exploited to make maintenance scheduling of power converters when functioning in a wide selection of applications. The outcome can be useful for the provision of early forecasts of failures in an effort to keep unscheduled maintenance at a minimum, prolonging the time between maintenance actions and consequently lowering failure-affiliated downtime.

5.1 Framework

In this Section, a procedure that is practised to detect when power converters have reached the end-of-life is given. The procedure benefits from the degradation of a diverse selection of components simultaneously and, at the same time, accounts for every possible operating condition. The procedure accounts for each defined operating condition and its effect on the collective health indicator, demonstrating the presented procedure's usefulness. With the aim of depicting the potential of the presented procedure, it is again outlined via the case study used in the preceding chapters, using the power processing unit shown in Fig. 3.2. The procedure also considers the same parameter shifts of the same studied components. The useful life of the individual components is, as previously stated, determined by a defined end-

of-life benchmark that is rooted in certain factual awareness of the destruct restraint plus some incorporated margin in an effort to counteract failure-caused downtime. The general degradation trend of a health indicator is (re)introduced in Fig. 5.1, with y being the observed value of the health precursor, Δy is the parameter deviation concerning its lead-off value y_0. The

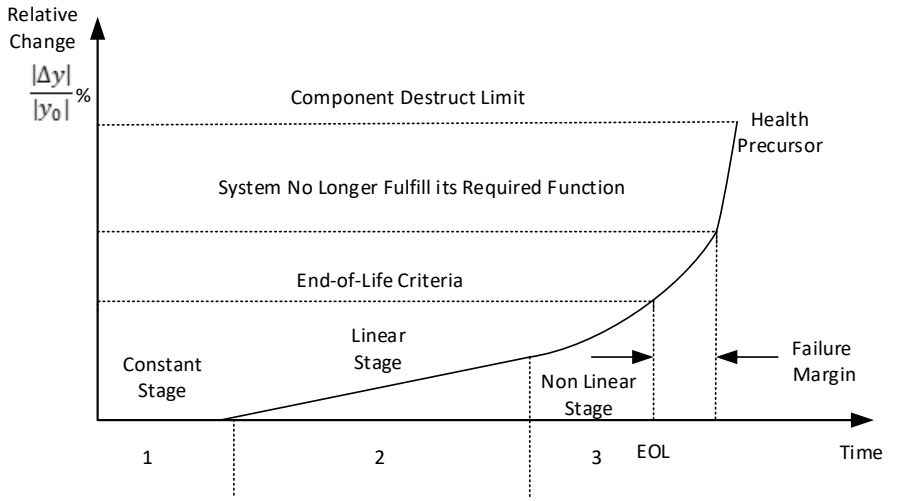

Fig. 5.1: A general degradation curve showing the three typical stages of the power electronic component degradation process. Δy is the parameter drift of the given health precursor y, y_0 is the initial state of a component operating in an "as good as new" state **[J2]**.

y-axis is scaled to display the absolute value of the deviation in percentage. The three distinct degradation stages are described in Chapter 1, and the allowed parameter drift of the components are enlisted in Table 3.1.

The framework associated with the presented procedure is summarized in Fig. 5.2, which covers three central parts, i.e. the leading part is the modelling and loss characterization that was presented in Section 3.2. The second part covers the collection and management of the data regarding the development of a data ensemble for administrating the large bulk of data so that it is consistent with the employed classification algorithm. The greatest signature signal attributes of the data ensemble are determined and adopted in order to gain supreme classifier performance. Subsets of the signal attributes are used for training and testing the performance of the end-of-life detection approach. Conclusively, the procedure's capability is demonstrated by highlighting the clear separation of active converters from those which has arrived at their end-of-life state by the use of an assigned safe operational area.

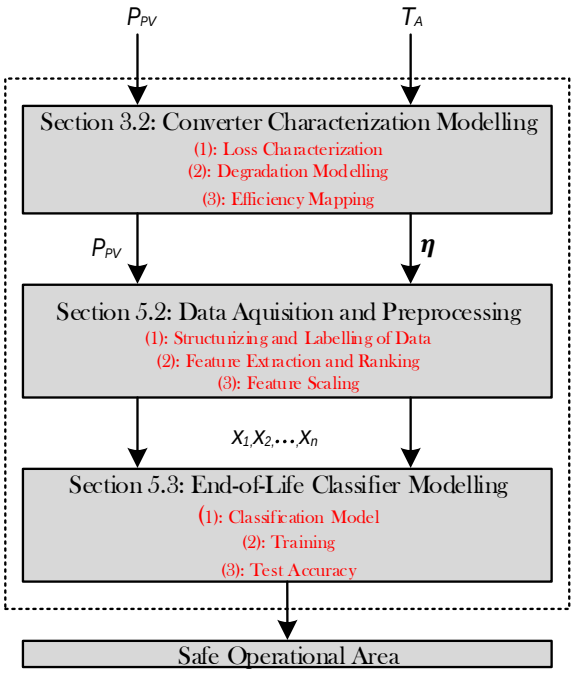

Fig. 5.2: The framework linked to the proposed detection method and its corresponding chapter sections. The system used in this Chapter is the PV-based generation unit shown in Fig. 3.2, where P_{pv} is the input power that subjects the unit. T_a is the ambient temperature surrounding the unit and η is the efficiency when considering the input power P_{pv} and output power P_{grid} in Fig. 3.2 **[J2]**.

5.2 Data Acquisition and Pre-processing

In any case of using a health precursor, data analysis is the groundwork of whichever condition monitoring scheme. In this Section, a data ensemble is made for organizing and labelling a large amount of data, which are needed to establish the end-of-life detection algorithm. The blueprint of the data ensemble is that it must describe a life-cycle record of the system mode of operation, i.e. run-to-failure data. Furthermore, supplementary to accounting for every possible health state, it must include every operating condition option due to its significant impact on the health precursor. Lastly, it is necessary to arrange the data in a manner which enables the condition monitoring algorithm to track which condition any of the large quantity of data designates.

Grounded in the previously declared reflections and specifications, the data set group contains 70 members, including members representing the unit operating in an "as good as new" state or progressively degraded. This portion of members is appointed a binary condition label of zero. The remaining part of existing members characterizes the converter condition as being completely degraded, and those members are appointed a binary condition label of one. Every member includes the required data variables, such as the monitoring data of the efficiency and loading of the unit. Each of these monitored data variables encompasses time series of 6000 sample instants using a sample rate of one minute, which roughly amounts to four days of operation [**J2**]. The arrangement of the data ensemble is detailed in Table 5.1. Even though

Table 5.1: Arrangement of the data ensemble developed for end-of-life detection [**J2**]

Member ID	Efficiency η	Loading P_{pv}	Fault Code
1	$6000x1$ Time series data	$6000x1$ Time series data	1
2	$6000x1$ Time series data	$6000x1$ Time series data	0
...	...	...	...
70	$6000x1$ Time series data	$6000x1$ Time series data	0

the raw data is organized, it is still required to process it as well so that the numerical features that provide the ideal condition monitoring classification algorithm outcome and simultaneously sustain the basic data information of the data ensemble can be obtained. The signal features are extracted manually, and it is therefore required to employ a technique which can deduce which features of the data are most appropriate in an efficient manner. More specifically, discover the feature data of which the performance alternates in an anticipated mode as the converter degrades, but also is able to dispose of the insignificant signal features as these can promote the event of overfitting the model due to unnecessary model complexity and consequently, this can result in biased prediction outcomes. The feature selection techniques for binary classification, founded on filters, assesses each respective signal feature in terms of measuring to which degree it is able to separate the defined condition classes. The ideal features are considered to be those that can distinguish between perfectly healthy and partly degraded from the units that have entered their defined end-of-life state. This distinguishing should ideally show as little overlap of the condition classes as possible when clustering the identical conditions together [**J2**]. At first, a preliminary analysis that aims to determine each feature's usefulness is made by the use of fea-

ture histogram illustrations. The histograms provide an initial sense of how well the features perform. Thus a good perception of which feature subset is meaningful to include in the more detailed quantifiable evaluation by use of filter-founded techniques. Furthermore, the histogram plot envisions the data separation of the labeled groups within the data ensemble by binning the feature data and using color codes to distinguish between the binary condition label of the distinct condition category. The histogram technique is illustrated in Fig. 5.3, where the separation of the feature variables' mean efficiency and distribution skewness of the units operating efficiency is presented. The blue color designates the condition value of zero, i.e. a perfectly

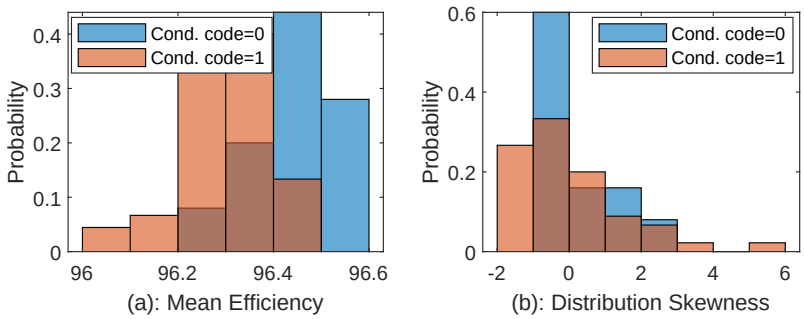

Fig. 5.3: Histograms used for visualization of the condition-based feature separation [**J2**].

healthy or partly degraded operation, whereas the orange color designates the condition value of one, i.e. the system being active in its end-of-life state. As it can be perceived in the histogram that exhibits the mean efficiency, the greater share of the healthy feature data is situated in between the two most right bins, while the larger share of the fully degraded data samples is located within the rest of the bins. In spite of the data not showing complete separation, the mean efficiency could potentially perform well when combined with a feature that holds insights into the state of the applied loading. On the contrary, the histogram that portrays the distribution skewness demonstrates significant overlap of the feature data. The certain bins that do not display any overlap are located near the extreme low and high values even though these bins represent the same condition class in both cases. The result is, therefore, ambivalent and not useful in terms of detecting the end-of-life [**J2**]. It is noteworthy that in spite of the selected efficiency feature, it is central that this feature is merged with a feature that can inform of the applied loading of the unit. For instance, assuming that the peak efficiency is favored, it cannot be assured that the specific condition leading to the peak of the efficiency/loading curve occurs within every sample window. This will especially prove to be critical during low load seasons such as winter time, and if the loading is not accounted for, it may lead to a false alarm and con-

sequently no failure affiliated maintenance.

The concluding feature pick of the feature subset favored based on the histogram conception, will be rooted in the Kolmogorov-Sminor (KS) test, which is a quantitative measure of how well the condition variables separated themselves from each other. The approach is superior to the approaches that make use of the mean, which is caused by the reality that the two feature distributions can very well have a significant amount of overlap even though their individual means vary, which is on account of the dissimilarity of the distribution spread. The KS statistic is essentially the measure of the most significant divergence of the two distributions sampled from the distinct condition types. The KS statistic can be obtained as follows [118]

$$D = \underset{x \in \mathbb{R}}{sup} |F_{cond.1}(x) - F_{cond.0}(x)| \tag{5.1}$$

where D is the KS statistic value, $F_{cond.0}$ and $F_{cond.1}$ are the cumulative distributions of each of the respective condition class samples. The interpretation of the KS statistic outcome is that the greater its value is, the less likely it is that these two distributions originate from the same data variable, i.e. the condition classes demonstrate a good amount of separation. In Fig. 5.4, the fitted probability distribution functions of the mean efficiency originating from each of the condition classes are presented in the company with the greatest distance of those classes. Derived from the unrivaled separation

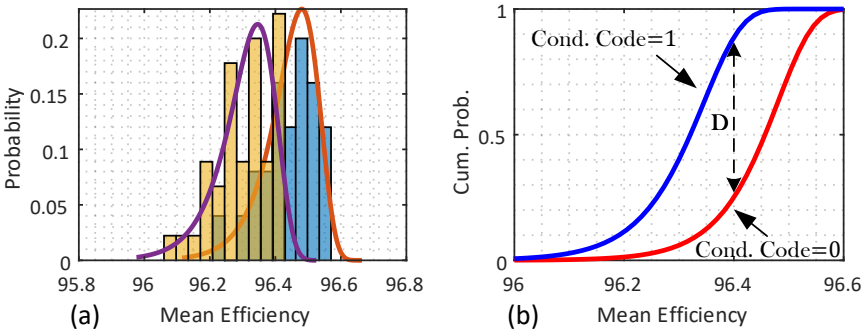

Fig. 5.4: (a): Weibull distribution function fit of each of the condition classes of the mean efficiency. (b): Corresponding cumulative distribution functions of the condition classes that show good separation properties by having a relatively large Kolmogorov-Sminor statistic. **[J2]**.

character, the mean efficiency is selected in coalition with the mean loading as the signal features utilized for condition monitoring. Nonetheless, before the data utilization for training the classification algorithm, it is obligatory to abolish the comparatively considerable variation in the scale level of the loading and the efficiency. If this significant difference in the feature scale is

not dealt with by normalizing them to a comparable level, it can produce a biased classification outcome in favour of the relatively high-valued loading data [**J2**]. This is caused by the usage of the distance among the data points when establishing the decision boundary. Therefore, if one of the features has a vast extent of values, the distance will be highly impacted by that certain feature. The ideal selection of either scaling or standardization-founded practices rely on the application that is practiced. In the event of a clustering or distance-formed analysis, the z-score standardization can be a powerful option to gain favorable results. The result of applying the z-score standardization is that the feature data is scaled in a manner making it adopt the characteristics of a standard normal distribution. The standardized scores of the feature data are obtained by the following

$$z_i = \frac{(x_i - \mu)}{\sigma} \tag{5.2}$$

where μ is the sample mean and σ is the standard deviation from the mean [**J2**].

5.3 End-of-life Classifier Modelling

Now that the considered features are thoroughly processed, the feature space is ready to be divided, in a manner that separates the respective health state classes, by the use of a decision boundary. The decision boundary will be created using the support vector machine (SVM) algorithm, which takes advantage of the kernel trick for modelling a non-linear decision boundary, that is mandatory in this context [119]. By noting the feature space, which is presented in Fig. 5.5(a), it is evident that the feature data of the health precursor is not linearly separable, i.e. any given straight line, that can be sketched throughout the feature space will not be able to isolate the fully-degraded samples from the non-fully-degraded ones. There may be an endless amount of solutions that are able to isolate the health classes into two distinct areas, and thus, the aim is to seek the one that produces the least generalization error. The SVM algorithm approaches this challenge using the conception of a margin, identified as the minimum distance between the decision boundary and any feature sample, as demonstrated in Fig. 5.5(b). SVM appoints and uses the decision boundary that will maximize the margin [120]. The decision rule utilizes the decision boundary in a sense that can be grasped by examining the random sample observation, denoted $\bar{x}$ in Fig. 5.5(b). For the reason of getting awareness of which side of the decision boundary the random sample observation is located at, the vector denoting the sample coordinates is projected upon the weighting vector $\bar{w}$, which is perpendicular to the decision boundary [**J2**]. The effectuation of the vector projection enables the distance of a feature sample can be gained in the form of proportionality

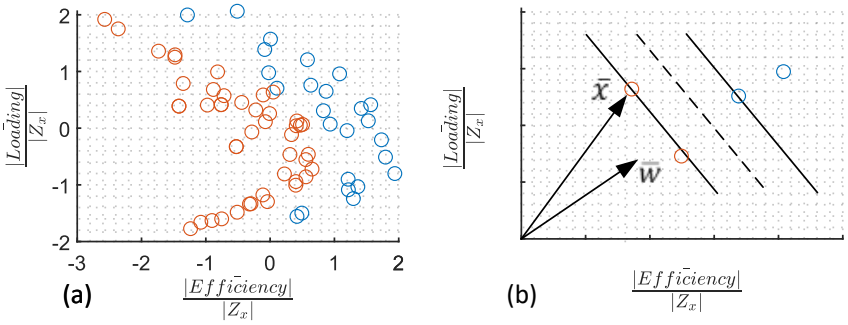

Fig. 5.5: (a): Feature space where the red circles represent the fully degraded converter data, and the blue circles represent new or partially degraded converter data. (b): Concept of Support Vector Machine, where the margin is defined as the perpendicular distance between the decision boundary and the nearest data points. The dashed line represents the decision boundary, and the solid lines represent the margins. The data located on the margin lines are known as support vectors. $\bar{w}$ is the weighting vector, $\bar{x}$ is a random data observation, and Z_x denotes that the data is standardized using the z-score standardization presented in Equation (5.2) **[J2]**.

to the weighting vector $\bar{w}$ in the same orientation as the weighting vector. Given the circumstances and concepts mentioned, the decision rule can be mathematically expressed as

$$y(x) = w^T \phi(x) + b \tag{5.3}$$

where $\phi(x)$ indicates a feature-space transformation and b denotes the explicit bias parameter. At this point, the expression is not subjected to an adequate amount of constraints that will ensure fixed values of b and $\bar{w}$, which involves the annotation of the target values so that $t_n \in \{-1, 1\}$ and that the sample points are classified based on the sign of $y(x)$. So in the event of a sample instant representing a partially degraded unit, the sum of the dot product and the bias parameter will be positive, whereas the contrasting health state will result in the outcome of a negative value. Inevitably, there will exist one or more sets of values for $\bar{w}$ such that the function given in (5.3) fulfills that $y(x_n) > 0$ for $t_n = 1$ and $y(x_n) < 0$ for $t_n = -1$, which conveniently causes $t_n y(x_n) > 0$ for all sample instants **[J2]**.

As mentioned earlier, the SVM selects the specific decision boundary, which guarantees that the margin is maximized. The distance from a point to a hyperplane can be used to formulate a maximization principle as $|y(x)|/||w||$, where w is the width of the decision surface. Furthermore, since we strictly want to be concerned with rightly classified sample instants that are able to fulfill that $t_n y(x_n) > 0$ for all n, the distance of a sample point to the surface

can be expressed as

$$\frac{t_n y(x_n)}{||w||} = \frac{t_n(w^T\phi(x_n) + b)}{||w||} \tag{5.4}$$

The distance can be declared as an optimization problem, which strives to optimize the b and w parameters as a means to maximize the margin

$$\underset{w,b}{max}\left\{ \frac{1}{||w||}\underset{n}{min}[t_n(w^T\phi(x_n) + b)] \right\} \tag{5.5}$$

An explicit solution to (5.5) is rather difficult to obtain, and therefore a rescaling of the expression is done in a manner that assumes that the nearest data sample has a distance of one. This is achieved by letting $w \rightarrow cw$ and $b \rightarrow cb$ such that

$$\underset{n}{min}\, t_n(w^T\phi(x_n) + b) = 1 \tag{5.6}$$

The optimization problem is then simply condensed only to include the maximization of $||w||^{-1}$ or equally minimizing $||w||$, which results in the optimization problem can be rewritten as

$$\underset{w}{min}\, \frac{1}{2}||w||^2 \tag{5.7}$$

and due to the nearest point being of a distance of one, the minimization problem has to comply with the given constraint

$$t_n(w^T\phi(x_n) + b) \geq 1 \tag{5.8}$$

Expression (5.8) is commonly referred to as the primal form of SVM, which is comprised through the assumption that the data is fully separable and no misclassifications occur. However, in reality, the condition classes may well coincide and show overlapping distributions, which is also seen in this case when observing Fig. 5.3, which implies that a strict and full separation can lead to inferior generalization, i.e. poor ability to predict future samples correctly. The procedure is consequently revised in a manner that will permit misclassifications within and across the margin boundary but will assign any given misclassifications a penalty, which amount depends on the distance from the boundary, i.e. the more severe case of misclassification, the larger the assigned penalty is **[J2]**. Due to the increased practicality with respect to the optimization problem, the penalty is represented by a linear function of the distance being $\zeta_n \geq 0$. It holds for the values of $\zeta_n \geq 1$ in the event of misclassifications, as demonstrated in Fig. 5.6(a) [121]. This approach is typically known as using a soft margin considering that it eases the hard margin constraint, and it can be expressed as

$$t_n(w^T\phi(x_n) + b) \geq 1 - \zeta_n \tag{5.9}$$

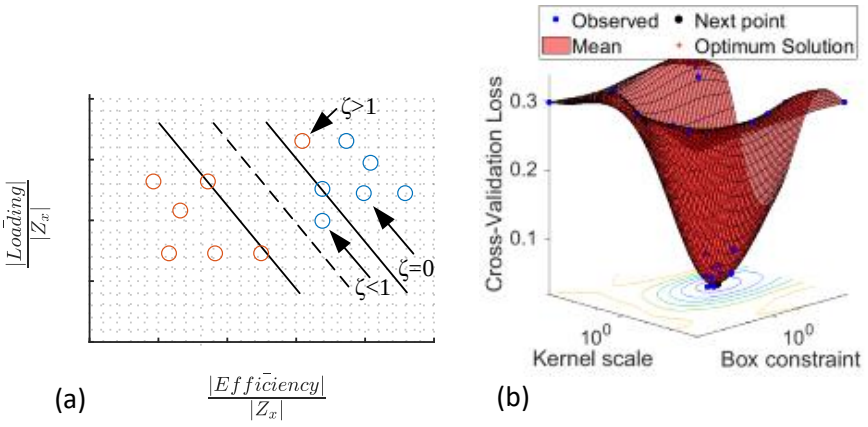

Fig. 5.6: (a): Visual interpretation of the approach of including slack variables for soft margin classification. (b): Cross-validation loss evaluation for different sets of the box constraint and the kernel scale. **[J2]**.

The optimization objective has now turned into maximizing the margin and, at the same time, penalizing the sample data that is situated at the wrong side of the boundary. The minimization problem presented in expression (5.7) is now modified so it involves misclassification slack

$$\min_{w} C \sum_{n=1}^{N} \zeta_n + \frac{1}{2}||w||^2 \tag{5.10}$$

where C denotes the box constraint which manages the level of trade-off between the induced penalty and the margin. Now assume that $C = 0$, which will remove any slack penalization, and thus, the optimization can allow it to be used whenever it desires, and no matter how severe the misclassification is, they will all be approved. This would produce a linear decision boundary and result in underfitting. On the other hand, a large C value will cause even a small amount of slack to be greatly penalized, and the classifier can, therefore, not allow any misclassifications regardless of the severity. This will create a highly complex decision boundary, also known as a case of overfitting **[J2]**.

The problem at hand is a convex quadratic optimization problem as we are coping with a quadratic objective function subjected to linear constraints. As a means to gain a solution to the constrained optimization problem, the technique of Lagrange multipliers is used. The representing Lagrangian function

can be expressed as

$$L = (w, b, \zeta, \alpha, \lambda) = \frac{1}{2}||w||^2 + C\sum_{n=1}^{N}\zeta_n - \sum_{n-1}^{N}\alpha_n[t_n y(x_n) - 1 + \zeta_n] - \sum_{n=1}^{N}\lambda_n\zeta_n \quad (5.11)$$

where α_n and λ_n are the respective Lagrance multipliers. At this point, it is appropriate to acquire the optimization problem stated in what is known as the dual form, which excludes the primal variables w, b, and ζ and consequently lessens the reliance on the optimization problem to only include pairs of sample data points. In an effort to discard the primal variables, the expression presented in (5.11) is differentiated with respect to w,b, and ζ_n and then equalized with zero. The expressions that are gained through those computations are then utilized to eliminate those specific variables in the Lagrangian expression, and conclusively, the optimization problem can be stated in dual form as [121]

$$\underset{\alpha_i}{max}(\sum_{n=1}^{N}\alpha_n - \frac{1}{2}\sum_{n=1}^{N}\sum_{m=1}^{N}\alpha_n\alpha_m t_n t_m k(x_n, x_m)) \quad (5.12)$$

where $k(x_n, x_m)$ represents the kernel function that consistently assesses the SVMs in higher dimensions and consequently makes it possible to achieve excellent separation qualities of the classifier when coping with linearly inseparable data. Because of the characteristics of kernelization, it permits to function in the primary two-dimensional feature space, and not it is not required to compute the data coordinates in higher dimensional spaces, meaning that the inner product only involves the base features as detailed in expression (5.13)

$$k(x_n, x_m) = \phi(x_n) \cdot \phi(x_m) \quad (5.13)$$

where ϕ designates the feature space transformation. The applied kernel function used in this study is commonly referred to as the radial basis function, which can be stated as

$$k(x_n, x_m) = exp(-\gamma||x_n - x_m||^2) \quad (5.14)$$

where γ denotes the scaling parameter that scales the data when assessing the kernel [119]. Now there is obtained an optimization problem which can be solved with relatively low effort. The problem does now include the maximization of expression (5.12) with respect to α_n while being subjected to the following constraints

$$\sum_{n=1}^{N}\alpha_n t_n = 0 \quad (5.15)$$

$$0 \leq \alpha_n \leq C \tag{5.16}$$

The dataset is split into a training and test dataset. However, beforehand, the complete feature set is randomly permuted to make certain that all sorts of operating conditions of all seasons are well represented within both the training and test data sets **[J2]**. Additionally, a five-fold partition of the training data is formed, which is made use of for performing cross-validation during the training of the model. This is done to ensure that the model exploits the degradation data to the fullest by training and testing the model five times on different subsets of training data and thereby developing an estimate of the performance of an SVM model on unseen data. During the training of the model, the ideal parameter values of the kernel scale γ and the box constraint C are acquired by examining which parameter pair will generate the minimum amount of cross-validation loss. The assessment of the optimal parameters is illustrated in Fig. 5.6(b), which leads to $C = 11.761$ and $\gamma = 1.8711$. The accuracy of the developed model is after that examined by analysing if the model outputs do match the known condition labels of the separate test data set

$$Accuracy = \frac{\sum(\text{Model predictions}(x_{test}) == y_{test})}{N_{test}} \cdot 100 \tag{5.17}$$

where x_{test} is the test feature set, y_{test} is the known condition labels belonging to the test feature set, and N_{test} is the size of the test feature set. In Fig. 5.7, the solid dots portrays the training data, the encircled dots denote the data points that are used for the support vectors, and the crosses refer to the test data **[J2]**. From Fig. 5.7, it can be recognized that the hyperplane separates the

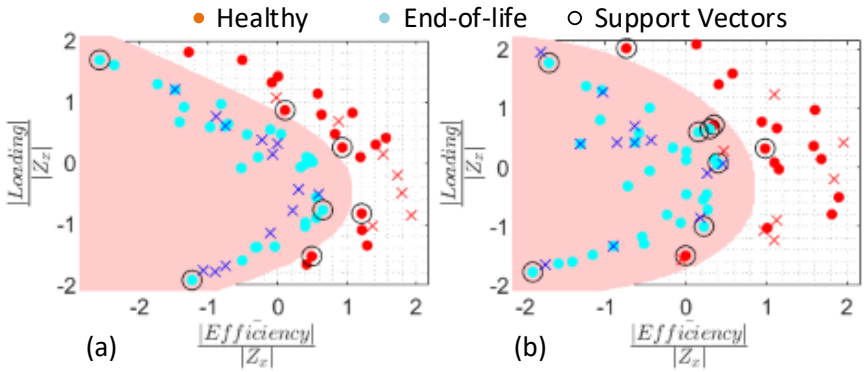

Fig. 5.7: Visualization of the hyperplane separating the feature space's white and red areas containing the standardised values of mean efficiency and mean loading. (a): Idealised results with 100 percent accuracy. (b): Case including measurement inaccuracies, which introduces a few cases of overlapping and leads to 90 percent accuracy according to Equation (5.17). **[J2]**.

health categories of the test data flawlessly with full accuracy. It can also be observed that this approach deals with and resolves the influence of the loading on the health precursor in terms of the standardized data, which can not be resolved through a single-valued end-of-life criteria. The red shaded area symbolizes the entire range of the end-of-life conditions, whereas the white area designate the safe operational area. The outcomes that are presented in Fig. 5.7(a) are attained under idealistic circumstances, where an almost unlimited extent of information is accessible from simulating the particular system that was presented in Fig. 3.2 [**J2**]. The likely measurement inaccuracies are considered to gain an authentic apprehension of how well the model accomplishes to detect the end-of-life in real applied usage. The simulated data consisting of a resolution of approximately 2 MHz, is downsampled to 20 kHz, a standard sampling rate of the type of sensors, often used in connection with prognostic applications. When having almost unlimited data availability from the simulation models, the approach is to perform regular averaging of the efficiency response using an averaging window corresponding to the fundamental period, which provides a constant efficiency signal for one specific condition. An efficiency value is then sampled each minute, which corresponds to the input mission profile resolution, and finally, the efficiency value of 6000 samples within four days is computed. Reducing the available information by resampling the data output at 20 kHz eliminates the potential of obtaining perfect periodical averaging and consequently leads to a measurement error of up to 0.03%. Furthermore, a 0.1% error is also added with the intention of modelling the potential sensor inaccuracies, in which the chosen value is based on the assumption of using sensors of sensor class 0.1.

Lastly, the addition of Gaussian white noise is added to the efficiency signal with a signal-to-noise ratio of 80 using the Additive Gaussian White Noise function in MATLAB. The total added errors are randomly added or subtracted from the original idealized data, and the outcome can be seen in Fig. 5.7(b). As seen by observing Fig. 5.7(b), there is introduced a degree of overlapping of the health state classes, which causes some incidents of misclassifications. However, on account of the usage of soft margins, the few incidents of misclassifications do not result in hyperplanes with poor outcomes, caused by the box constraint being determined to achieve supreme performance by minimizing the cross-validation loss during training as depicted in Fig. 5.6(b). In this particular case, it resulted in that two of the test observations were misclassified, which are the two observations that are denoted with red crosses even though they are situated within the red-shaded end-of-life area. Including those two misclassifications, the prediction accuracy ended up being 90%, which must still be regarded as being quite satisfying considering that no real competitive alternatives are available at this

time.

5.4 Summary

On account of the costly consequences of failure associated with downtime of power converters that are functioning in a broad assortment of applications, it is crucial to earn the capability of asserting the lifetime with high accuracy. A considerable share of uncertainty is tied to the existing reliability assessment methods, namely the PoF approach, which can give rise to erroneous lifetime estimations. One encouraging alternative is the PHM-founded approach, in which the electro-thermal parameters are exploited for health pointers. Even so, every current approach is limited to only cover single unique components, which is regarded as a critical shortcoming due to the fact that the event of degradation will presumably occur on several components simultaneously. This chapter has presented an approach which makes use of efficiency as an application-level health indicator, which allows the surveillance of complete power converters. Furthermore, the subject of the efficiency being conditional on how the converter is loaded was addressed by using an SVM-founded classifier when assessing the end-of-life. The SVM classifier is capable of establishing non-linear decision boundaries to deal with this reliance and at the same time, being computationally efficient due to its ability not to require any computations being executed in higher dimensional spaces.

In order to not solely state the conclusive outcomes using idealized conditions, the influence of the possible measurement inaccuracies was considered, which produced a moderate amount of overlapping health classes. The overall influence of the particular misclassifications did not cause badly separated hyperplanes with inferior outcomes due to the usage of soft margins that are regulated by an optimal amount of penalized slack. As a result of the proposed detection approach, the planning personnel can be provided with warnings of impending failures and consequently reduce the events of unscheduled maintenance, prolong the maintenance cycles, and thereby sustain timely and effective repairs, which can all contribute to a decrease in downtime and inspection expenses and therefore a lowering of the total life-cycle cost

Chapter 6

Conclusions

This Chapter concludes the primary findings and results of this Ph.D. project. In addition, the chapter includes a summary of the thesis, the highlighted main contributions, a discussion of potential research perspectives, and an outline of relevant future work tasks.

6.1 Summary

This Ph.D. thesis sought to conduct research to improve the reliability of power electronics-based power systems by lowering the risk of not supplying the system loads due to converter-affiliated generation unit downtime. This is mainly approached by investigating how to model and assess the reliability of converter-based generation units while coping with the challenges that arise when the system is transitioning from power generation based on fully dispatchable generation units to the intermittent generation linked to RES. In addition, a great deal of attention was put on understanding the shortcomings and issues related to the existing reliability assessment methods of power converters and presenting alternative methods to deal with those issues. The proposed methods aimed to counteract system downtime by predicting imminent converter failure and exploiting this knowledge to execute timely maintenance measures. A summary of each of the thesis chapters is now given:

In *Chapter 1*, research gaps and shortcomings in the existing reliability modelling of power converters were identified. The research gaps and the existing shortcomings were used to formulate the motivation and objectives of this Ph.D. thesis. The research objectives were divided into two main topics: objectives linked to securing system adequacy in RES-based power systems and objectives related to the lifetime prediction issues in the existing

power electronics reliability assessment methods. The identified objectives were then addressed in the chapters that followed.

Chapter 2 provided a comprehensive analysis of how existing PoF-based power electronics reliability methods can be applied to power systems by bridging the gap that enables the merging of the converter assessment methods with those of power system reliability. This included a methodology that deals with the non-exponential failure distributions of power converters. The commonly used method to gain converter systems' reliability is to merge the respective failure distributions of the components using the reliability block diagram. However, this method is not suited for power system reliability evaluations, as it inherently assumes instant repair, and the use of this method would therefore not lead to realistic results. Alternatively, the chapter made use of stochastic processes to model the state probability of the converter-based generation units, i.e. the converter availability, which accounts for the repair process. The conventional availability modelling methods based on Markov processes, only apply to homogeneous systems and are therefore not directly applicable as a result of the non-exponential failure tendency of power converters.

Chapter 2 presented a method to deal with this issue by splitting up the non-homogeneous systems states into a number of exponentially distributed states. However, a comparison of gaining the availability using non-constant and constant failure rates proved that there was a significant difference in both the transient phase and the limiting-state probabilities. The use of constant failure rates that are based on static lifetime measures will therefore lead to incorrect risk evaluations. In addition, due to the severe impracticability of the availability modelling of systems with more than a few non-identical units, conventional Markov process modelling methods proved to be very exhaustive and computationally demanding. *Chapter 2* presented a method that discretized the continuous Markov process by defining a time step, which could ensure that the probability of two or more state transitions is unlikely and thereby transform the problem into one, which can be solved using Markov Chain methods instead. This proved to be very convenient as one of the leading modelling tools in Markov chains is the stochastic transitional matrix. The stochastic transitional matrix has superior computational efficiency, in terms of lowered mathematical complexity and significantly reduced computational time. Also, in contrast to the use of solving large systems of equations when using Markov process modelling methods, the use of the stochastic transitional method is scalable. It can be applied even to large systems as adding a system unit only requires an additional dimension in the matrix, that only contains the failure and repair rate of the system units. *Chapter 2* was concluded with a method that showed how to use the risk of

losing the load to base the maintenance scheduling of the power electronic-based generation units. The subjects of the thesis then moved into the domain of physics-of-degradation-based concepts, with the purpose of improving reliability assessments that are based on the static lifetime estimations using the physics-of-failure analysis.

Chapter 3 introduced an application-level health precursor, which main benefit is that it enables the possibility to assess the current health state of the converter through means of condition monitoring. The monitoring concept can lead to a more accurate end-of-life prediction for a unique unit compared to the use of a failure percentage in large populations of units obtained from failure distributions that inhibits a relatively large lifetime variance. The subject of condition monitoring is widely known. It is increasingly seen in practical use, but all existing methods are restricted to only cover single components, which is a severe limitation as it does not indicate the health state of the entire converter. One common phenomenon that occurs across the different power electronic components, as they degrade, is the increase in the amount of dissipated losses. *Chapter 3* exploited the increase in losses by proposing a method which makes use of the operating efficiency as a unified health precursor of power converters. The health precursor is realized through modelling of the losses dissipated in the converter when it is affected both by different loading conditions and also due to the combined component degradation. The models are combined with the knowledge of the general degradation tendency of power electronic components, particularly the fact that the rate-of-change in the amount of dissipated power losses will differ as the degradation process develops. The combination of these models enabled the definition of degradation bounds, which was based on the general degradation stages of power electronic components, which involved stages of different rate-of-change of efficiency. The chapter concluded with an end-of-life detection mechanism based on the rate-of-change of the monitored samples that crosses the defined degradation bounds.

Chapter 4 extended the theory of the converter-level health precursor presented in *Chapter 3* with the intention of developing remaining useful life estimations for use in strategic reliability-based decision-making. The efficiency-based health precursor was used to assess the residual lifetime continuously as the degradation process evolves throughout the converter life cycle. This is realized by exploiting a stochastic degradation model founded on the concept of Bayesian inference. The procedure proved to be effective, as the distribution spread of the residual life decreased as the degradation trend of the particular unit became increasingly transparent. When end-of-life was imminent, the residual life could be stated with relatively high precision relative to the lifetime predictions based on the PoF concept. In addition, a procedure

was presented on how to state the residual life distribution by Weibull probability density function parameters, which enabled the computation of the availability at different levels of consumed life. This continuous evaluation of availability proved to be a great advantage with respect to existing methods, which often compute the lifetime prediction at an early life cycle stage and then assume identical loading through its remaining life cycle. Finally, a comparison of the availability was made using residual life assessments at different life stages. A significant difference was observed in the steady-state failure probability from an availability computation made at an early stage versus a reassessed availability computation made far into the converter's operational life. This is an indication of the procedure being superior when compared to the availability assessed using a static measure. The procedure can therefore lead to an improvement when evaluating the risk of power electronic-based power systems.

Chapter 5 also used the efficiency-based health precursor presented in *Chapter 3*, now with the intention to develop an end-of-life detection mechanism. The end-of-life assessment procedure used the concept of Support Vector Machine, which is able to overcome the issue of the efficiency being highly dependent on the loading conditions due to its ability to construct a non-linear decision boundary in the feature plane. The method was able to map linearly inseparable data into higher dimensions, where the data is separable, by use of the kernel trick. The chapter concluded by accounting for sensor inaccuracies, intending not to conclude the results solely on idealized conditions, which resulted in health class overlap. Even though the data did include health state overlap, it did not result in poorly separated hyperplanes due to the use of soft margins, which could be controlled by regulating incorporated penalizing slack. The approach proposed in *Chapter 5* can be merged with the remaining useful life estimation updating mechanism that was presented in *Chapter 4* in order to obtain a holistic approach, which deals with the future perspective in terms of long-term planning but also imminent maintenance requirement. It can also be an advantage to combine the Support Vector Machine-based detection approach with the rate-of-change of the health precursor, which was discussed in Chapter 3. This can deal with the issue of being forced to assume that all the components degrade in a homogeneous manner by paying attention to sudden changes that can be provoked by immediate health changes in unique components.

6.2 Main Thesis Contributions

The primary research outcomes and main contributions are stated based on the research objectives presented in *Chapter 1*. These contributions are sum-

marized below:

Understand and deal with the reliability issues caused by the intermittent nature of renewable-based energy sources and the incorporation of power electronic converters in system-level reliability assessment
An in-depth analysis was given, which can be used to assess the reliability of modern power systems. The existing power system reliability assessment methods are developed for systems consisting solely of fully dispatchable generators. In contrast, the analysis given in this thesis was based on a case study using a low-voltage distribution network consisting solely of RES-based units. The study presented a methodology on how to guarantee adequate system operation of RES-based power systems, which involved the following

- Physics-of-failure-based reliability assessment of the power converters using real-field mission profiles
- The inclusion and design of storage units to compensate for the intermittent energy supply and thereby adding to the system's flexibility
- Risk modelling strategies, which can increase the security of supply by assessing the risk of generator downtime and exploiting that knowledge for maintenance planning

Model and investigate the impact of using time-varying failure rates that reflect realistic wear-out tendencies in power converter-based generation units
The existing reliability studies on the integration of renewable-based generators assume that the failure tendency of these generators can be described using simple constant failure rates. This is an unrealistic assumption as this does not reflect the renewable-based generators' true nature. To deal with this, a concept was presented that enabled the availability evaluation of power converters by transforming their non-homogeneous failure state into a number of homogeneous states, including their corresponding state transitions. A comparison of the converter state probability using non-constant and constant failure rates was presented, showing that the assumption of constant failure rates led to false availability predictions and should be avoided. The presented procedure enables the incorporation of power electronics into the power system reliability assessment methods, which thereby aids in gaining more realistic risk rates induced by RES-based generators.

Develop a monitoring concept that utilizes a health precursor, which can indicate the health state of entire converters
Physics-of-degradation-based methods were one of the main concepts of this study, which should deal with the prediction uncertainties related to the existing time-to-failure assessment methods. This was approached by utilizing

the parameter drifts in the power electronics components that take place as these components degrade. The existing degradation-based condition monitoring methods are limited to only cover individual components and are therefore insufficient for obtaining the remaining useful life of power converters. This study presented a converter-level health precursor, which took advantage of the change of dissipated losses in power electronic components as these parameter drifts occurred and made use of the converter efficiency to gain insights into the current health state of RES-based generation units. The study included detailed thermal models and component loss calculations, accounting for the temperature and frequency dependency. The converter-level health precursor was further used to obtain the following reliability metrics.

- Continuously reassessed time-to-failure estimations with relatively low distribution spread during later stage life-cycle
- Time of imminent failure based on end-of-life detection concepts, which dealt with the health precursor's reliance on loading conditions

Understand and deal with the challenges of the existing physics-of-failure-based method, which can lead to inaccurate lifetime predictions
Great efforts were made to identify the challenges and assumptions of the existing time-to-failure assessment methods. One of those challenges was identified as being a large distribution spread in the failure distributions caused by multiple uncertainties, such as the extrapolation of accelerated test results to real-field usage conditions. This was addressed by a method that obtained the time-to-failure distribution via monitoring the unified converter health precursor. The method used a stochastic degradation model capable of reassessing the estimations as new monitoring data arrived. These continuously updated remaining useful life distributions were realized by modelling based on exploiting the concept of Bayesian inference. Furthermore, due to the relatively large amount of information contained in a degradation curve, when compared to single-point lifetime estimations, the methodology was capable of decreasing the distribution spread as a unique degradation path got increasingly transparent. The time-to-failure could therefore be stated with relatively high precision at the crucial time of imminent failure. Another common issue related to the PoF-based reliability studies is the consistent use of Miner's rule, which assumes linear damage accumulation even though it is well documented that interactions in the driving forces of failure cause the evolution of damage to accelerate as the components degrade. The methods presented in this study account for the accelerating damage by using exponential degradation models, which continuously reassess the current health state. The existing literature has previously abstained from using efficiency as a health precursor due to its dependency on loading conditions. This study presented a method to detect when the end-of-life of converters is reached and which could overcome the loading dependence issue

by using a maximum margin classifier, capable of constructing a non-linear decision boundary in the feature plane. This included a modelling methodology, which outlined how to determine the optimal signal features of the loading and efficiency that would lead to maximum separation of the health classes. The classifier was modelled based on support vector machines, and the concept of the kernel trick was incorporated, which maps the data into higher dimensions where the linearly inseparable data could be separated. Additionally, the study presented a method that could minimize the negative effect of the data being affected by sensor noise and the resulting negative impact of health class overlap. The detection mechanism still proved to be highly effective, despite health class overlap, due to the incorporated concept of soft margins, which allows certain misclassifications so the margin can be kept as wide as possible and the remaining data points can be classified correctly. This detection mechanism can be useful regarding maintenance coordination, which can help to advance the reliability of power electronic-based power systems.

6.3 Research Perspectives and Future Work

In addition to the presented work in this thesis, there are some relevant future research perspective, which could improve the study and help to make it a general approach for usage in large-scale power system analysis. Some of these relevant perspectives and possible future work are now summarized.

1. The reliability analysis conducted in this thesis was solely based on power converters. However, in power systems, there are numerous other components which can malfunction, such as transformers, transmission lines and busbars. It would be interesting to include these components and simulate each for a large number of outage events to see how they affect the overall system reliability. Each of these components can be included in a sensitivity analysis by the use of a Monte Carlo analysis or other relevant modelling tools. Another relevant addition to the system analysis could be to incorporate the total transfer capacity limits of the system by first identifying the critical transfer sections and then incorporate the limitations of these sections with respect to thermal and voltage levels in case of an outage.

2. In this study, it was chosen only to analyse a system operating in islanded mode to quantify what was required to guarantee localized reliability. This resulted in harsh requirements for each individual generation unit, and their respective maintenance frequency was high as their respective failures greatly impacted the system reliability. In most cases, small localized grids operate in grid-connected mode. Therefore, it is

relevant to analyze the case of interconnected systems, which generally provide a higher level of adequacy of generation capacity. Furthermore, it would be relevant to investigate to what degree each system reserve could be lowered while maintaining the same amount of system risk due to the introduced tie capacity. Of course, this reliability advancement would rely on things such as the total tie capacity, the outage rates of the tie lines, and the sort of agreement that exist between each system operator. The Loss of Load Expectation of the combined systems could then be assessed by the use of concepts of probability arrays, which can cover all possible capacity outages of the interconnected systems.

3. During the degradation-based efficiency study presented in this Thesis, some degradation process distributions were assumed based on typical failure distribution shape factors. This was necessary due to the lack of sufficient experimental degradation data availability which could describe the time difference in when each unit reached the defined degradation limit. In reality, degradation processes will differ as a result of differences in the applied conditions and dissimilarity in electrical parameters due to variations in the components manufacturing process. Therefore, this study will greatly benefit from experimental validation in the form of conducting tests on power electronics components while monitoring the individual component health precursors that impact the converter's efficiency. This should not only include the data acquisition of when each respective component reaches the parameter drift limits but the entire degradation process including the trends. Ideally, the test data should be of sufficient population size to constitute the distribution spread of degradation processes. This would remove the need to use common failure distributions gained from the physics-of-failure analysis.

4. The study did also assume homogeneous degradation in each of the studied converter components, meaning that all of them reached their defined degradation limit and similar types of components provide an equal share to the lowering of efficiency. The result of this homogeneous degradation assumption is that the end-of-life of all converters is at the exact same efficiency change, when in reality, one unique component could be inferior to the remaining due to manufacturing defects, and it could therefore fail relatively faster. In the case of single inferior components, the total combined efficiency change would not be of the same size as if all of them reached their full degradation limit. The thesis presented a rate-of-change of efficiency-based end-of-life detection methodology, which can provide some indication of when a single component is within imminent failure by noting abrupt changes in the efficiency samples. Still, more effort should be put into developing

methods that are able to predict if abrupt failure is imminent in one single component at a relatively early life cycle stage when compared to the remaining converter components.

5. The research would also benefit from including a study which characterizes each of the relevant failure modes individual impact on efficiency. The presented study mainly accounted for the on-state voltage increase due to degradation related lowered quality of the electrical connections. Phenomenons such as e.g., the increase of the thermal resistance caused by solder fatigue leads to a relatively high junction temperature and does therefore affect the efficiency. By considering the change in on-state voltage and the applied conditions, a separation strategy might be attainable that can be able to observe which changes are caused by bond wire-related degradation and which are caused by solder fatigue.

References

[1] R. Billington and R. N. Allen, *Reliability Evaluation of Power Systems*, 1st ed. Plenum Press, 1984.

[2] International Renewable Energy Agency (IRENA). (2021) Renewable capacity statistics 2021. [Online]. Available: http://www.irena.org/-/media/Files/IRENA/Agency/Publication/2021/Apr/IRENA_RE.pdf

[3] J. Carrasco, L. Franquelo, J. Bialasiewicz, E. Galvan, R. PortilloGuisado, M. Prats, J. Leon, and N. Moreno-Alfonso, "Power-electronic systems for the grid integration of renewable energy sources: A survey," *IEEE Transactions on Industrial Electronics*, vol. 53, no. 4, pp. 1002–1016, 2006.

[4] F. Blaabjerg, Y. Yang, D. Yang, and X. Wang, "Distributed power-generation systems and protection," *Proceedings of the IEEE*, vol. 105, no. 7, pp. 1311–1331, 2017.

[5] S. Yang, A. Bryant, P. Mawby, D. Xiang, L. Ran, and P. Tavner, "An industry-based survey of reliability in power electronic converters," in *2009 IEEE Energy Conversion Congress and Exposition*, 2009, pp. 3151–3157.

[6] H. Wang, K. Ma, and F. Blaabjerg, "Design for reliability of power electronic systems," in *IECON 2012 - 38th Annual Conference on IEEE Industrial Electronics Society*, 2012, pp. 33–44.

[7] Cigre Working Group C1.27, "The Future of Reliability - Definition of Reliability in Light of New Developments in Various Devices and Services Which Offer Customers and System Operators New Levels of Flexibility," Cigre, Technical Report, 2018.

[8] G. B. Sheblé, *Power system Planning (Reliability)*, 1st ed. Boca Raton: CRC Press LLC, 2001.

[9] Energinet, "Security of Electricity Supply Report 2020," Energinet, Technical Report, 2020.

[10] European Network of Transmission Operators for Electricity, "Nordic and Baltic Grid Disturbance Statistics 2020," entsoe, Technical Report, 2021.

[11] European Commision, "The cost of blackouts in Europe," European Commision, Technical Report, 2022.

[12] U.S. Department of Energy, "Economic Benefits of Increasing Grid Resilience to Weather Outages," U.S. Department of Energy's Office of Electricity Delivery and Energy Reliability, Technical Report, 2013.

[13] F. Blaabjerg, Y. Yang, K. Ma, and X. Wang, "Power electronics - the key technology for renewable energy system integration," in *2015 International Conference on Renewable Energy Research and Applications (ICRERA)*, 2015, pp. 1618–1626.

[14] Cigre Working Group C1.27, "The Future of Reliability - In Light of New Developements in Various Devices and Services Which Offer Customers and System Operators New Levels of Flexibility ," Cigre, Technical Report, 2018.

[15] M. Bollen and F. Hassan, *Integration of Distributed Generation in the Power System*, 1st ed. Wiley, 2011.

[16] F. Katiraei, R. Iravani, N. Hatziargyriou, and A. Dimeas, "Microgrids management," *IEEE Power and Energy Magazine*, vol. 6, no. 3, pp. 54–65, 2008.

[17] K. Ma, M. Liserre, F. Blaabjerg, and T. Kerekes, "Thermal loading and lifetime estimation for power device considering mission profiles in wind power converter," *IEEE Transactions on Power Electronics*, vol. 30, no. 2, pp. 590–602, 2015.

[18] Y. Wang, P. Zhang, W. Li, W. Xiao, and A. Abdollahi, "Online overvoltage prevention control of photovoltaic generators in microgrids," *IEEE Transactions on Smart Grid*, vol. 3, no. 4, pp. 2071–2078, 2012.

[19] H. Yang, Z. Cai, X. Li, and C. Yu, "Assessment of commutation failure in hvdc systems considering spatial-temporal discreteness of ac system faults," *Journal of Modern Power Systems and Clean Energy*, vol. 6, no. 5, pp. 1055–1065, 2018.

[20] L. Shen, Q. Tang, T. Li, Y. Wang, and F. Song, "A review on VSC-HVDC reliability modeling and evaluation techniques," *IOP Conference Series: Materials Science and Engineering*, vol. 199, p. 012133, 24-26 March 2017. [Online]. Available: https://doi.org/10.1088/1757-899x/199/1/012133

[21] Y. Guo, H. Gao, and Q. Wu, "A combined reliability model of vsc-hvdc connected offshore wind farms considering wind speed correlation," *IEEE Transactions on Sustainable Energy*, vol. 8, no. 4, pp. 1637–1646, 2017.

[22] C. MacIver, K. R. W. Bell, and D. P. Nedić, "A reliability evaluation of offshore hvdc grid configuration options," *IEEE Transactions on Power Delivery*, vol. 31, no. 2, pp. 810–819, 2016.

[23] S. Sulaeman, M. Benidris, J. Mitra, and C. Singh, "A wind farm reliability model considering both wind variability and turbine forced outages," *IEEE Transactions on Sustainable Energy*, vol. 8, no. 2, pp. 629–637, 2017.

[24] H. J. Bahirat, G. H. Kjølle, B. A. Mork, and H. K. Høidalen, "Reliability assessment of dc wind farms," in *2012 IEEE Power and Energy Society General Meeting*, 2012, pp. 1–7.

[25] P. Wang, Z. Gao, and L. Bertling, "Operational adequacy studies of power systems with wind farms and energy storages," *IEEE Transactions on Power Systems*, vol. 27, no. 4, pp. 2377–2384, 2012.

[26] H. Wang, M. Liserre, and F. Blaabjerg, "Toward reliable power electronics: Challenges, design tools, and opportunities," *IEEE Industrial Electronics Magazine*, vol. 7, no. 2, pp. 17–26, 2013.

[27] Reliawind, "Report on wind turbine reliability profiles - field data reliability analysis," Reliawind, Technical Report, 2011.

[28] L. Moore and H. Post, "Five years of operating experience at a large, utility-scale photovoltaic generating plant," *Progress in Photovoltaics: Research and Applications*, vol. 16, pp. 249 – 259, 05 2008.

[29] F. Kulenkampff, S. Franz, K. Kiefer, and L. Sans, "Reliability of inverters in photovoltaic power systems – a detailed field data analysis," in *PCIM Europe 2022; International Exhibition and Conference for Power Electronics, Intelligent Motion, Renewable Energy and Energy Management*, 2022, pp. 1–7.

[30] P. D. T. O'Connor and A. Kleyner, *Practical Reliability Engineering*, 5th ed. John Wiley & Sons, Ltd, 2012.

[31] C. e. a. Byrne, *Zvei - Handbook for Robustness Validation*, 2013, :18-05-2020.

[32] H. Wang, M. Liserre, F. Blaabjerg, P. de Place Rimmen, J. B. Jacobsen, T. Kvisgaard, and J. Landkildehus, "Transitioning to physics-of-failure

as a reliability driver in power electronics," *IEEE Journal of Emerging and Selected Topics in Power Electronics*, vol. 2, no. 1, pp. 97–114, 2014.

[33] H. Chung, H. Wang, F. Blaabjerg, and M. Pecht, *Reliability of Power Electronic Converter Systems*, ser. IET Power and Energy Series. the Institution of Engineering and Technology, London, United Kingdom, 2015, no. ISBN-978: 1-84919-901-8.

[34] A. Hanif, Y. Yu, D. DeVoto, and F. Khan, "A comprehensive review toward the state-of-the-art in failure and lifetime predictions of power electronic devices," *IEEE Transactions on Power Electronics*, vol. 34, no. 5, pp. 4729–4746, 2019.

[35] R. Bayerer, T. Herrmann, T. Licht, J. Lutz, and M. Feller, "Model for power cycling lifetime of igbt modules - various factors influencing lifetime," in *5th International Conference on Integrated Power Electronics Systems*, 2008, pp. 1–6.

[36] J. Gu, D. Barker, and M. Pecht, "Uncertainty assessment of prognostics of electronics subject to random vibration," *AAAI Fall Symposium - Technical Report*, 01 2007.

[37] A. Sangwongwanich, Y. Yang, D. Sera, and F. Blaabjerg, "Mission profile-oriented control for reliability and lifetime of photovoltaic inverters," *IEEE Transactions on Industry Applications*, vol. 56, no. 1, pp. 601–610, 2020.

[38] D. Xiang, L. Ran, P. Tavner, S. Yang, A. Bryant, and P. Mawby, "Condition monitoring power module solder fatigue using inverter harmonic identification," *IEEE Transactions on Power Electronics*, vol. 27, no. 1, pp. 235–247, 2012.

[39] Infineon, *Application Note 2019-05 - PC and TC Diagrams*, 2019, :18-06-2022.

[40] R. Schmidt, F. Zeyss, and U. Scheuermann, "Impact of absolute junction temperature on power cycling lifetime," in *2013 15th European Conference on Power Electronics and Applications, EPE 2013*, 09 2013, pp. 1–10.

[41] H. Wang and F. Blaabjerg, "Power electronics reliability: State of the art and outlook," *IEEE Journal of Emerging and Selected Topics in Power Electronics*, vol. 9, no. 6, pp. 6476–6493, 2021.

[42] H. Huang and P. A. Mawby, "A lifetime estimation technique for voltage source inverters," *IEEE Transactions on Power Electronics*, vol. 28, no. 8, pp. 4113–4119, 2013.

[43] K. Ma, N. He, M. Liserre, and F. Blaabjerg, "Frequency-domain thermal modeling and characterization of power semiconductor devices," *IEEE Transactions on Power Electronics*, vol. 31, no. 10, pp. 7183–7193, 2016.

[44] A. Wintrich, U. Nicolai, and W. Tursky, *Semikron Applictaion Manual Power Semiconductors*, 2015, : 19-05-2020, Semikron Int.GmbH.

[45] M. Held, P. Jacob, G. Nicoletti, P. Scacco, and M.-H. Poech, "Fast power cycling test of igbt modules in traction application," in *Proceedings of Second International Conference on Power Electronics and Drive Systems*, vol. 1, 1997, pp. 425–430.

[46] A. Hamidi, A. Stuck, N. Beck, and R. Zehringer, "Time dependent thermal fatigue of hv-igbt modules," in *In Proc. of the 27th Kolloquium Halbleiter-Leitungsbauelemente und Materialegüte von Silizium, Freiburg/Breisgau*, vol. 1, 1998.

[47] H. Wang and F. Blaabjerg, "Reliability of capacitors for dc-link applications in power electronic converters—an overview," *IEEE Transactions on Industry Applications*, vol. 50, no. 5, pp. 3569–3578, 2014.

[48] R. Alwitt and R. Hills, "The chemistry of failure of aluminum electrolytic capacitors," *IEEE Transactions on Parts, Materials and Packaging*, vol. 1, no. 2, pp. 28–34, 1965.

[49] B. W. Williams, *Principles and Elements of Power Electronics: Devices, Drivers, Applications, And Passive Components*, 1st ed. Barry W Williams, 2006.

[50] Y. Yang, K. Ma, H. Wang, and F. Blaabjerg, "Instantaneous thermal modeling of the dc-link capacitor in photovoltaic systems," in *2015 IEEE Applied Power Electronics Conference and Exposition (APEC)*, 2015, pp. 2733–2739.

[51] B. P. McGrath and D. G. Holmes, "A general analytical method for calculating inverter dc-link current harmonics," in *2008 IEEE Industry Applications Society Annual Meeting*, 2008, pp. 1–8.

[52] J. Stevens, J. Shaffer, and J. Vandenham, "The service life of large aluminum electrolytic capacitors: effects of construction and application," in *Conference Record of the 2001 IEEE Industry Applications Conference. 36th IAS Annual Meeting (Cat. No.01CH37248)*, vol. 4, 2001, pp. 2493–2499 vol.4.

[53] D. Zhou, G. Zhang, and F. Blaabjerg, "Optimal selection of power converter in dfig wind turbine with enhanced system-level reliability,"

IEEE Transactions on Industry Applications, vol. 54, no. 4, pp. 3637–3644, 2018.

[54] Y. Avenas, L. Dupont, N. Baker, H. Zara, and F. Barruel, "Condition monitoring: A decade of proposed techniques," *IEEE Industrial Electronics Magazine*, vol. 9, no. 4, pp. 22–36, 2015.

[55] X. Perpiñà, L. Navarro, X. Jordà, M. Vellvehi, J.-F. Serviere, and M. Mermet-Guyennet, "Reliability and lifetime prediction for igbt modules in railway traction chains," in *Reliability and Safety in Railway*, X. Perpinya, Ed. Rijeka: IntechOpen, 2012, ch. 7. [Online]. Available: https://doi.org/10.5772/38268

[56] W. Wu, M. Held, P. Jacob, P. Scacco, and A. Birolini, "Investigation on the long term reliability of power igbt modules," in *Proceedings of International Symposium on Power Semiconductor Devices and IC's: ISPSD '95*, 1995, pp. 443–448.

[57] M. Bouarroudj, Z. Khatir, J. Ousten, F. Badel, L. Dupont, and S. Lefebvre, "Degradation behavior of 600 v-200 a igbt modules under power cycling and high temperature environment conditions," *Microelectronics Reliability*, vol. 47, pp. 1719–1724, 09 2007.

[58] L. Dupont, S. Lefebvre, M. Bouarroudj Berkani, Z. Khatir, and J. Faugières, "Failure modes on low voltage power mosfets under high temperature application," *Microelectronics Reliability*, vol. 47, pp. 1767–1772, 09 2007.

[59] P. Jacob, M. Held, P. Scacco, and W. Wu, "Reliability testing and analysis of igbt power semiconductor modules," in *IEE Colloquium on IGBT Propulsion Drives*, 1995, pp. 4/1–4/5.

[60] P. Cova and F. Fantini, "On the effect of power cycling stress on igbt modules," *Microelectronics Reliability*, vol. 38, no. 6, pp. 1347–1352, 1998, reliability of Electron Devices, Failure Physics and Analysis. [Online]. Available: https://www.sciencedirect.com/science/article/pii/S002627149800081X

[61] D. Katsis and J. van Wyk, "Experimental measurement and simulation of thermal performance due to aging in power semiconductor devices," in *Conference Record of the 2002 IEEE Industry Applications Conference. 37th IAS Annual Meeting (Cat. No.02CH37344)*, vol. 3, 2002, pp. 1746–1751.

[62] Z. Zhao, P. Davari, W. Lu, H. Wang, and F. Blaabjerg, "An overview of condition monitoring techniques for capacitors in dc-link

applications," *IEEE Transactions on Power Electronics*, vol. 36, no. 4, pp. 3692–3716, 2021.

[63] ECPE, *Guideline AQG 324: Qualification of Power Modules for Use in Power Electronic Converter Units in Motor Vehicles*, 2019, :15-07-2022.

[64] H. Oh, B. Han, P. McCluskey, C. Han, and B. D. Youn, "Physics-of-failure, condition monitoring, and prognostics of insulated gate bipolar transistor modules: A review," *IEEE Transactions on Power Electronics*, vol. 30, no. 5, pp. 2413–2426, 2015.

[65] T. Krone, L. Dang Hung, M. Jung, and A. Mertens, "Advanced condition monitoring system based on on-line semiconductor loss measurements," in *2016 IEEE Energy Conversion Congress and Exposition (ECCE)*, 2016, pp. 1–8.

[66] H. Al-Nasseri, B. Wood, and A. Al-Hinai, *Generation System Reliability Overview*, Oman Power and Water Procurement CO.

[67] R. Billinton and R. Allan, *Reliability Assessment of Large Electrical Power Systems*, 1st ed. Springer, 1988.

[68] K. Fischer, K. Pelka, A. Bartschat, B. Tegtmeier, D. Coronado, C. Broer, and J. Wenske, "Reliability of power converters in wind turbines: Exploratory analysis of failure and operating data from a worldwide turbine fleet," *IEEE Transactions on Power Electronics*, vol. 34, no. 7, pp. 6332–6344, 2019.

[69] M. J. A. Husain Saleh, S. A. Abbas Hasan Abdulla, A. M. A. Aziz Altaweel, and I. S. Qamber, "Lolp and lole calculation for smart cities power plants," in *2019 International Conference on Innovation and Intelligence for Informatics, Computing, and Technologies (3ICT)*, 2019, pp. 1–6.

[70] K. Struntz, E. Abbasi, C. Abbey, C. Andrieu, U. Annakkage, S. Barsali, R. Campbell, R. Fletcher, F. Gao, and T. Gaunt, "Benchmark Systems for Network Integration of Renewable and Distributed Energy Resources ," CIGRE, Technical Report, 2014.

[71] Y. Yang, K. Ma, H. Wang, and F. Blaabjerg, "Mission profile translation to capacitor stresses in grid-connected photovoltaic systems," in *2014 IEEE Energy Conversion Congress and Exposition (ECCE)*, 2014, pp. 5479–5486.

[72] Y. Li, Y. Zheng, N. Zhu, and F. Zhao, "Wind turbine kinetic energy accumulation and release regulation for wind farm optimization," in *2019 4th International Conference on Mechanical, Control and Computer Engineering (ICMCCE)*, 2019, pp. 231–2314.

[73] Thy Windpower. [Online]. Available: http://thymoellen.dk/wp-content/uploads/2014/01/Brochure-TWP-40-6-10kW-DK.pdf

[74] Permanent Magnet Synchronous Motors for Inverter Operation. [Online]. Available: http://www.vem-group-com/fileadmin/content/pdf/Download/Kataloge

[75] D. Sera, R. Teodorescu, and P. Rodriguez, "Pv panel model based on datasheet values," in *2007 IEEE International Symposium on Industrial Electronics*, 2007, pp. 2392–2396.

[76] R. Billinton and D. Huang, "Basic concepts in generating capacity adequacy evaluation," in *9th International Conference on Probabilistic Methods Applied to Power Systems, PMAPS*, 07 2006, pp. 1 – 6.

[77] Energy Numbers. [Online]. Available: http://energynumbers.info/capacity-factors-at-danish-offshore-wind-farms

[78] U.S. Energy Information Administration. [Online]. Available: http://www.eia.gov/electricity/monthly/

[79] SUNmetrix. [Online]. Available: http://sunmetrix.com

[80] A. Anvari-Moghaddam, T. Dragicevic, J. C. Vasquez, and J. M. Guerrero, "Optimal utilization of microgrids supplemented with battery energy storage systems in grid support applications," in *2015 IEEE First International Conference on DC Microgrids (ICDCM)*, 2015, pp. 57–61.

[81] M. Sandelic, A. Sangwongwanich, and F. Blaabjerg, "Robustness evaluation of pv-battery sizing principle under mission profile variations," in *2020 IEEE Energy Conversion Congress and Exposition (ECCE)*, 2020, pp. 545–552.

[82] D.-I. Stroe, M. Swierczynski, A.-I. Stroe, R. Laerke, P. C. Kjaer, and R. Teodorescu, "Degradation behavior of lithium-ion batteries based on lifetime models and field measured frequency regulation mission profile," *IEEE Transactions on Industry Applications*, vol. 52, no. 6, pp. 5009–5018, 2016.

[83] T. B. Reddy, *Linden's Handbook of Batteries*, 4th ed. McGraw-Hill Education, 2011.

[84] V. Svoboda, H. Wenzl, R. Kaiser, A. Jossen, I. Baring-Gould, J. Manwell, P. Lundsager, H. Bindner, T. Cronin, P. Nørgård, A. Ruddell, A. Perujo, K. Douglas, C. Rodrigues, A. Joyce, S. Tselepis, N. van der Borg, F. Nieuwenhout, N. Wilmot, F. Mattera, and D. U.

Sauer, "Operating conditions of batteries in off-grid renewable energy systems," *Solar Energy*, vol. 81, no. 11, pp. 1409–1425, 2007. [Online]. Available: https://www.sciencedirect.com/science/article/pii/S0038092X07000291

[85] G. Zhang, D. Zhou, F. Blaabjerg, and J. Yang, "Consumed lifetime estimation of dfig power converter with constructed high-resolution mission profile," in *2018 20th European Conference on Power Electronics and Applications (EPE'18 ECCE Europe)*, 2018, pp. P.1–P.10.

[86] D. Zhou, H. Wang, F. Blaabjerg, S. K. Kaer, and D. Blom-Hansen, "Real mission profile based lifetime estimation of fuel-cell power converter," in *2016 IEEE 8th International Power Electronics and Motion Control Conference (IPEMC-ECCE Asia)*, 2016, pp. 2798–2805.

[87] P. D. Reigosa, H. Wang, Y. Yang, and F. Blaabjerg, "Prediction of bond wire fatigue of igbts in a pv inverter under a long-term operation," *IEEE Transactions on Power Electronics*, vol. 31, no. 10, pp. 7171–7182, 2016.

[88] A. Sangwongwanich, Y. Yang, D. Sera, and F. Blaabjerg, "Lifetime evaluation of grid-connected pv inverters considering panel degradation rates and installation sites," *IEEE Transactions on Power Electronics*, vol. 33, no. 2, pp. 1225–1236, 2018.

[89] I. Vernica, H. Wang, and F. Blaabjerg, "A mission-profile-based tool for the reliability evaluation of power semiconductor devices in hybrid electric vehicles," in *2020 32nd International Symposium on Power Semiconductor Devices and ICs (ISPSD)*, 2020, pp. 380–383.

[90] G. Zhang, D. Zhou, F. Blaabjerg, and J. Yang, "Mission profile resolution effects on lifetime estimation of doubly-fed induction generator power converter," in *2017 IEEE Southern Power Electronics Conference (SPEC)*, 2017, pp. 1–6.

[91] A. Golnas, "Pv system reliability: An operator's perspective," *IEEE Journal of Photovoltaics*, vol. 3, no. 1, pp. 416–421, 2013.

[92] U. Scheuermann, R. Schmidt, and P. Newman, "Power cycling testing with different load pulse durations," in *7th IET International Conference on Power Electronics, Machines and Drives (PEMD 2014)*, 2014, pp. 1–6.

[93] Infineon, *Technical Information IGBT Modules Use of Power Cycling Curves for IGBT 4*, 2010, Infineon.

[94] S. G. Parler and P. Dubilier, "Deriving life multipliers for electrolytic capacitors," in *IEEE Power Electronics Society Newsletter*, vol. 16, no. 1, 2004, pp. 11–12.

[95] Infineon, "Fs300r12oe4 igbt data sheet," Data sheet, 2013. [Online]. Available: https://www.infineon.com/dgdl/Infineon-FS300R12OE4-DS-v03_01-en_de.pdf?fileId=db3a304335f1f4b601363fdf1629503d

[96] R. Billington and R. N. Allen, *Reliability Evaluation of Engineering Systems - Concepts and Techniques*, 2nd ed. Springer New York, 1992.

[97] A. Lisnianski, I. Frenkel, and Y. Ding, *Multi-state System Reliability Analysis and Optimization for Engineers and Industrial Managers*, 1st ed. Springer London, 2010.

[98] D. R. Cox, "The analysis of non-markovian stochastic processes by the inclusion of supplementary variables," *Mathematical Proceedings of the Cambridge Philosophical Society*, vol. 51, no. 3, p. 433–441, 1955.

[99] C. Singh and R. Billinton, *System Reliability Modelling and Evaluation*, 1st ed. Hutchinson Educational Publishers, 1977.

[100] R. Billinton and J. Satish, "Adequacy evaluation in generation, transmission and distribution systems of an electric power system," in *IEEE WESCANEX 93 Communications, Computers and Power in the Modern Environment - Conference Proceedings*, 1993, pp. 120–126.

[101] M. Cepin, *Assessment of Power System Reliability*, 1st ed. Springer London, 2011.

[102] J. Gu and M. Pecht, "Prognostics and health management using physics-of-failure," in *2008 Annual Reliability and Maintainability Symposium*, 2008, pp. 481–487.

[103] S. Zhao, S. Chen, F. Yang, E. Ugur, B. Akin, and H. Wang, "A composite failure precursor for condition monitoring and remaining useful life prediction of discrete power devices," *IEEE Transactions on Industrial Informatics*, vol. 17, no. 1, pp. 688–698, 2021.

[104] *Aluminium Electrolytic Capacitor Application Guide*, Cornell Dubilier. [Online]. Available: https://www.cde.com/resources/technical-papers/AEappGuide.pdf

[105] Z. Yin, Y. Yang, and H. Wang, "Thermal modeling of an electrolytic capacitor bank," in *2020 IEEE 21st Workshop on Control and Modeling for Power Electronics (COMPEL)*, 2020, pp. 1–5.

[106] Infineon, "Fs25r12w1t7 igbt data sheet," Data sheet, 2020. [Online]. Available: https://www.infineon.com/dgdl/Infineon-FS25R12W1T7-DataSheet-v02_00-EN.pdf?fileId=5546d46270c4f93e0170f188efca7334

[107] EPCOS, "Aluminum electrolytic capacitors datasheet," Data sheet, 2010. [Online]. Available: http://4donline.ihs.com/images/VipMasterIC/IC/EPCO/EPCOS16904/EPCOS16904-1.pdf?hkey=6D3A4C79FDBF58556ACFDE234799DDF0

[108] C. Kulkarni, G. Biswas, X. Koutsoukos, J. Celaya, and K. Goebel, "Experimental studies of ageing in electrolytic capacitors," in *Annual Conference of the Prognostics and Health Management Society, Portland, Oregon, USA*, 10 2010.

[109] N. Z. Gebraeel, M. A. Lawley, R. Li, and J. K. Ryan, "Residual-life distributions from component degradation signals: A bayesian approach," *IIE Transactions*, vol. 37, no. 6, pp. 543–557, 2005.

[110] B. M. Ayyub and R. H. McCuen, *Probability, Statistics, and Reliability for Engineers and Scientists*, ser. 3rd Edition. Taylor and Francis Group, Boca Raton, Florida, US, 2012, no. ISBN-9780429112478.

[111] X. Ye, C. Chen, Y. Wang, G. Zhai, and G. J. Vachtsevanos, "Online condition monitoring of power mosfet gate oxide degradation based on miller platform voltage," *IEEE Transactions on Power Electronics*, vol. 32, no. 6, pp. 4776–4784, 2017.

[112] C. Song and K. Liu, "Statistical degradation modeling and prognostics of multiple sensor signals via data fusion: A composite health index approach," *IISE Transactions*, vol. 50, no. 10, pp. 853–867, 2018.

[113] N. Gebraeel, "Sensory-updated residual life distributions for components with exponential degradation patterns," *IEEE Transactions on Automation Science and Engineering*, vol. 3, no. 4, pp. 382–393, 2006.

[114] K. Liu, N. Z. Gebraeel, and J. Shi, "A data-level fusion model for developing composite health indices for degradation modeling and prognostic analysis," *IEEE Transactions on Automation Science and Engineering*, vol. 10, no. 3, pp. 652–664, 2013.

[115] D. W. Scott, *Multivariate Density Estimation: Theory, Practice and Visualization*, 1st ed. John Wiley and Sons, 1992.

[116] C. Wong and M. Easton, "An efficient method for weighted sampling without replacement." *SIAM J. Comput.*, vol. 9, pp. 111–113, 02 1980.

[117] A. Hamidi, N. Beck, K. Thomas, and E. Herr, "Reliability and lifetime evaluation of different wire bonding technologies for high power igbt modules," *Microelectronics Reliability*, vol. 39, no. 6, pp. 1153–1158, 1999, european Symposium on Reliability of Electron Devices, Failure Physics and Analysis. [Online]. Available: https://www.sciencedirect.com/science/article/pii/S002627149900164X

[118] Y. Fu, J. Zhu, S. Wang, and Z. Xi, "Reduced complexity snr estimation via kolmogorov-smirnov test," *IEEE Communications Letters*, vol. 19, no. 9, pp. 1568–1571, 2015.

[119] B. E. Boser, I. M. Guyon, and V. N. Vapnik, "A training algorithm for optimal margin classifiers," in *Proceedings of the Fifth Annual Workshop on Computational Learning Theory*, ser. COLT '92. New York, NY, USA: Association for Computing Machinery, 1992, pp. 144–152.

[120] S. Tong and D. Koller, "Restricted bayes optimal classifiers," in *The Seventeenth National Conference on Artificial Intelligence and Twelfth Conference on Innovative Applications of Artificial Intelligence, AAAI Press*, 2000, pp. 658–664.

[121] C. Cortes and V. Vapnik, "Support vector networks," *Machine Learning*, vol. 20, no. 3, pp. 273–297, 1995.

ISSN (online): 2446-1636
ISBN (online): 978-87-7573-687-4

AALBORG UNIVERSITY PRESS